

Fast Solvers for Time-Harmonic Maxwell's Equations in 3D

by

Dhavide Arjunan Aruliah

BSc. Simon Fraser University 1993

MSc. Simon Fraser University 1996

A THESIS SUBMITTED IN PARTIAL FULFILLMENT OF
THE REQUIREMENTS FOR THE DEGREE OF

Doctor of Philosophy

in

THE FACULTY OF GRADUATE STUDIES

(Department of Computer Science)

We accept this thesis as conforming
to the required standard

The University of British Columbia

August 2001

© Dhavide Arjunan Aruliah, 2001

In presenting this thesis in partial fulfilment of the requirements for an advanced degree at the University of British Columbia, I agree that the Library shall make it freely available for reference and study. I further agree that permission for extensive copying of this thesis for scholarly purposes may be granted by the head of my department or by his or her representatives. It is understood that copying or publication of this thesis for financial gain shall not be allowed without my written permission.

Department of Computer Science

The University of British Columbia
Vancouver, Canada

Date Aug. 13, 2001

Abstract

The speed of iterative solvers for discretizations of partial differential equations (PDEs) is a significant bottleneck in the performance of codes designed to solve large-scale electromagnetic inverse problems. A single data inversion requires solving Maxwell's equations dozens if not hundreds of times. An inherent difficulty in geophysical contexts is that the conductivity and permeability coefficients may exhibit discontinuities spanning several orders of magnitude. Furthermore, in the air, the conductivity effectively vanishes. In standard formulations of Maxwell's equations, the **curl** operator that dominates the PDE operator leads to strong mixing of field components and ill-conditioning of linear systems resulting from standard discretizations.

The primary objective of this research is to build fast iterative solvers for the forward-modeling problem associated with electromagnetic inverse problems in the frequency domain. Toward this goal, a Helmholtz decomposition of the electric field using a Coulomb gauge condition recasts the PDE problem in terms of scalar and vector potentials. The resulting indefinite system is then stabilized by addition of a vanishing term that lies in the kernel of the dominant **curl** operator. Finally, an extra differentiation recasts the PDE system in a diagonally-dominant form reminiscent of a “pressure-Poisson” formulation for incompressible fluid flow. The continuous PDE problem obtained is equivalent to the original Maxwell's system but has a structure that is amenable to reliable solution techniques.

Using a finite-volume scheme, the PDE is discretized on a staggered grid in three dimensions. The discretization obtained possesses conservation properties typical of finite-volume methods. Furthermore, interface conditions imposed by discontinuities in the material coefficients are sensibly accounted for in deriving the discretization. Although the simple representation of the

media on a Cartesian tensor-product grid uses staircase approximations of surfaces of discontinuity of the material coefficients, some analysis and a numerical study demonstrate the suitability of such coarse approximations for diffusive problems.

The discretization yields a non-Hermitian sparse linear system of algebraic equations; various preconditioners for Krylov-subspace methods are described, analyzed, implemented, and tested. Of particular interest is a multigrid preconditioner that exploits both the structure of the PDE problem and the availability of well-established solvers for elliptic PDE problems (in particular, Dendy's BOXMG solver). The end result is a robust solver for the forward-modeling equations that can be incorporated within a competitive inverse problem code.

Contents

Abstract	ii
Contents	iv
List of Tables	vii
List of Figures	viii
Acknowledgements	ix
Dedication	x
1 Introduction	1
1.1 Background Sketch	3
1.2 Outline of research	9
2 Background Theory of Electromagnetism	14
2.1 Maxwell's Equations	14
2.2 Derived Models	16
2.2.1 Constitutive Relations	17

2.2.2	Stationary Models: Electrostatics and Magnetostatics	19
2.2.3	The Time-Harmonic Model	21
2.2.4	The Quasistatic Model	22
2.2.5	Electric Source Currents	23
2.2.6	Magnetic Source Currents	25
2.2.7	The Magnetotelluric Model	26
2.3	Boundary Conditions	29
2.3.1	Frequency-Domain Boundary Conditions	31
2.3.2	Interface Conditions	33
2.4	Second-order PDE Formulations	36
2.5	Weak Formulations	38
3	Vector and Scalar Potential Formulations	43
3.1	The Forward-modeling Problem	44
3.1.1	Helmholtz Decomposition	47
3.1.2	Stabilization	49
3.1.3	“Pressure-Poisson” Formulation	50
3.2	Boundary Conditions	53
3.2.1	Interface Conditions	59
3.3	Weak Formulations	61
4	Finite-Volume Discretizations	63
4.1	Domain of Discretization	63
4.2	The Yee Discretization	66
4.2.1	The Discrete Fields	68

4.2.2	Derivation of Yee Scheme	70
4.3	Discretization Using Potentials	74
4.3.1	The Discrete Fields	76
4.3.2	Derivation of the Finite-Volume Scheme	78
4.3.3	The Discrete Linear System	84
4.4	Grid Effects	87
4.4.1	Model Problem Analysis	89
4.4.2	Numerical Study	95
5	Construction and Analysis of Iterative Solvers	103
5.1	Iterative Methods	104
5.1.1	Preconditioned Krylov-Subspace Methods	104
5.2	Analytical Framework	110
5.2.1	Discrete Operators on a Periodic Grid	111
5.3	Spectral Bounds	114
5.4	Numerical Experiments	121
6	Conclusions	132
6.1	Research Summary	132
6.2	Future Research	136
Bibliography		139

List of Tables

2.1	Field quantities in Maxwell's equations.	15
2.2	Constitutive parameters for Maxwell's equations.	18
4.1	$\sigma = \sigma_{HS}$: results with vertical shifts	98
4.2	$\sigma = \sigma_E$: results with vertical shifts	100
4.3	$\sigma = \sigma_E$: results with fine & coarse resolutions	102
5.1	$\sigma = \sigma_B$ and electric dipole source on uniform grids.	125
5.2	$\sigma = \sigma_B$ and electric dipole source on nonuniform grids.	126
5.3	$\sigma = \sigma_B$ and magnetic dipole source on uniform grids.	127
5.4	$\sigma = \sigma_B$ and magnetic dipole source on nonuniform grids.	127
5.5	$\sigma = \sigma_E$ and electric dipole source on uniform grids.	128
5.6	$\sigma = \sigma_B$ over a range of frequencies.	128

List of Figures

2.1	Infinitesimal volume V_δ for interface conditions	34
3.1	A typical geophysical scenario	45
4.1	Primary and dual grids for discretization	66
4.2	Staggering of components of \mathbf{E}^h for Yee scheme	70
4.3	Staggering of components of \mathbf{H}^h for Yee scheme	71
4.4	Cross-sections of σ , $\tilde{\sigma}$, and the support S^h of $\tilde{\sigma} - \sigma$	91
4.5	Cross-sections of σ_{HS} and σ_{E}	97
4.6	Cross-sections of σ_{E} resolved on fine and coarse grids.	99
5.1	Eigenvalue range and condition number vs. χ	119
5.2	Cross-section of σ_{B}	124
5.3	Comparison of AMG and M_M	131

Acknowledgements

I have many people to thank. To start, the staff and members of the Dept. of Computer Science and the Institute of Applied Mathematics at UBC have been wonderfully helpful. I offer thanks also to my friends; too many to list, they know who they are. And of course, my family has always given me unconditional love and support without which I could not have gotten so far.

My graduate experiences have taught me much about scientific inquiry and collaboration. I want to thank the members of the Scientific Computation and Visualization group as well as the UBC-GIF for greatly broadening my perspective. Drs. David Moulton and Joel Dendy assisted me greatly with the generous loan of their codes, as did Dr. Yair Shapira. I thank Drs. Doug Oldenburg, Jim Varah, and Brian Wetton for their helpful advice as members of my supervisory committee. I am also deeply grateful for the unbounded enthusiasm and scientific insight of my friend and colleague Dr. Eldad Haber. It is encouraging that the spirit of cooperation and camaraderie thrives in my scientific peers in spite of other pressures.

Finally, I am extremely indebted to my research supervisor, Dr. Uri Ascher. He has set an example as a scientific researcher, as a teacher, and as a person that will be difficult to live up to in my future career. His support, guidance, inspiration, and friendship have been essential through difficult times over the last few years. Thank you, Uri, for everything.

DHAVIDE ARJUNAN ARULIAH

*The University of British Columbia
August 2001*

To my mother's parents,
Daniel Chellathurai Arulanantham and
Grace Emily Athisayam Arulanantham,
and my father's parents,
Vethakutty Charles Aruliah and
Clara Arunothayam Sinnathangam Aruliah.

I wish I had been able to know you better and I hope have made you proud.

Chapter 1

Introduction

A crucial bottleneck in the performance of computational inverse problems is the efficiency of available solvers for the associated forward-modeling problems. Generic strategies for parameter function estimation are based on an iteration within which the forward-modeling problem is solved using the current parameters, the obtained solution is somehow used to update the parameters, and the process is repeated until the parameter function converges in some suitable norm [40]. For large-scale inverse problems, inversion of the forward-modeling problem within each iteration of the inverse problem generally requires some iterative algorithm in itself. Since, in principle, dozens if not hundreds of forward-modeling solves are needed for a single data inversion, the embedded forward-modelling solver must be quick and robust.

Within the geophysical community, an important family of inverse problems used for prospecting derives from electromagnetic surveys [2, 42, 52, 75, 83, 85, 86]. In particular, the electromagnetic response due to some ground-based or aerial transmitter is measured over some terrain. The basic geophysi-

cal inverse problem considered, then, is to construct a model of the conductivity profile under the terrain based on the knowledge of the applied electromagnetic sources and the measured responses. The corresponding mathematical problem is ill-posed as is usual for inverse problems [40, 107].

The goal of this thesis is to derive fast solvers for time-harmonic Maxwell's equations for low or moderate frequencies. Toward this goal, key hindrances in the forward problem are identified that point to analytic reformulations of the partial differential equations (PDEs) in terms of scalar and vector potentials. This analytic model lends itself to a straightforward discretization applying finite-volume techniques. The discretization has conservative properties on the discrete level typical of finite-volume methods and also successfully approximates interface conditions imposed by discontinuities in the material parameters. Finally, a set of preconditioners for Krylov-subspace methods applied to the resulting non-Hermitian sparse linear systems of algebraic equations is explored. Of particular interest is a multigrid preconditioner that exploits both the structure of the PDE problem at hand and well-established solvers for elliptic PDE problems [19, 35, 61, 60, 92]. The combination of the aforementioned efforts leads to a robust solver for the forward-modeling equations. Although the analysis and techniques presented here focus explicitly on geophysical applications, extensions exist to other low-frequency electromagnetic applications such as medical imaging.

1.1 Background Sketch

The past decades have seen the development of many numerical techniques for the computation of electromagnetic fields as well as significant advances in computer hardware, both in processor speed and memory capacity. Fast and accurate methods for predicting electromagnetic phenomena are more readily available. Three-dimensional numerical simulation of the interaction of electromagnetic fields with matter is attainable on modern desktop machines.

The basic physics of electromagnetic fields is governed by Maxwell's equations. Among alternative mathematical formulations of Maxwell's equations, integral equations (IEs) and partial differential equations (PDEs) lead to very different computational approaches. With computational methods derived from IEs, a three-dimensional boundary-value problem reduces to a two-dimensional problem over the boundary of the domain of interest (e.g. boundary element methods or the method of moments [59, 98]). However, even with a significant reduction in the number of unknowns, the computational cost of generating the full system matrix and difficulties in solving the linear equations often makes this approach more costly than comparable PDE methods [77]. It is also difficult to formulate the appropriate IE for geometrically complex inhomogeneous structures, possibly requiring a nontrivial derivation of a geometry-dependent Green's function; PDE solutions are much more flexible in dealing with such media. Thus, PDE formulations of electromagnetics and consequent numerical techniques are the focus of this thesis.

For static problems, scalar and vector potentials for Maxwell's equations

are commonly used [69]. As observed in [16], the paradigmatic equation for electromagnetics in the static case was long thought to be the diffusion problem

$$\operatorname{div}(\epsilon \operatorname{grad} \phi) = \rho$$

for the electrostatic potential ϕ . During the 1970's, advances in finite element methods popularized simulation and analysis for diffusion problems of this form [23, 69, 102]. In two dimensions, the corresponding equation for magnetostatics

$$\operatorname{curl}(\mu^{-1} \operatorname{curl} \mathbf{a}) = \mathbf{J}$$

has only one component for the vector potential \mathbf{a} and reduces to a similar scalar **div-grad** problem. Thus, it was commonly perceived that the **div-grad** and the **curl-curl** equations are effectively equivalent. However, in three dimensions, this is not the case; complications including the nontrivial kernel of the **curl** operator and coupling of field components in three dimensions make the latter operator much more difficult to handle. This realization led to intense research activity into suitable computational methods in three dimensions (e.g. edge elements [11, 16]).

Although finite-element methods are rich in theoretical tools and provide great geometric flexibility, finite-difference methods and finite-volume methods are simpler to implement and can still provide accurate descriptions of solutions for many realistic electromagnetic phenomena [6, 25, 44, 79]. The first finite-difference codes to model Maxwell's equations in three dimensions were based on the well-known Yee method [115]. This spatial discretization

scheme uses a staggered grid to explicitly enforce discrete analogues of conservation properties; this is important for certain applications including electromagnetic scattering, radiation, and waveguides [69, 104]. Although used mostly in electrical engineering applications, Yee’s discretization has over the last ten years been applied in both time- and frequency-domain problems by geophysical researchers [3, 84, 100, 109].

Beyond the need for accurate discretizations in electromagnetic simulation, the large sparse systems of linear equations that typically arise from the discretization of PDEs in three dimensions must be solved efficiently. Direct methods have long been known to be inadequate with the exception of certain cases with unique structure (see, e.g., [48]). With the dramatic increases in processor speeds and growth of memory capacity in modern computers, computations on a large scale are more common and iterative methods become crucial [10, 49, 93].

Although originally conceived as a direct method, the widely-known method of conjugate gradients has had a great impact as an iterative method for the solution of linear systems obtained from discretizations of elliptic PDE problems [60, 61]. One appealing feature is that the convergence behavior of the conjugate-gradient method for elliptic problems is understood. Specifically, for a square linear system $Hx = b$ with a Hermitian positive-definite matrix H , the number of iterations required for the residual $b - Hx_i$ of the approximate solution x_i to converge within a set tolerance is $O(\sqrt{\text{cond}(H)}) = O(\sqrt{\lambda_{\max}/\lambda_{\min}})$, where $\text{cond}(H)$ is the ℓ_2 -condition number of H and λ_{\max} and

λ_{\min} are respectively the largest and smallest eigenvalues of H [49, 93]. For discretizations of second-order elliptic PDEs with grid spacing h , the bound on the number of iterations typically increases as $O(h^{-1})$ since the condition number is $O(h^{-2})$ (see, e.g., [49, Chap. 9]).

Unfortunately, a great number of linear problems are non-Hermitian and indefinite or both, including discrete systems associated with Maxwell's equations. Throughout the 1980's and 1990's, much effort went into the development of *Krylov-subspace methods* for the solution of more general linear algebraic equations. Methods such as GMRES, QMR, and BiCGStab [10, 45, 49, 93, 94] provide generalizations of the conjugate-gradient method that apply for non-Hermitian problems. However, the theory guaranteeing convergence behavior of non-Hermitian matrix iterations is scarce. In spite of the lack of such theoretical results, non-Hermitian Krylov-subspace iterations are applied in most areas of physical science with great success (see, e.g., [6, 26, 28, 54] for examples relating to electromagnetics).

In many ways, more important than the search for more variants of Krylov-subspace methods themselves is the search for suitable *preconditioners* for matrix iterations. Given an invertible square matrix A , a preconditioner is a matrix M that in some way approximates A^{-1} so that MA (or AM) has better spectral properties than A itself. The preconditioner M is selected so that the matrix-vector product Mz is cheap to evaluate for any column vector z (e.g. by FFT, fast Poisson solvers, ADI methods, multigrid methods, etc.) since that product has to be computed within each iteration of a Krylov-subspace

method. While preconditioners based on classical stationary iterative methods are simple to implement in a black-box solver and may have other advantages, many important preconditioners exploit properties of the continuous problem underlying the discrete linear system. For comprehensive summaries of Krylov-subspace methods and some standard preconditioners, see [10, 49, 93].

Over the last thirty years, an important class of iterative methods for elliptic PDE problems emerged, namely the family of *multigrid methods* [17, 18, 19, 22, 56, 92]. Multigrid methods rely on the fact that the error of a fine-grid discrete approximation of the solution of an elliptic PDE can be split into high- and low-wavenumber components; the high-wavenumber components are damped rapidly by the action of a *smoother* (e.g. iterations of a classical stationary iterative method like Gauss-Seidel or SOR) on a fine grid, while the low-wavenumber components can be eliminated on a coarser grid where the number of discrete unknowns is fewer.

Given a discretization of an elliptic PDE, the key components of a multigrid method are a hierarchy of fine and coarse grids, a basic smoothing or relaxation method for improving discrete solution approximations, a *restriction* operator and an *interpolation* operator for transferring grid functions between grids, and a *coarse-grid operator* approximating the action of the discrete operator on the coarse grid (see [18, 22] for more details). A multigrid method is constructed based on the following two-grid heuristic:

1. *Pre-smoothing*: Given a guess for the discrete solution resolved on the fine grid, smooth out the error with a few sweeps of the smoother.

2. *Restriction*: Compute the residual of the current solution on the fine grid and project the result onto the coarse grid with the restriction operator.
3. *Coarse-grid solve*: Obtain the coarse-grid error by applying the inverse of the coarse-grid operator to the coarse-grid residual.
4. *Prolongation*: Interpolate the coarse-grid error up to the fine grid with the interpolation operator, giving an approximation of the fine-grid error of the current fine-grid solution.
5. *Post-smoothing*: Update the current fine-grid solution using the fine-grid error and perform a few more smoothing sweeps to improve the solution.

At the level of the coarsest grid, the appropriate grid equations are solved exactly or nearly exactly to eliminate the low-wavenumber components of the error.

A multigrid method is based on a recursive implementation of the above two-grid scheme on a hierarchy of grids (i.e. applying the same two-grid heuristic for the coarse-grid solve in step 3). Such a recursive iteration is called a *V-cycle* since problems are solved on progressively coarser grids until reaching the coarsest grid, after which the grids are revisited in reverse order. A variant of a V-cycle where the coarsest grid is visited twice in a single iteration is called a *W-cycle*.

Multigrid methods stand out amongst other iterative methods applied to discretizations of elliptic PDEs since well-constructed multigrid methods have grid-independent rates of convergence. Specifically, for a problem dis-

cretized on a fine grid of spacing h , if a multigrid method is constructed and applied, then the number of multigrid W-cycles required to reduce the error within a set tolerance is constant as the grid spacing h is decreased [17, 19]. The same is not true for Krylov-subspace methods, such as the method of conjugate gradients, where the corresponding number of iterations increases as $O(h^{-1})$ for standard discretizations of elliptic PDEs [10, 49]. Thus, although multigrid software can be tricky to implement, for sufficiently large problems (i.e. problems resolved with small grid spacings), the pay-off can be highly significant. For more detailed surveys and background on multigrid methods, consult [17, 18, 19, 22, 56, 92].

1.2 Outline of research

A background survey of electromagnetic theory needed to describe basic electromagnetic phenomena is presented in Chapter 2 with a particular focus on geophysical problems. Starting from Maxwell's equations, various physical assumptions used in practice are described, including, among others, constitutive relations, time-harmonic and quasistatic models, and boundary conditions. A clear understanding of the modeling assumptions imposed is crucial from physical, mathematical, and computational perspectives; it is desirable that all assumptions yield a description that is consistent with the actual physics, that is mathematically sound and solvable, and that is amenable to reliable computational techniques.

Thus, in Chapter 3, the forward-modeling problem is formulated in the

frequency-domain drawing particular attention to the physical properties of the systems being modeled. First, the frequencies of interest are of moderate magnitude, so the effective wavelengths of the scattered fields are much greater than the length scales considered. Secondly, the material properties to be recovered in the inverse problem are isotropic and inhomogeneous with jump discontinuities of several orders of magnitude occurring at media interfaces. Finally, the conductivity coefficient effectively vanishes in the air, so traditional PDE formulations, although well-posed under suitable assumptions, lead to ill-conditioned linear systems when discretized with standard techniques.

Although the latter two of the preceding observations are hindrances, the first is actually an advantage. For sufficiently low frequencies (and parameter ranges suitable for geophysical problems), the prevalent flow of solutions of Maxwell's equations in the time-domain is parabolic rather than hyperbolic; that is, the physics of the electromagnetic field is prevalently diffusive rather than dispersive as in high-frequency electromagnetics. This feature is eventually exploited to construct preconditioners, but it relates also to the selection of suitable analytic formulations of Maxwell's equations.

Scalar and vector potentials are introduced with a Coulomb gauge condition in Chapter 3 to circumvent the problems induced by the dominant **curl-curl** operator in the frequency-domain PDE. The resulting indefinite system is then stabilized by addition of a vanishing term that lies in the kernel of the dominant **curl** operator. Finally, an extra differentiation recasts the PDE system in a diagonally-dominant form reminiscent of a pressure-Poisson

formulation for incompressible fluid flow. Unlike the related problem in fluid flow, there is some freedom to choose boundary conditions for the potential fields so that this formulation leads to robust discretizations. Sections 3.2 and 3.3 fill in the remaining details by deriving suitable boundary and interface conditions for the scalar and vector potential fields and by providing a discussion of a related weak formulation.

After recalling the Yee (or FD-FD) discretization at the beginning of Chapter 4, a finite-volume method is derived with discrete scalar and vector potential fields as unknowns on a staggered grid [53, 54]. An important feature of the discretization is that it retains the important conservation properties of Yee’s discretization while pointing to logical ways to represent the material inhomogeneities within the discrete equations. In particular, the conductivity at the interface of discontinuity between adjacent cells is calculated using harmonic averages, while the permeability at the edges between adjacent cells is given by arithmetic averages.

The discretization of material parameters typically used throughout the geophysical community consists of a grid composed of cells within each of which the material parameters are assumed constant (e.g., [37, 84]). While convenient for inverse problems, this model can only resolve interfaces between distinct media with a staircase approximation of the actual geometry. For high-frequency problems, failure to resolve the geometry accurately may cause great difficulty in practice (e.g. [105]). However, for low-frequency problems, the diffusive nature of the PDE operator tends to smooth out computed

errors and the solutions are not as sensitive to perturbations in the coefficients. In Section 4.4, some analysis of a simple inhomogeneous diffusion problem is presented to estimate the nature of the bounds on the perturbations in the fields induced by staircasing. The analysis is accompanied by supporting experiments in three dimensions.

In Chapter 5, a new family of preconditioners based on sparse approximations of the original linear systems is constructed. Specifically, in the low-frequency limit, the diagonal blocks of the linear system are dominant and thus suggest an obvious block diagonal preconditioner. The diagonal blocks are effectively discretizations of scalar Poisson and inhomogeneous diffusion problems in three dimensions. The blocks can be inverted exactly, or approximate inversion can be achieved either by Incomplete-LU (ILU) factorization or by a multigrid solver such as BOXMG [35, 36]. All of these strategies are compared in the experiments presented.

Since the coefficient matrix is complex and non-Hermitian, the performance of Krylov-subspace methods on the preconditioned system is not well understood. However, a Fourier analysis yields frequency-dependent bounds on the spectrum of the preconditioned system from which a condition bound can also be derived under some simplifying assumptions [5]. The analysis, although limited by the assumptions, does indeed capture the local behavior of the discrete system being solved. Indeed, the numerical tests show grid-independent rates of convergence of the resulting multigrid-preconditioned solver in spite of the non-Hermitian character of the linear system. The ef-

fectiveness of analyzing local behavior of the discrete operators in this case follows largely due the physical assumptions inherent in the model.

Finally, a summary of this research and some future research directions are presented in Chapter 6.

Chapter 2

Background Theory of Electromagnetism

James Clerk Maxwell elegantly formulated the classical theory of electromagnetism in 1864. Maxwell unified previous theoretical and experimental knowledge of electromagnetic phenomena into a more general and advanced theory summarized in a system of partial differential equations (PDEs) known as Maxwell's equations. Physical scientists have studied this particular model of macroscopic electromagnetic phenomena extensively for over a hundred years, laying out the theoretical foundation on which modern electronic technology is built.

2.1 Maxwell's Equations

Maxwell's equations can be formulated using the language of differential forms [16, 67, 73], but the more common language of vector analysis suffices. Written as partial differential equations in Minkowski form (see [68, 76]),

Maxwell's equations are

$$\operatorname{curl} \mathbf{E} + \partial_t \mathbf{B} = \mathbf{0}, \quad (\text{Faraday's law}) \quad (2.1\text{a})$$

$$\operatorname{curl} \mathbf{H} - \partial_t \mathbf{D} = \mathbf{J}, \quad (\text{Maxwell-Ampère law}) \quad (2.1\text{b})$$

$$\operatorname{div} \mathbf{D} = \rho_e, \quad (2.1\text{c})$$

$$\operatorname{div} \mathbf{B} = 0. \quad (2.1\text{d})$$

The quantities represented in (2.1) are distinct fields that are functions of spatial position \mathbf{x} and time t . The vector fields are \mathbf{E} (the *electric field intensity*), \mathbf{D} (the *electric flux density*), \mathbf{H} (the *magnetic field intensity*), \mathbf{B} (the *magnetic flux density*), \mathbf{J} (the *electric current density*), and ρ_e (the *electric charge density*). The four fields \mathbf{E} , \mathbf{D} , \mathbf{H} , and \mathbf{B} describe the total electromagnetic field. The PDEs (2.1) hold in an inertial frame in which the material media are at rest and the charges that interact with the electromagnetic field can move and produce currents [68, 101]. Table 2.1 summarizes these fields in terms of fundamental dimensions of mass (M), length (L), time (T), and current (I).

	Quantity	Units	
\mathbf{E}	Electric field intensity	volts/meter (V/m)	$MLT^{-3}I^{-1}$
\mathbf{D}	Electric flux density	coulombs/meter ² (C/m ²)	$L^{-2}TI$
\mathbf{H}	Magnetic field intensity	amperes/meter (A/m)	$L^{-1}I$
\mathbf{B}	Magnetic flux density	webers/meter ² (W/m ²)	$MT^{-2}I^{-1}$
\mathbf{J}	Electric current density	amperes/meter ² (A/m ²)	$L^{-2}I$
ρ_e	Electric charge density	coulombs/meter ³ (C/m ³)	$L^{-3}TI$

Table 2.1: Field quantities in Maxwell's equations.

There is an additional continuity equation

$$\operatorname{div} \mathbf{J} + \partial_t \rho_e = 0 \quad (2.2)$$

that expresses the conservation of electric charge. In three dimensions, only 7 of the 9 scalar equations (2.1) and (2.2) are independent since (2.1d) follows directly from (2.1a) (with the assumption $\operatorname{div} \mathbf{B} \equiv 0$ at $t = 0$) and (2.2) is a consequence of (2.1b,c). Usually, (2.1a-c) or (2.1a,b) and (2.2) are chosen as the independent equations.

2.2 Derived Models

Maxwell's equations (2.1) in their most general form describe a great range of phenomena. There are a variety of physical models in applied sciences that arise from some simplifying assumptions in (2.1). Among possible models, there are a number of further assumptions that can be made:

1. Constitutive relations
2. Stationary models: electrostatics and magnetostatics
3. The time-harmonic model
4. The quasistatic model
5. Electric source currents
6. Magnetic source currents
7. The magnetotelluric model

Of these possible modeling assumptions, the constitutive relations (2.3) are crucial. The time-harmonic model is considered in this thesis, occasionally

making use of the quasistatic assumption. Stationary models are not studied in this thesis, although much of the standard theory developed for static problems (in particular, the use of potentials) is applied. Assumptions dealing with boundary conditions are discussed in Section 2.3.

2.2.1 Constitutive Relations

Since there are 7 independent scalar equations from (2.1-2.2) that involve 16 scalar unknowns (including the components of the vector fields), the system is underdetermined. A determinate system requires further assumptions. Towards this end, impose *constitutive relations* between the field quantities in order to make the system (2.1) definite [16, 76]. These take the form

$$\mathbf{D} = \epsilon \mathbf{E}, \tag{2.3a}$$

$$\mathbf{B} = \mu \mathbf{H}, \text{ and} \tag{2.3b}$$

$$\mathbf{J} = \sigma \mathbf{E} + \mathbf{J}_e, \tag{2.3c}$$

where ϵ is the *electric permittivity*, μ is the *magnetic permeability*, and σ is the *specific conductivity* of the macroscopic media in which the electromagnetic field exists. The current density \mathbf{J} is decomposed into \mathbf{J}_e (the current density due to some external applied electric source), and $\sigma \mathbf{E}$ (the current density induced in conducting matter by the source current \mathbf{J}_e). The quantities in (2.3) are summarized in fundamental units of mass, length, time, and current in Table 2.2.

The quantities ϵ , μ , and σ are macroscopic properties of matter. They are generally tensor fields that depend on the fields \mathbf{E} and \mathbf{H} as well as the

Quantity	Units
σ	siemens/meter
ϵ	farads/meter
μ	henrys/meter

$M^{-1}L^{-3}T^3I^2$

$M^{-1}L^{-3}T^4I^2$

$MLT^{-2}I^{-2}$

Table 2.2: Constitutive parameters for Maxwell's equations.

spatial variables \mathbf{x} and the time t . The tensor fields ϵ and μ are positive definite while the tensor field σ is positive semi-definite (because it is physically plausible for σ to vanish). For *isotropic* media, the tensor fields for ϵ , μ , and σ reduce to scalar multiples of an identity tensor, so they are essentially scalar fields; for *linear* media, they are independent of the state of the electromagnetic field (i.e. of \mathbf{E} and \mathbf{H}); for *homogeneous* media, they are independent of position \mathbf{x} ; and, for *dispersive* media, they depend on the frequencies of the electromagnetic fields.

In free space, ϵ and μ are isotropic and homogeneous; the corresponding *permittivity of free space* is denoted ϵ_0 and has the value $\epsilon_0 := 8.85 \times 10^{-12}$ F/m in SI units, while the *permeability of free space* is denoted μ_0 and $\mu_0 := 4\pi \times 10^{-7}$ H/m. Free space is nonconductive, so $\sigma = 0$ in free space; Elementary analysis of propagation of electromagnetic waves within isotropic, homogeneous media allows exact solutions of Maxwell's equations to be determined [101]. For more realistic physical simulations of electronic devices, for scattering experiments, or for geophysical data inversion, the material tensors are at the very least inhomogeneous, usually with discontinuities across material boundaries.

It is typical to choose either (\mathbf{E}, \mathbf{H}) or (\mathbf{D}, \mathbf{B}) as the unknown fields

once the constitutive relations (2.3) are assumed. Opting for the unknown fields (\mathbf{E}, \mathbf{H}) , Maxwell's equations (2.1) become

$$\operatorname{curl} \mathbf{E} + \mu \partial_t \mathbf{H} = \mathbf{0}, \quad (2.4a)$$

$$\operatorname{curl} \mathbf{H} - \sigma \mathbf{E} - \epsilon \partial_t \mathbf{E} = \mathbf{J}_e, \quad (2.4b)$$

$$\operatorname{div} (\epsilon \mathbf{E}) = \rho_e, \quad (2.4c)$$

$$\operatorname{div} (\mu \mathbf{H}) = 0. \quad (2.4d)$$

The system (2.4) is a linear, first-order, hyperbolic system of PDEs [89]. Within this work, the material properties ϵ , μ , and σ are assumed to be independent of time t and of the frequencies of the electromagnetic fields (i.e. nondispersive); this permits moving the quantities ϵ and μ through the operator ∂_t in (2.4a,b) without concern. However, great care is required in manipulating the operator div in (2.4c,d) unless ϵ and μ are spatially constant (i.e. homogeneous).

2.2.2 Stationary Models: Electrostatics and Magneto-statics

The most obvious simplification is to assume that the electromagnetic fields do not vary in time. As such, all terms with time derivatives vanish in (2.4). An immediate consequence is the *electrostatic* model

$$\begin{aligned} \operatorname{curl} \mathbf{E} &= \mathbf{0}, \\ \mathbf{D} &= \epsilon \mathbf{E}, \\ \operatorname{div} \mathbf{D} &= \rho_e. \end{aligned} \quad (2.5)$$

Assuming the static charge density is known, it is possible to identify the electric field \mathbf{E} as the gradient of a scalar potential field, so $\mathbf{E} = -\mathbf{grad} \phi$. With this notation, the essential model of linear electrostatics is the inhomogeneous diffusion equation

$$-\operatorname{div}(\epsilon \mathbf{grad} \phi) = \rho_e. \quad (2.6)$$

With a suitable domain and boundary conditions specified, the diffusion PDE (2.6) yields a well-posed boundary-value problem [46, 89]. In the case where $\epsilon = \epsilon_0$ (i.e. the permittivity is everywhere constant) and where the domain is all of \mathbb{R}^3 , standard analysis (e.g. [101]) gives the electrostatic potential

$$\phi(\mathbf{x}) = \frac{1}{4\pi\epsilon_0} \iiint_{\mathbb{R}^3} \frac{\rho_e(\mathbf{y})}{|\mathbf{x} - \mathbf{y}|} d\mathbf{y}. \quad (2.7)$$

In a similar way, the model of *magnetostatics* is given by

$$\begin{aligned} \mathbf{curl} \mathbf{H} &= \mathbf{J}, \\ \mathbf{B} &= \mu \mathbf{H}, \\ \operatorname{div} \mathbf{B} &= 0, \end{aligned} \quad (2.8)$$

for some known time-independent source current density \mathbf{J} (the effects of conduction are not included in this model, so there is no $\sigma \mathbf{E}$ term). The vanishing divergence of \mathbf{B} usually implies the existence of a vector potential field for \mathbf{B} , so $\mathbf{H} = \mu^{-1} \mathbf{curl} \mathbf{a}$ for some vector field \mathbf{a} . Thus, the essential equation describing linear magnetostatics is the double-curl equation

$$\mathbf{curl}(\mu^{-1} \mathbf{curl} \mathbf{a}) = \mathbf{J}. \quad (2.9)$$

If $\mu = \mu_0$, the vector potential over all space is

$$\mathbf{a}(\mathbf{x}) = \frac{\mu_0}{4\pi} \iiint_{\mathbb{R}^3} \frac{\mathbf{J}}{|\mathbf{x} - \mathbf{y}|} d\mathbf{y}. \quad (2.10)$$

The magnetic field can be recovered naturally with the Biot-Savart law [43, 76]

$$\mathbf{H}(\mathbf{x}) = \frac{1}{4\pi} \iiint_{\mathbb{R}^3} \frac{\mathbf{J} \times (\mathbf{x} - \mathbf{y})}{|\mathbf{x} - \mathbf{y}|^3} d\mathbf{y}. \quad (2.11)$$

2.2.3 The Time-Harmonic Model

For this model, all the scalar fields and the components of the vector fields in (2.4) are assumed to be of the form $u(\mathbf{x}, t) \equiv \text{Re}(u(\mathbf{x}, \omega)e^{-i\omega t})$ for some constant frequency $\omega \in \mathbb{R}$. The resulting model of electromagnetism is commonly called *time-harmonic*. Then, Maxwell's equations (2.4) become

$$\operatorname{curl} \mathbf{E} - i\omega\mu\mathbf{H} = \mathbf{0}, \quad (2.12a)$$

$$\operatorname{curl} \mathbf{H} - \hat{\sigma}\mathbf{E} = \mathbf{J}_e, \quad (2.12b)$$

$$\operatorname{div} (\epsilon\mathbf{E}) = \rho_e, \quad (2.12c)$$

$$\operatorname{div} (\mu\mathbf{H}) = 0. \quad (2.12d)$$

In (2.12b), the complex conductivity

$$\hat{\sigma} := \sigma - i\omega\epsilon \quad (2.13)$$

is introduced for notational convenience. The equations (2.4) are *Maxwell's equations in the time domain*, whereas the equations (2.12) are *Maxwell's equations in the frequency domain* (sometimes called *time-harmonic Maxwell's*

equations). One advantage of the frequency-domain formulation of Maxwell's equations is that, in principle, solutions of (2.12) can be found for a few key frequencies of interest. Formally, the system (2.12) is obtained by substituting $-\imath\omega\epsilon$ for every occurrence of ∂_t in (2.4). Within this thesis, the same notation is used for fields $u \equiv u(\mathbf{x}, t)$ in the time domain and the corresponding fields $u \equiv u(\mathbf{x}, \omega)$ in the frequency domain; the meaning is always clear from the context.

2.2.4 The Quasistatic Model

For many physical applications, it is possible to neglect the Maxwellian displacement current term $\imath\omega\mathbf{D}$ from (2.12b) (or $\partial_t\mathbf{D}$ from (2.1b) in the time-domain formulation); in the frequency-domain, this amounts to substituting $\hat{\sigma} \leftarrow \sigma$ in (2.12b). This *quasistatic assumption* (also called the *eddy-current approximation*) is reasonable assuming that the displacement current $\imath\omega\mathbf{D}$ is negligible relative to the other terms in the Maxwell-Ampère law (2.12b). One key indicator of the validity of the quasistatic assumption in the frequency-domain model is the magnitude of the ratio $\omega\epsilon/\sigma$; for low-frequency experiments within conductors, this ratio can vary from 10^{-16} to 10^{-1} (see [16, 111]). In many high-frequency electromagnetic applications (e.g. waveguides) or applications in vacuum (e.g. radar scattering), the displacement current's contribution to the evolution of the electromagnetic field cannot be ignored as readily. For a discussion of parameter ranges in which the quasistatic assumption is valid, see [16, 111].

The mathematical importance of the quasistatic assumption is that it changes the underlying character of Maxwell's equations. Ordinarily, the time-domain equations (2.4) constitute a hyperbolic system of PDEs; dropping the displacement current $\partial_t \mathbf{D}$ makes the PDE system parabolic. The ratio of the magnitude of the conduction current $\sigma \mathbf{E}$ to the magnitude of the displacement current $\partial_t \mathbf{D} = \epsilon \partial_t \mathbf{E}$ reflects the relative importance of diffusion to dispersion in transmission of electromagnetic energy on the time scales considered. The balance between these physical processes strongly influences the development of mathematical models and discretization schemes in low- and high-frequency electromagnetics.

2.2.5 Electric Source Currents

Generally, the conduction currents within matter as described by Maxwell's equations (2.4) (2.12) are induced by some time-varying field driven by some external electric current density \mathbf{J}_e . Within the domain of geophysical applications, certain source currents are naturally occurring, such as ionospheric currents that cause geomagnetic variation, while others are artificial, such as current loops used in geophysical prospecting [111]. In either case, the source of electromagnetic induction is incorporated into Maxwell's equations through the constitutive relation (2.3c), namely

$$\mathbf{J} = \sigma \mathbf{E} + \mathbf{J}_e.$$

In the following, let \mathbf{e}_x , \mathbf{e}_y , and \mathbf{e}_z denote the orthogonal Cartesian coordinate unit vectors. Let $\mathbf{x} := (x, y, z)^T$ denote the coordinates of a point

in space. The function δ refers to the usual Dirac- δ function and H refers to the Heaviside-step function (see e.g. [101]). The sources are understood as distributions that act on a space of testing functions (see [46, 89] for definitions of distributions).

Examples of source fields include:

1. A vertical electric dipole

$$\mathbf{J}_e(\mathbf{x}, t) = I(t)\delta(x)\delta(y)(H(z - \ell) - H(z))\mathbf{e}_z. \quad (2.14a)$$

In (2.14a), $\ell > 0$ is the separation of the electrodes between which a potential difference is maintained that generates the dipole field. The function $I(t)$ describes the current that flows between the electrodes as a function of time.

2. A vertical magnetic dipole

$$\begin{aligned} \mathbf{J}_e(\mathbf{x}, t) = & I(t)\delta(z)[(H(x) - H(x - \ell))(\delta(y) - \delta(y - \ell))\mathbf{e}_x \\ & - (\delta(x) - \delta(x - \ell))(H(y) - H(y - \ell))\mathbf{e}_y]. \end{aligned} \quad (2.14b)$$

The magnetic dipole field is generated by a current loop with normal direction \mathbf{e}_z . Again, $I(t)$ is the current flowing through the loop as a function of time and ℓ is the sidelength of the loop.

3. A source current along a line

$$\mathbf{J}_e(\mathbf{x}, t) = I(t)\delta(y)\delta(z)\mathbf{e}_x. \quad (2.14c)$$

The current $I(t)$ flows in the x -direction. Notice that, unlike the previous source fields, this field has unbounded support. Other source fields of unbounded support include current sheets in a horizontal or vertical plane [111].

The sources in (2.14) are used in time-domain modeling. If the current inducing the source is of the form $I(t) = I_0 e^{-t/\tau}$ in (2.14b-d), the sources are referred to as transient (that are of interest in geophysical prospecting [110]). For frequency-domain models, the applied currents are of the form $I(t) = I_0 e^{-i\omega t}$ in (2.14b-d). Exact solutions of Maxwell's equations are known for all of the above with time-harmonic sources in vacuum and in half-space conductivity models due to the high degree of symmetry [76, 101, 110, 111].

2.2.6 Magnetic Source Currents

Given the apparent symmetries in the curl equations (2.12a-b), it is reasonable from a mathematical perspective to place some kind of a source term on the right-hand side of (2.12a). Under this assumption, the time-domain curl equations become

$$\text{curl } \mathbf{E} + \mu \partial_t \mathbf{H} = \mathbf{J}_m, \quad (2.15a)$$

$$\text{curl } \mathbf{H} - (\sigma + \epsilon \partial_t) \mathbf{E} = \mathbf{J}_e, \quad (2.15b)$$

$$\text{div } (\epsilon \mathbf{E}) = \rho_e, \quad (2.15c)$$

$$\text{div } (\mu \mathbf{H}) = \rho_m, \quad (2.15d)$$

and in the frequency domain,

$$\operatorname{curl} \mathbf{E} - i\omega\mu\mathbf{H} = \mathbf{J}_m, \quad (2.16a)$$

$$\operatorname{curl} \mathbf{H} - \hat{\sigma}\mathbf{E} = \mathbf{J}_e, \quad (2.16b)$$

$$\operatorname{div} (\epsilon\mathbf{E}) = \rho_e, \quad (2.16c)$$

$$\operatorname{div} (\mu\mathbf{H}) = \rho_m. \quad (2.16d)$$

In (2.15) and (2.16), \mathbf{J}_m is a magnetic current density and ρ_m is a magnetic charge density. Such magnetic currents and charges are not physically realistic; magnetic charges correspond to magnetic monopoles that have never been observed experimentally. As a result, \mathbf{J}_m and ρ_m are null in all physically relevant situations [43, 68, 101].

However, (2.15) and (2.16) are useful for the purpose of analysis and derivation of numerical schemes. For instance, in the forward-modeling problem, if there is a known primary field $(\mathbf{E}^p, \mathbf{H}^p)$ in the background, it may be more convenient to solve for the unknown *secondary field* $(\mathbf{E}^s, \mathbf{H}^s)$, assuming that the total electromagnetic field is given by $(\mathbf{E}^p + \mathbf{E}^s, \mathbf{H}^p + \mathbf{H}^s)$ [6, 14]. Solving for a secondary field may be more useful in the event that the secondary field is significantly smaller in magnitude than the primary field. Magnetotelluric models provide an example of a physical model in which secondary fields and hence magnetic source currents enter the mathematical formulation of Maxwell's equations.

2.2.7 The Magnetotelluric Model

In a large class of geophysical problems, the flow of electromagnetic fields in the higher atmosphere induces currents in conductive matter underground; this is the basic principle of the *magnetotelluric (or MT) experiment* (see [71, 77, 95]). To derive the basic physical model for the MT experiment, assume that the total electromagnetic field satisfies Maxwell's curl equations in the frequency domain with no applied source currents, i.e.,

$$\operatorname{curl} \mathbf{E} - \imath\omega\mu\mathbf{H} = \mathbf{0}, \quad (2.17a)$$

$$\operatorname{curl} \mathbf{H} - (\sigma - \imath\omega\epsilon)\mathbf{E} = \mathbf{0}. \quad (2.17b)$$

The equations (2.17) are assumed to hold throughout all of space. The material tensors σ , ϵ , and μ are isotropic, but inhomogeneous; in particular, they are assumed to be piecewise constant scalar fields throughout \mathbb{R}^3 .

Assume that the field admits the decomposition

$$\mathbf{E} = \mathbf{E}^p + \mathbf{E}^s, \text{ and} \quad (2.18a)$$

$$\mathbf{H} = \mathbf{H}^p + \mathbf{H}^s. \quad (2.18b)$$

The field $(\mathbf{E}^p, \mathbf{H}^p)$ in (2.18) is a *primary field* that is assumed to satisfy Maxwell's equations with some known coefficients and source terms. If the primary field is known, then solving the original system (2.17) amounts to solving a similar PDE for the *secondary field* $(\mathbf{E}^s, \mathbf{H}^s)$ induced by the primary field. The left-hand side of the PDE for the secondary field is determined by the primary field and describes the response of the secondary field due to the primary one [6, 14].

For the magnetotelluric modeling, it is sensible to use a half-space or a

1-D layered-earth solution (i.e., piecewise constant functions of z only, see [111, 110]) of Maxwell's equations for the primary field based on the assumption that the earth being modeled has that basic structure far away from the region of interest [71]. Thus, assuming that the primary field satisfies Maxwell's equations with no source currents in a half-space model, then

$$\operatorname{curl} \mathbf{E}^p = \imath\omega\tilde{\mu}\mathbf{H}^p, \quad (2.19a)$$

$$\operatorname{curl} \mathbf{H}^p = (\tilde{\sigma} - \imath\omega\tilde{\epsilon})\mathbf{E}^p \quad (2.19b)$$

where $\tilde{\sigma}$, $\tilde{\epsilon}$, and $\tilde{\mu}$ are models for a half-space or 1D layered earth. The equations (2.19) admit analytic solutions provided that the coefficients in (2.19) have such a simple one-dimensional structure.

Under the assumption (2.19), since $\mathbf{J}_e = \mathbf{0}$ for the primary field, the secondary field satisfies

$$\operatorname{curl} \mathbf{E}^s - \imath\omega\mu\mathbf{H}^s = \mathbf{J}_m, \quad (2.20a)$$

$$\operatorname{curl} \mathbf{H}^s - (\sigma - \imath\omega\epsilon)\mathbf{E}^s = \mathbf{J}_e, \quad (2.20b)$$

where

$$\mathbf{J}_m := \imath\omega(\mu - \tilde{\mu})\mathbf{H}^p, \quad (2.21a)$$

$$\mathbf{J}_e := [(\sigma - \tilde{\sigma}) - \imath\omega(\epsilon - \tilde{\epsilon})]\mathbf{E}^p. \quad (2.21b)$$

In decomposing the total field, the PDE for the secondary field has a magnetic current source term \mathbf{J}_m as well. The sources in (2.21) generally have unbounded support since the fields \mathbf{E}^p and \mathbf{H}^p will generally have unbounded support. However, if it is known *a priori* that $\sigma \equiv \tilde{\sigma}$, $\epsilon \equiv \tilde{\epsilon}$, and $\mu \equiv \tilde{\mu}$ outside

some bounded domain, then the source terms indeed have compact support. In fact, if the computational domain is large enough, the normal and tangential components of \mathbf{J}_m and \mathbf{J}_e in (2.21) on the boundary of the computational domain Ω vanish, and these fields do not affect the boundary conditions. If there is a more complicated structure to the material tensors outside Ω , then the source terms may enter into the boundary conditions. Suitable boundary conditions are presented in the next section.

2.3 Boundary Conditions

The *forward-modeling problem* refers to determining the unknown fields \mathbf{E} , \mathbf{H} , and ρ_e under the assumption that the quantities ω (in the frequency domain), \mathbf{J}_e , ϵ , μ , and σ are all known. The forward-modeling problem can be solved in the time domain with (2.4) or in the frequency domain with (2.12). In either case, the system consists of 8 differential equations involving 7 unknown quantities. In practice, the divergence equation (2.4c) (or (2.12c) in the frequency domain) defines the charge density ρ_e once the field \mathbf{E} is determined. Moreover, (2.12d) can be derived from (2.12a) under the assumption $\omega \neq 0$. Thus, consider (2.1d) as a differential invariant and use the curl equations (2.4a,b) (or (2.12a,b)) as the system of PDEs determining \mathbf{E} and \mathbf{H} in the forward-modeling problem.

Even with the constitutive relations (2.3) and various modeling assumptions about the source fields, a suitable set of boundary and initial (in the time domain) conditions is needed to make the forward-modeling problem

well posed. For an unbounded domain $\Omega \subset \mathbb{R}^3$, suitable boundary conditions at infinity are well known [69, 91]. However, the question of what boundary conditions to apply on the boundary $\partial\Omega$ of a bounded computational domain $\Omega \subset \mathbb{R}^3$ is actively debated due to the inherent difficulty of balancing the need for physically relevant boundary data with the desire for an elegant, consistent, mathematical formulation. This direction of research in electromagnetics parallels the search for open boundary conditions in computational fluid mechanics [51, 50]. Absorbing boundary conditions have been used for over twenty years in electromagnetic codes to absorb outgoing waves at $\partial\Omega$ and to ensure that reflected waves do not corrupt the solution [41]. As a first-order approximation, absorbing boundary conditions correspond to Sommerfeld's radiation condition for the Helmholtz equation; at high frequencies where greater accuracy may be required, higher-order absorbing boundary condition are also possible [58, 57, 69]. A different class of approximate boundary conditions stems from a perfectly matched layer technique (PML) [12] in which some absorbing matter is placed immediately outside the artificial boundary $\partial\Omega$ to absorb outgoing waves; for a numerical study of implementations of various artificial boundary conditions, see [104].

It is not necessary to assign boundary conditions on the artificial boundary with certain formulations. One alternative is to use boundary integrals (e.g. boundary element methods [59]) to connect the problem within the finite computational domain to the unbounded exterior region. The use of infinite elements also allows a computational framework that incorporates the behav-

ior of the fields at infinity into the solution [47]. Both of these techniques have some advantages but may introduce other computational difficulties. For a detailed review of different techniques used for the numerical solution of problems on unbounded domains, see [106].

It is important to recognize that for the classes of geophysical applications studied herein, the time-harmonic fields are driven by low- or moderate-frequency sources; as such, the influence of boundary conditions at the artificial boundary $\partial\Omega$ is minimal. This is in contrast with the situation in high-frequency scattering applications where errors in the computation of the electromagnetic field at $\partial\Omega$ contaminate the entire solution. For the diffusion-dominated flow of the electromagnetic field on geophysical length scales, the accuracy of the artificial boundary condition is not as crucial as it would be at higher frequencies.

This thesis focuses on frequency-domain formulations of Maxwell's equations. As such, the discussion that follows is limited to well-posed PDE problems in the frequency domain. For results describing initial and boundary conditions for well-posed PDE problems based on Maxwell's equations in the time domain, see [4, 11, 70, 73, 97].

2.3.1 Frequency-Domain Boundary Conditions

First, consider the time-harmonic PDE problem (2.12) specified in an

unbounded spatial domain $\Omega \subset \mathbb{R}^3$. Then, as $|\mathbf{x}| \rightarrow \infty$, provided that

$$\begin{aligned} |\mathbf{x}| \mathbf{E}(\mathbf{x}, \omega) \text{ and } |\mathbf{x}| \mathbf{H}(\mathbf{x}, \omega) \text{ are bounded and that} \\ \mathbf{E}(\mathbf{x}, \omega) + \frac{\mathbf{x} \times \mathbf{H}(\mathbf{x}, \omega)}{|\mathbf{x}|} = o\left(\frac{1}{|\mathbf{x}|}\right) \end{aligned} \quad (2.22)$$

uniformly in all directions, then the frequency-domain problem (2.12) is guaranteed to have a unique solution [97]. The conditions (2.22) are the *Silver-Müller radiation conditions* that are analogous to the Sommerfeld radiation condition for the Helmholtz equation [69, 91].

On a bounded domain $\Omega \subset \mathbb{R}^3$, suppose that the boundary $\partial\Omega$ is partitioned into two disjoint parts, $\partial\Omega^E$ and $\partial\Omega^H := \partial\Omega \setminus \partial\Omega^E$, one of which may be empty. Then, the following inhomogeneous boundary-value problem is well-posed (see [16, chap. 9] or [15]):

$$\begin{aligned} \operatorname{curl} \mathbf{E} - i\omega\mu\mathbf{H} &= \mathbf{J}_m \quad (\mathbf{x} \in \Omega); \\ \operatorname{curl} \mathbf{H} - \hat{\sigma}\mathbf{E} &= \mathbf{J}_e \quad (\mathbf{x} \in \Omega); \\ \mathbf{n} \times \mathbf{E} &= \mathbf{n} \times \mathbf{e} \quad (\mathbf{x} \in \partial\Omega^E); \\ \mathbf{n} \times \mathbf{H} &= \mathbf{n} \times \mathbf{h} \quad (\mathbf{x} \in \partial\Omega^H), \end{aligned} \quad (2.23)$$

where \mathbf{e} and \mathbf{h} are some known fields whose tangential traces are well-defined. The explicit spaces in which the solution (\mathbf{E}, \mathbf{H}) is sought are detailed in Section 2.5 where equivalent integral formulations are specified.

The specification of the tangential trace $\mathbf{n} \times \mathbf{E} = \mathbf{0}$ is the boundary condition that applies at the boundary of a perfect electric conductor (PEC); hence, this boundary condition is often called a PEC boundary condition. The corresponding boundary condition $\mathbf{n} \times \mathbf{H} = \mathbf{0}$ is the boundary condition for a perfect magnetic conductor (PMC). While both PEC and PMC boundary

conditions represent idealizations that do not exist in nature, they are reasonable approximations and are used in many electromagnetic models for their simplicity [11, 63].

A standard first-order absorbing boundary condition is of the form

$$\mathbf{n} \times (-\mathbf{n} \times \mathbf{E} + \mathbf{H}) = \mathbf{n} \times \mathbf{g} \quad (\mathbf{x} \in \partial\Omega), \quad (2.24)$$

where \mathbf{g} is the tangential trace of some known field [41, 97]. The particular absorbing boundary condition (2.24) ensures that electromagnetic waves normally incident on the boundary will be completely absorbed. This is more physically reasonable than a PEC or PMC, although there will be some reflections due to waves striking the boundary obliquely. However, if the wavevector \mathbf{k} of an incident electromagnetic wave is known (for instance, the wave that generates the primary solution in the MT experiment in Section 2.2.7), a slightly different absorbing boundary condition applies, namely

$$-\mathbf{n} \times \mathbf{n} \times \left(\epsilon - \frac{i\sigma}{\omega}\right)^{\frac{1}{2}} \mathbf{E} + A(\mathbf{k}, \mathbf{n}) \mathbf{n} \times \mu^{\frac{1}{2}} \mathbf{H} = \mathbf{g} \quad (\mathbf{x} \in \partial\Omega), \quad (2.25)$$

where $A(\mathbf{k}, \mathbf{n})$ is a symmetric positive-definite matrix chosen so that waves on $\partial\Omega$ with wavevector \mathbf{k} are completely absorbed [97]. Well-posedness of time-harmonic Maxwell's equations with boundary conditions (2.24) or (2.25) is shown in [95, 97]. Higher-order absorbing boundary conditions are discussed in [69].

2.3.2 Interface Conditions

The material tensors ϵ , μ , and σ are generally discontinuous at interfaces between distinct kinds of matter. Due to such discontinuities, the differential equations (2.4) and (2.12) (and their generalizations (2.15) and (2.16)) do not apply at the interfaces; they hold strictly within regions wherein the material tensors are continuous. Thus, in addition to boundary conditions that describe the behavior of the electromagnetic field at the artificial boundary $\partial\Omega$, *interface conditions* apply at material interfaces.

To derive the associated interface conditions, let $\Gamma \subset \Omega$ be any surface that divides Ω into two disconnected portions, Ω^I and Ω^{II} . Consider an infinitesimal cylinder $V_\delta \subset \Omega$ of height $\delta > 0$ that straddles Γ . The cylinder V_δ intersects Γ in a surface Γ_0 . Let the boundary of V_δ consist of three disjoint parts: the sides, top, and bottom respectively (see Figure 2.1), so

$$\partial V_\delta = \partial V_\delta^{\text{sides}} \cup \partial V_\delta^I \cup \partial V_\delta^{II}. \quad (2.26)$$

Finally, let \mathbf{n}^I and \mathbf{n}^{II} denote the unit normal vectors on ∂V_δ^I and ∂V_δ^{II} respectively with the conventional outward orientation.

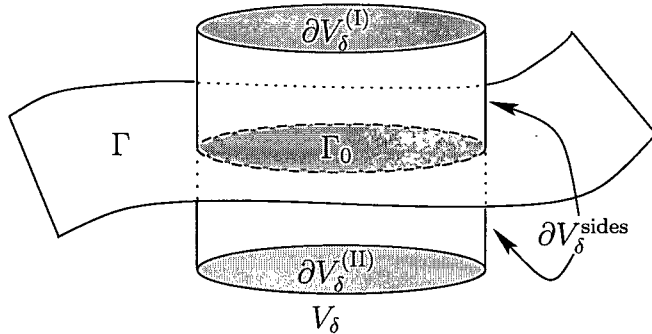


Figure 2.1: Infinitesimal cylinder V_δ for deriving interface conditions.

Multiplying the divergence equation (2.1c) by some arbitrary smooth

function ψ and integrating by parts yields

$$\begin{aligned} \int_{\partial V_\delta^I} \psi \mathbf{n}^I \cdot \mathbf{D} dS + \int_{\partial V_\delta^{II}} \psi \mathbf{n}^{II} \cdot \mathbf{D} dS &= \int_{V_\delta} \psi \rho_e dV \\ &+ \int_{V_\delta} \mathbf{grad} \psi \cdot \mathbf{D} dV - \int_{\partial V_\delta^{\text{sides}}} \psi \mathbf{n} \cdot \mathbf{D} dS. \end{aligned} \quad (2.27a)$$

Choose the test function ψ in (2.27a) so that $\psi \equiv 0$ on $\partial V_\delta^{\text{sides}}$. Then,

$$\begin{aligned} \int_{\partial V_\delta^I} \psi \mathbf{n}^I \cdot \mathbf{D} dS + \int_{\partial V_\delta^{II}} \psi \mathbf{n}^{II} \cdot \mathbf{D} dS &= \int_{V_\delta} \psi \rho_e dV \\ &+ \int_{V_\delta} \mathbf{grad} \psi \cdot \mathbf{D} dV. \end{aligned} \quad (2.27b)$$

As $\delta \downarrow 0$, the second volume integral on the right-hand side of (2.27b) vanishes assuming that \mathbf{D} and $\mathbf{grad} \psi$ do not have surface singularities. The other volume integral on the right-hand side reduces to a surface integral of a surface electric charge density. The preceding argument holds for any surface $\Gamma \subset \Omega$ (not just interfaces), so it follows that

$$\mathbf{n}^I \cdot [\mathbf{D}^I - \mathbf{D}^{II}] = \varrho_e, \quad (2.28a)$$

holds pointwise on Γ , where ϱ_e is the surface electric charge density. The expression \mathbf{D}^I in (2.28a) is the limiting value of \mathbf{D} approaching a point on Γ from within Ω^I and \mathbf{D}^{II} is similarly defined.

In a similar manner (see, e.g. [68, 69, 76, 101]), the conditions

$$\mathbf{n}^I \cdot [\mathbf{B}^I - \mathbf{B}^{II}] = \varrho_m, \quad (2.28b)$$

$$\mathbf{n}^I \cdot [\mathbf{J}^I - \mathbf{J}^{II}] = -\partial_t \varrho_e, \quad (2.28c)$$

$$\mathbf{n}^I \times [\mathbf{H}^I - \mathbf{H}^{II}] = \mathbf{j}_e, \quad (2.28d)$$

$$\mathbf{n}^I \times [\mathbf{E}^I - \mathbf{E}^{II}] = \mathbf{j}_m \quad (2.28e)$$

also apply across any surface $\Gamma \subset \Omega$. In (2.28), ϱ_e and ϱ_m are surface electric and magnetic charge densities while \mathbf{j}_e and \mathbf{j}_m are surface electric and magnetic current densities respectively.

The interface conditions (2.28) are derived explicitly assuming the fields \mathbf{E} , \mathbf{H} , \mathbf{D} , and \mathbf{B} do not have singularities in any of their components. This modeling assumption rules out the possibility of singular layers that might occur in cracks or tiny air gaps in a conductor (see [16]). For the geophysical problems considered in this thesis, this assumption is reasonable. Further, even where magnetic charges and currents are formally used for mathematical purposes (cf. Section 2.2.6), the surface densities ϱ_m and \mathbf{j}_m are assumed to vanish, assuring the continuity of $\mathbf{n} \cdot \mathbf{B}$ and $\mathbf{n} \times \mathbf{E}$ throughout Ω . Moreover, between media of finite conductivities, no surface electric current density \mathbf{j}_e exists, so $\mathbf{n} \times \mathbf{H}$ is continuous as well [67, 110]. With the preceding assumptions, the interface conditions (2.28) imply that the tangential components of the fields \mathbf{E} and \mathbf{H} are continuous across any surface in Ω , as is the normal component of \mathbf{B} . The normal component $\mathbf{n} \cdot \mathbf{D}$ may be discontinuous, as a surface electric charge density ϱ_e might be induced by the applied source current \mathbf{J}_e .

2.4 Second-order PDE Formulations

It is often not necessary to determine both \mathbf{E} and \mathbf{H} , as one of these two vector fields can be eliminated. Eliminating \mathbf{H} from (2.12) gives the

second-order vector Helmholtz equation

$$\operatorname{curl} (\mu^{-1} \operatorname{curl} \mathbf{E}) - \omega \hat{\sigma} \mathbf{E} = \omega \mathbf{J}_e. \quad (2.29)$$

The corresponding PDE in the time domain is the hyperbolic evolutionary PDE

$$\operatorname{curl} (\mu^{-1} \operatorname{curl} \mathbf{E}) + \sigma \partial_t \mathbf{E} + \epsilon \partial_{tt} \mathbf{E} = -\partial_t \mathbf{J}_e. \quad (2.30)$$

After solving for \mathbf{E} in either the frequency domain using (2.29) or the time domain using (2.30), the magnetic field intensity \mathbf{H} can be recovered if needed using the appropriate form of Faraday's law (i.e. with (2.12a) or (2.4a) respectively).

With the other approach, \mathbf{E} can be eliminated from (2.12) in the frequency domain, giving

$$\operatorname{curl} (\hat{\sigma}^{-1} \operatorname{curl} \mathbf{H}) - \omega \mu \mathbf{H} = \operatorname{curl} (\hat{\sigma}^{-1} \mathbf{J}_e). \quad (2.31)$$

Eliminating \mathbf{E} in the time domain, however, is less straightforward; dividing by $\hat{\sigma}$ in (2.31) formally corresponds to computing the operator $(\sigma + \epsilon \partial_t)^{-1}$ in the time-domain problem. However, with the quasistatic assumption, the term $\epsilon \partial_t \mathbf{E}$ is ignored wherever it occurs, so the time-domain system is

$$\operatorname{curl} (\sigma^{-1} \operatorname{curl} \mathbf{H}) + \mu \partial_t \mathbf{H} = \operatorname{curl} (\sigma^{-1} \mathbf{J}_e). \quad (2.32)$$

Notice that (2.32) assumes $\sigma \neq 0$ which is not necessarily the case in nonconducting media such as air.

The equations (2.32) are called the equations of magnetic diffusion (see [66, 68]), as they describe a parabolic (rather than hyperbolic) evolutionary

system for the magnetic field intensity. The time-domain PDE system for \mathbf{E} with the same quasistatic assumption is obtained by dropping the term $\epsilon\partial_{tt}\mathbf{E}$ in (2.30). The frequency-domain systems for \mathbf{E} and \mathbf{H} under the quasistatic assumption are found by substituting $\hat{\sigma} \leftarrow \sigma$ in (2.29) and (2.31) respectively.

2.5 Weak Formulations

Since the classical or strong forms of Maxwell's equations (2.4) or (2.12) implicitly assume high degrees of smoothness in all the fields involved, weak equations posed over suitable functional spaces are required. It suffices to consider spaces consisting of vector fields of finite energy; that is, application of the differential operators **grad**, **curl**, and **div** should not result in fields with unbounded energy in the standard \mathcal{L}_2 -norm.

With the domain $\Omega \subset \mathbb{R}^3$ given, define the mappings

$$(f, g)_\Omega := \int_\Omega f g^* dV, \quad (2.33a)$$

$$(\boldsymbol{\xi}, \boldsymbol{\eta})_\Omega := \int_\Omega \boldsymbol{\xi} \cdot \boldsymbol{\eta}^* dV, \quad (2.33b)$$

$$\langle f, g \rangle_{\partial\Omega} := \int_{\partial\Omega} f g^* dS, \quad (2.33c)$$

$$\langle \boldsymbol{\xi}, \boldsymbol{\eta} \rangle_{\partial\Omega} := \int_{\partial\Omega} \boldsymbol{\xi} \cdot \boldsymbol{\eta}^* dS, \quad (2.33d)$$

where $*$ denotes the usual complex conjugate taken pointwise. Suitable norms on spaces of complex scalar and vector fields can be defined in terms of the

notation of (2.33a-b), namely,

$$\|f\|_{\Omega} := \sqrt{(f, f)_{\Omega}}, \quad (2.34a)$$

$$\|\boldsymbol{\xi}\|_{\Omega} := \sqrt{(\boldsymbol{\xi}, \boldsymbol{\xi})_{\Omega}}. \quad (2.34b)$$

With the inner products and norms in (2.34) and (2.33a-b), the spaces

$$\mathcal{L}_2(\Omega) := \{f : \|f\|_{\Omega} < \infty\}, \text{ and} \quad (2.35a)$$

$$\mathcal{L}_2(\Omega) := [\mathcal{L}_2(\Omega)]^3 = \mathcal{L}_2(\Omega) \times \mathcal{L}_2(\Omega) \times \mathcal{L}_2(\Omega), \quad (2.35b)$$

are Hilbert spaces of complex-valued fields [16, 46]. For variational problems in electromagnetics, the Hilbert spaces $\mathcal{L}_2(\Omega)$ and $\mathcal{L}_2(\Omega)$ give rise to the spaces

$$\mathcal{H}(\mathbf{grad}; \Omega) := \{f \in \mathcal{L}_2(\Omega) : \mathbf{grad} f \in \mathcal{L}_2(\Omega)\}, \quad (2.35c)$$

$$\mathcal{H}(\mathbf{curl}; \Omega) := \{\boldsymbol{\eta} \in \mathcal{L}_2(\Omega) : \mathbf{curl} \boldsymbol{\eta} \in \mathcal{L}_2(\Omega)\}, \quad (2.35d)$$

$$\mathcal{H}(\mathbf{div}; \Omega) := \{\boldsymbol{v} \in \mathcal{L}_2(\Omega) : \mathbf{div} \boldsymbol{v} \in \mathcal{L}_2(\Omega)\}. \quad (2.35e)$$

The operators **grad**, **curl**, and **div** as they occur in (2.35c-e) must be interpreted in a weak sense (i.e. as continuous extensions of strong differential operators as they apply to smooth functions; see [16, Chap. 5] for details.) The complex spaces (2.35c-e) are also Hilbert spaces, but not when endowed with the standard \mathcal{L}_2 -inner-products. The appropriate inner product for each

space can be inferred from the corresponding Hilbert-space norms:

$$\|f\|_{\mathcal{H}(\mathbf{grad};\Omega)}^2 := \|f\|_\Omega^2 + \|\mathbf{grad} f\|_\Omega^2, \quad (2.36a)$$

$$\|\boldsymbol{\eta}\|_{\mathcal{H}(\mathbf{curl};\Omega)}^2 := \|\boldsymbol{\eta}\|_\Omega^2 + \|\mathbf{curl} \boldsymbol{\eta}\|_\Omega^2, \text{ and} \quad (2.36b)$$

$$\|\mathbf{v}\|_{\mathcal{H}(\mathbf{div};\Omega)}^2 := \|\mathbf{v}\|_\Omega^2 + \|\mathbf{div} \mathbf{v}\|_\Omega^2. \quad (2.36c)$$

All of the spaces (2.35) are Hilbert spaces with their respective norms and inner products in (2.34) and (2.36). Detailed discussions of the required background in functional analysis can be found in [16, 46, 78, 89]).

In terms of the above notation, the strong PDE problem (2.23) leads to at least two weak formulations that correspond to equivalent second-order PDE formulations. To see this, given the data $\mathbf{e}, \mathbf{h} \in \mathcal{L}_2(\Omega)$, define the spaces

$$\mathbb{E}^e := \{\boldsymbol{\xi} \in \mathcal{H}(\mathbf{curl};\Omega) : \mathbf{n} \times \boldsymbol{\xi} = \mathbf{e} \text{ on } \partial\Omega^E\}, \quad (2.37a)$$

$$\mathbb{H}^h := \{\boldsymbol{\eta} \in \mathcal{H}(\mathbf{curl};\Omega) : \mathbf{n} \times \boldsymbol{\eta} = \mathbf{h} \text{ on } \partial\Omega^H\}, \quad (2.37b)$$

and their homogeneous counterparts

$$\mathbb{E}^0 := \{\boldsymbol{\xi} \in \mathcal{H}(\mathbf{curl};\Omega) : \mathbf{n} \times \boldsymbol{\xi} = \mathbf{0} \text{ on } \partial\Omega^E\}, \quad (2.37c)$$

$$\mathbb{H}^0 := \{\boldsymbol{\eta} \in \mathcal{H}(\mathbf{curl};\Omega) : \mathbf{n} \times \boldsymbol{\eta} = \mathbf{0} \text{ on } \partial\Omega^H\}. \quad (2.37d)$$

The tangential traces $\mathbf{n} \times \mathbf{e}$ and $\mathbf{n} \times \mathbf{h}$ are understood in a distributional sense (\mathcal{L}_2 fields do not have tangential traces in the strictest sense [46]).

With this terminology, the second-order boundary-value PDE

$$\begin{aligned} \mathbf{curl}((\omega\mu)^{-1}\mathbf{curl} \mathbf{E}) - \hat{\sigma} \mathbf{E} &= \\ \mathbf{J}_e + \mathbf{curl}((\omega\mu)^{-1}\mathbf{J}_m) &\quad (\mathbf{x} \in \Omega), \\ \mathbf{n} \times \mathbf{E} = \mathbf{n} \times \mathbf{e} &\quad (\mathbf{x} \in \partial\Omega^E), \\ \mathbf{n} \times (\omega\mu)^{-1}[\mathbf{curl} \mathbf{E} - \mathbf{J}_m] = \mathbf{n} \times \mathbf{h} &\quad (\mathbf{x} \in \partial\Omega^H), \end{aligned} \quad (2.38)$$

leads to the weak problem

Find $\mathbf{E} \in \mathbb{E}^e$ such that, for every $\boldsymbol{\xi} \in \mathbb{E}^0$,

$$\begin{aligned} & ((\omega\mu)^{-1}\mathbf{curl} \mathbf{E}, \mathbf{curl} \boldsymbol{\xi})_\Omega - (\widehat{\sigma} \mathbf{E}, \boldsymbol{\xi})_\Omega = \\ & (\mathbf{J}_e, \boldsymbol{\xi})_\Omega + ((\omega\mu)^{-1}\mathbf{J}_m, \mathbf{curl} \boldsymbol{\xi})_\Omega - \langle \mathbf{n} \times \mathbf{h}, \boldsymbol{\xi} \rangle_{\partial\Omega}. \end{aligned} \quad (2.39)$$

That is, any strong solution \mathbf{E} of (2.38) is also a weak solution of (2.39). Notice that the Dirichlet boundary condition for \mathbf{H} in (2.23) is replaced by a Neumann boundary condition for \mathbf{E} that includes the source field \mathbf{J}_m when \mathbf{H} is eliminated. Assuming that the frequency ω is not an eigenvalue of the associated homogeneous problem

$$((\omega\mu)^{-1}\mathbf{curl} \mathbf{E}, \mathbf{curl} \boldsymbol{\xi})_\Omega - (\widehat{\sigma} \mathbf{E}, \boldsymbol{\xi})_\Omega = 0,$$

the weak problem (2.39) is well-posed [15].

Alternatively, rather than eliminating the magnetic field \mathbf{H} , eliminating \mathbf{E} gives the boundary-value PDE problem

$$\begin{aligned} & \mathbf{curl} (\widehat{\sigma}^{-1} \mathbf{curl} \mathbf{H}) - \omega\mu \mathbf{H} = \\ & \mathbf{J}_m + \mathbf{curl} (\widehat{\sigma}^{-1} \mathbf{J}_e), \quad (\mathbf{x} \in \Omega) \\ & \mathbf{n} \times \mathbf{H} = \mathbf{n} \times \mathbf{h}, \quad (\mathbf{x} \in \partial\Omega^H) \\ & \mathbf{n} \times \widehat{\sigma}^{-1} [\mathbf{curl} \mathbf{H} - \mathbf{J}_e] = \mathbf{n} \times \mathbf{e}, \quad (\mathbf{x} \in \partial\Omega^E). \end{aligned} \quad (2.40)$$

and the corresponding weak problem

Find $\mathbf{H} \in \mathbb{H}^h$ such that, for every $\boldsymbol{\eta} \in \mathbb{H}^0$

$$\begin{aligned} & (\widehat{\sigma}^{-1} \mathbf{curl} \mathbf{H}, \mathbf{curl} \boldsymbol{\eta})_\Omega - \omega (\mu \mathbf{H}, \boldsymbol{\eta})_\Omega = (\mathbf{J}_m, \boldsymbol{\eta})_\Omega \\ & + (\widehat{\sigma}^{-1} \mathbf{J}_e, \mathbf{curl} \boldsymbol{\eta})_\Omega - \langle \mathbf{n} \times \mathbf{e}, \boldsymbol{\eta} \rangle_{\partial\Omega}. \end{aligned} \quad (2.41)$$

In eliminating either \mathbf{E} or \mathbf{H} from the original first-order Maxwell's system (2.23), one of the source fields \mathbf{J}_m or \mathbf{J}_e gets incorporated into the boundary conditions and both are combined in the right-hand side of the second-order double-curl PDE.

Either of (2.39) or (2.41) can be discretized to find a weak solution describing the desired electromagnetic fields. As is typically for many PDE problems, a single PDE admits numerous weak formulations that are equivalent in the event that the solution is sufficiently smooth that a classical solution exists. In a mixed variational formulation, the constitutive relations are not explicitly included in the PDE formulation [20, 21]; this is the approach taken for eddy current and magnetostatic problems in [88, 87].

Weak formulations of boundary-value PDEs are essential for analyses leading to existence of solutions (e.g. [4, 97]). More than being a purely theoretical tool, weak solutions exist for a number of physically-motivated problems where classical solutions do not. Weak formulations are natural for developing finite-element discretizations that are typically more flexible for dealing with difficult geometries [11, 63, 88]. For the class of geophysical problems studied in this thesis, however, classical PDE formulations leading to finite-volume methods—that are a middle ground between the simplicity of finite-difference methods and the practical strength of finite element methods—are sufficient.

Chapter 3

Vector and Scalar Potential Formulations

A problem of great importance in geophysics is to compute global electromagnetic fields in three dimensions given a known external source current and an electrical conductivity structure [111]. This is the forward-modeling problem that needs to be solved efficiently within each iteration of a remote-sensing inverse problem [40, 55, 86]. After a thorough description of the forward-modeling problem in Section 3.1, equivalent alternative PDE formulations are derived using a Helmholtz decomposition of the electric field. With a new PDE expressed in terms of scalar and vector potential field variables, boundary and interface conditions are presented in Section 3.2, followed by a weak formulation in Section 3.3.

3.1 The Forward-modeling Problem

The geophysical forward-modeling problem of interest is

$$\operatorname{curl} \mathbf{E} - i\omega\mu\mathbf{H} = \mathbf{J}_m \quad (\mathbf{x} \in \Omega), \quad (3.1a)$$

$$\operatorname{curl} \mathbf{H} - \hat{\sigma}\mathbf{E} = \mathbf{J}_e \quad (\mathbf{x} \in \Omega), \quad (3.1b)$$

$$\mathbf{n} \times \mathbf{H} = \mathbf{0} \quad (\mathbf{x} \in \partial\Omega) \quad (3.1c)$$

with $\hat{\sigma}$ as given in (2.13). Typically, $\mathbf{J}_m \equiv 0$, but the inclusion of \mathbf{J}_m in (3.1a) allows for the use of secondary fields (see Section 2.2.6). For most geophysical applications, the dielectric permittivity ϵ is effectively constant, so $\epsilon \equiv \epsilon_0$, where $\epsilon_0 := 8.85 \times 10^{-12}$ F/m is the permittivity of vacuum. The conductivity σ generally varies significantly between the air ($\sigma \approx 0$ S/m) and the ground ($\sigma \in [10^{-3}, 10^2]$ S/m). The magnetic permeability μ may vary over a range of one or two orders of magnitude from $\mu_0 := 4\pi \times 10^{-7}$ H/m, the permeability of vacuum. To keep the number of parameters manageable for purposes of the inverse problem, it is common to assume that σ is isotropic and piecewise constant. In magnetic ore bodies, assume μ is isotropic and piecewise constant like σ . For most situations, it is reasonable to assume $\mu \equiv \mu_0$ [84, 111]. Finally, in addition to the PDE and boundary condition in (3.1), the interface conditions (2.28) apply at interfaces between distinct material media. The general situation is illustrated in Figure 3.1; the length scale is typically from a few hundred meters to a kilometer.

Although an absorbing boundary condition such as (2.25) or even a higher-order absorbing boundary condition may be more physically reasonable

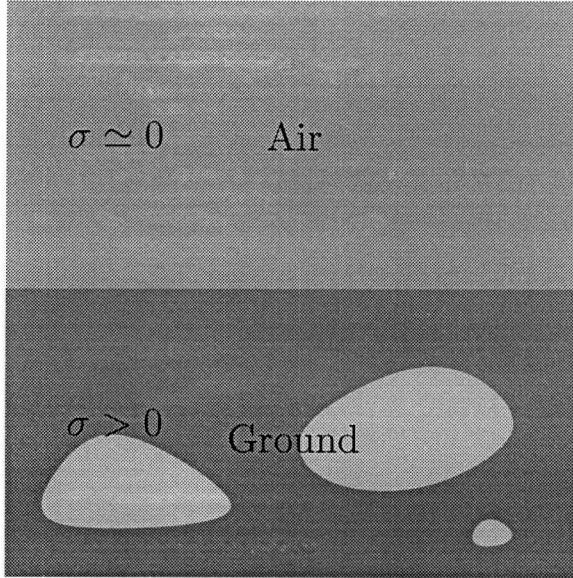


Figure 3.1: 2D cross-section of a typical geophysical scenario: ϵ is constant, σ and μ are piecewise constant.

than the homogeneous magnetic (PMC) boundary condition (3.1c), for low-to moderate-frequency ranges (say 0– 10^5 Hz) and for source fields \mathbf{J}_e and \mathbf{J}_m that have compact support in Ω , (3.1c) suffices. Under those assumptions, the induced electromagnetic fields decay as $|\mathbf{x}| \rightarrow \infty$ and the dominant behavior of Maxwell's equations is parabolic rather than hyperbolic. This will be the case for an electric or magnetic dipole source, as is common in many geophysical surveys [110, 111]. Thus, for a domain Ω that is sufficiently large, assume that a very small fraction of the total energy of the electromagnetic field is stored in the region near the boundary $\partial\Omega$; as such, a homogeneous boundary condition such as (3.1c) suffices for geophysical models. Even when \mathbf{J}_m and \mathbf{J}_e have unbounded support but most of the energy of each field (as measured in the \mathcal{L}_2 -norm) is stored away from $\partial\Omega$, such a homogeneous boundary condition

may still be reasonable.

The PDE (3.1a-b) can be reformulated in a second-order form by eliminating the magnetic field \mathbf{H} (cf. (2.29)), namely

$$(\omega)^{-1} \mathbf{curl} (\mu^{-1} \mathbf{curl} \mathbf{E}) - \hat{\sigma} \mathbf{E} = \mathbf{J}_e + (\omega)^{-1} \mathbf{curl} (\mu^{-1} \mathbf{J}_m). \quad (3.2)$$

It is alternatively possible to eliminate \mathbf{E} and derive a second-order PDE in the unknown \mathbf{H} (cf. (2.31)). For the ranges of conductivities considered here, (3.2) is more favorable; σ is much more strongly spatially inhomogeneous than μ , the former varying over seven or eight orders of magnitude as compared with two or three for the latter. The dominant term $\mathbf{curl} (\mu^{-1} \mathbf{curl} \mathbf{E})$ in (3.2) is far more preferable to the second-order term $\mathbf{curl} (\hat{\sigma}^{-1} \mathbf{curl} \mathbf{H})$ in (2.31) for this reason [53].

In the limit as $|\omega\hat{\sigma}| \rightarrow 0$, the second-order PDE (3.2) reduces to one of the form

$$\mathbf{curl} (\mu^{-1} \mathbf{curl} \mathbf{E}) = \omega \mathbf{J}_e + \mathbf{curl} (\mu^{-1} \mathbf{J}_m). \quad (3.3)$$

The **curl** operator has a nontrivial kernel consisting of any vector field that is a gradient of a scalar field [16, 46]. As such, the PDE (3.3) (with the boundary condition (3.1c)) is ill-posed in the sense that there are infinitely many solutions. Another equation prescribing $\operatorname{div} \mathbf{E}$ inside Ω and a suitable boundary condition is required in order to resolve this ill-posedness; usually, this is the divergence equation (2.12c) with some assumption made about the charge density ρ [6, 29].

For low frequencies, the displacement current $\omega\epsilon_0 \mathbf{E}$ is usually very

small. Given that the PDE problem (3.1) is ill-posed wherever $\widehat{\sigma} = 0$, practitioners often introduce a small, artificial conductivity, say, $\sigma \approx 10^{-6}\text{S/m}$ in those regions [84]. This regularizes the forward-modeling problem (3.1). However, any numerical discretization that faithfully models the continuous problem (3.1) produces an ill-conditioned system of linear algebraic equations, even with the artificial conductivity $0 < \sigma \ll 1$ in the air. The essential reason is that the small artificial conductivity term can regularize a large, second-order differential term only if it is added to its kernel; this is not the case in (3.1). It is the near-singular nature of the underlying continuous PDE problem that accounts for the ill-conditioned linear systems in experiments (see [84]). Since geophysical data inversions require solving this complex PDE dozens of times, alternative formulations of the analytic problem (3.1) are studied to develop efficient solvers and make computation times feasible.

3.1.1 Helmholtz Decomposition

For the time being, questions of differentiability are avoided. The various electromagnetic fields are assumed sufficiently smooth to allow application of the necessary differential operators. Discussion of boundary conditions and corresponding weak formulations are deferred to Section 3.2 and Section 3.3 respectively.

The strategy adopted splits the electric field \mathbf{E} into two parts. The first part lies in the *range* of the **curl** operator and the second part lies in the *kernel* of the **curl** operator. Introduction of the *Helmholtz decomposition* of \mathbf{E}

gives

$$\mathbf{E} = \mathbf{A} + \mathbf{grad} \phi \quad (3.4)$$

for some vector field \mathbf{A} and some scalar field ϕ [6, 13, 33, 46, 72].

Since $\mathbf{curl}(\mathbf{grad} \phi) = \mathbf{0}$, the field $\mathbf{grad} \phi$ lies in the kernel of the operator \mathbf{curl} in (3.1a). With the substitution (3.4) and the preceding observation, when \mathbf{E} and \mathbf{H} are eliminated, the PDE (3.1a) yields the equation

$$\begin{aligned} (\omega)^{-1} \mathbf{curl}(\mu^{-1} \mathbf{curl} \mathbf{A}) - \hat{\sigma}(\mathbf{A} + \mathbf{grad} \phi) &= \mathbf{J}_e \\ + (\omega)^{-1} \mathbf{curl}(\mu^{-1} \mathbf{J}_m) . \end{aligned} \quad (3.5)$$

The three unknown scalar fields in (3.2) (the components of \mathbf{E}) are replaced by four unknown scalar fields (the components of \mathbf{A} and the field ϕ). Thus, an extra scalar equation is required in addition to (3.5); a useful choice here is the *Coulomb gauge condition*

$$\mathbf{div} \mathbf{A} = 0. \quad (3.6)$$

The field \mathbf{A} is typically called a vector potential for the magnetic flux density \mathbf{B} since, in the event that $\mathbf{J}_m = \mathbf{0}$, (2.12) and (3.4) imply that

$$\mathbf{curl} \mathbf{A} = \mathbf{curl} \mathbf{E} = \omega \mathbf{B} = \omega \mu \mathbf{H}.$$

Similarly, the field ϕ is called a scalar potential.

Thus, the decomposition (3.4),(3.6) yields the new PDE

$$\begin{aligned} (\omega)^{-1} \mathbf{curl}(\mu^{-1} \mathbf{curl} \mathbf{A}) - \hat{\sigma}(\mathbf{A} + \mathbf{grad} \phi) &= \\ \mathbf{J}_e + (\omega)^{-1} \mathbf{curl}(\mu^{-1} \mathbf{J}_m) , \end{aligned} \quad (3.7a)$$

$$\mathbf{div} \mathbf{A} = 0. \quad (3.7b)$$

When $\mu \equiv \mu_0 = \text{constant}$, the dominant differential term $\mathbf{curl}(\mu^{-1}\mathbf{curl} \mathbf{A})$ in (3.7a) simplifies; in particular, denoting the *vector Laplacian* (the extension of the Laplacian operator for vector fields) by Δ ,

$$\begin{aligned}\mathbf{curl}(\mu_0^{-1}\mathbf{curl} \mathbf{A}) &\equiv \mu_0^{-1}(\mathbf{grad}(\operatorname{div} \mathbf{A}) - \Delta \mathbf{A}) \\ &\equiv -\mu_0^{-1}\Delta \mathbf{A},\end{aligned}\tag{3.8}$$

as a result of the Coulomb gauge condition (3.6) [6, 54]. The resulting PDE is

$$(\omega\mu_0)^{-1}\Delta \mathbf{A} + \widehat{\sigma}(\mathbf{A} + \mathbf{grad} \phi) = -\mathbf{J}_e - (\omega\mu_0)^{-1}\mathbf{curl}(\mathbf{J}_m),\tag{3.9a}$$

$$\operatorname{div} \mathbf{A} = 0.\tag{3.9b}$$

3.1.2 Stabilization

Generally, the permeability μ is inhomogeneous, so the dominant operator $\mathbf{curl}(\mu^{-1}\mathbf{curl})$ in (3.7a) cannot be replaced with the simpler vector Laplacian operator as in (3.9a). Moreover, the kernel of the dominant operator is nontrivial. A common strategy is to incorporate the gauge condition (3.6) into the equation (3.7a) (see, e.g., [29]). That is, rather than

$$\mathbf{curl}(\mu^{-1}\mathbf{curl}(\cdot)),$$

write the dominant operator in (3.7a) as

$$\mathbf{curl}(\mu^{-1}\mathbf{curl}(\cdot)) - \alpha \mathbf{grad}(\beta \operatorname{div}(\cdot))$$

for some scalar fields α and β . Given that

$$\mathbf{curl}(\mu_0^{-1}\mathbf{curl}(\cdot)) - \mathbf{grad}(\mu_0^{-1}\mathbf{div}(\cdot)) \equiv -\mu_0^{-1}\Delta$$

within a medium of homogeneous permeability, the appropriate vector Laplacian is recovered when $\mu \leftarrow \mu_0$ with the choice $\alpha \equiv 1$ and $\beta \equiv \mu^{-1}$.

Hence, the introduction of the vanishing term $\mathbf{grad}(\mu^{-1}\mathbf{div} \mathbf{A})$ into (3.7) effectively stabilizes (3.7a); the corresponding system is

$$(\imath\omega)^{-1} (\mathbf{curl}(\mu^{-1}\mathbf{curl} \mathbf{A}) - \mathbf{grad}(\mu^{-1}\mathbf{div} \mathbf{A})) - \widehat{\sigma}(\mathbf{A} + \mathbf{grad} \phi) = \mathbf{J}_e + (\imath\omega)^{-1}\mathbf{curl}(\mu^{-1}\mathbf{J}_m), \quad (3.10a)$$

$$\mathbf{div} \mathbf{A} = 0. \quad (3.10b)$$

The additional term is identically zero for the exact solution of the PDE (3.10), so introduction of the stabilizing term does not change the analytic solution of the problem. This is in contrast with penalty methods where the solution of the penalized problem fails to satisfy some of the constraints [21, 51]. In such cases, selection of a penalty parameter that is large enough to improve conditioning of the discrete equations while small enough to prevent excessive violation of the constraints is a significant challenge (e.g. [51]).

3.1.3 “Pressure-Poisson” Formulation

Again deferring the question of boundary conditions, there is a striking resemblance between the constant- μ electromagnetic equations (3.9), the

Stokes equations

$$\Delta \mathbf{u} + \mathbf{grad} p = \mathbf{s}, \quad (3.11a)$$

$$\operatorname{div} \mathbf{u} = 0, \quad (3.11b)$$

and the Oseen equations

$$\Delta \mathbf{u} + (\mathbf{w} \cdot \mathbf{grad}) \mathbf{u} + \mathbf{grad} p = \mathbf{s}, \quad (3.12a)$$

$$\operatorname{div} \mathbf{u} = 0, \quad (3.12b)$$

where (3.11) and (3.12) describe steady incompressible fluid flow [46, 51]. In particular, the vector potential field \mathbf{A} corresponds to a velocity field \mathbf{u} , the scalar potential ϕ corresponds to a pressure field p , and the Coulomb gauge condition (3.6) corresponds to the incompressibility condition $\operatorname{div} \mathbf{u} = 0$ in both (3.11) and (3.12). The PDE (3.9) for electromagnetics and the corresponding PDEs (3.11) and (3.12) for fluids differ in the (complex) Helmholtz shift $i\omega\widehat{\sigma}\mathbf{A}$ in (3.9a) and the advective term $(\mathbf{w} \cdot \mathbf{grad})\mathbf{u}$ in (3.12a); barring these differences, the systems (3.9), (3.11), and (3.12) have very similar structure in the dominant differential terms for (\mathbf{A}, ϕ) and (\mathbf{u}, p) respectively.

Motivated by the analogy with fluid flow, take the divergence of (3.1b) and replace the Coulomb gauge in (3.10) with the resulting equation. The PDE obtained is

$$(i\omega)^{-1} (\mathbf{curl} (\mu^{-1} \mathbf{curl} \mathbf{A}) - \mathbf{grad} (\mu^{-1} \operatorname{div} \mathbf{A})) - \widehat{\sigma}(\mathbf{A} + \mathbf{grad} \phi) = \mathbf{J}_e + (i\omega)^{-1} \mathbf{curl} (\mu^{-1} \mathbf{J}_m), \quad (3.13a)$$

$$\operatorname{div} (\widehat{\sigma}(\mathbf{A} + \mathbf{grad} \phi)) = -\operatorname{div} \mathbf{J}_e. \quad (3.13b)$$

The equation (3.13b) resembles the *pressure-Poisson equation* (PPE) used in incompressible flow [51, 99, 108]. The PDE (3.13) is used in [13] to derive a finite-element discretization of a PPE-type systems in (\mathbf{A}, ϕ) for a large scale geomagnetic problem where $\mu \equiv \mu_0$. The same PDE is studied in [6, 54] to yield finite-volume methods for other low-frequency geophysical applications. In [53], a discretization of a related PPE-type system in (\mathbf{A}, ϕ) is derived for the more general case of inhomogeneous permeability with the additional stabilizing term.

Solving direct discretizations of the indefinite PDE system (3.7) is possible by techniques analogous to those in [38, 39, 51] for the fluid-flow problems (3.11) and (3.12). The principle distinction between (3.7) or (3.10) and the fluid-flow problems (3.11) or (3.12) is that the decomposition (3.4),(3.6) is arbitrary (although \mathbf{A} and ϕ do have physical interpretations [6, 13]). There is, to a degree, more freedom in prescribing boundary conditions for the system (3.13) for this family of geophysical applications. This freedom contrasts the additional problems with boundary conditions arising in pressure-Poisson formulations for Stokes' flow [51, 99].

The left-hand side of the system (3.13) includes the linear differential operator

$$\mathcal{A} := \begin{pmatrix} (\omega)^{-1} \Delta_\mu - \widehat{\sigma} I & -\widehat{\sigma} \mathbf{grad}(\cdot) \\ \operatorname{div}(\widehat{\sigma} I) & \operatorname{div}(\widehat{\sigma} \mathbf{grad}(\cdot)) \end{pmatrix}, \text{ where} \quad (3.14a)$$

$$\Delta_\mu := \mathbf{curl}(\mu^{-1} \mathbf{curl}(\cdot)) - \mathbf{grad}(\mu^{-1} \operatorname{div}(\cdot)). \quad (3.14b)$$

If ω is not too large in magnitude, the differential operator in (3.14a) is di-

agonally dominant; that is, the leading order differential terms occur on the main diagonal. As a result, the corresponding scalar PDEs constituting (3.13) are weakly coupled. When (3.13) is discretized, the diagonal dominance of the operator leads to matrices with block-diagonal dominance; this property is used to advantage in devising iterative solvers. By contrast, standard formulations of Maxwell's equations (such as (3.2) for \mathbf{E}) have strong coupling between the scalar components. The poor convergence behavior of iterative methods applied to the corresponding discretizations of (3.2) relates to this coupling (see [53, 84]).

3.2 Boundary Conditions

To close the stabilized forward-modeling PDE (3.13), suitable boundary conditions for the unknowns (\mathbf{A}, ϕ) must be imposed. The key steps taken in the preceding derivation are:

- introduction of a Helmholtz decomposition with a Coulomb gauge;
- introduction of a stabilizing term;
- differentiation to obtain a “PPE” to replace the gauge condition.

The original PDE (3.1) has a single boundary condition and the final boundary-value problem has two additional boundary conditions derived below.

It is convenient to use auxiliary variables to derive the boundary conditions. Hence, introduce the generalized current density

$$\mathbf{j} := -\hat{\sigma}\mathbf{E} \tag{3.15}$$

into (3.1). In terms of \mathbf{j} , (3.1b) becomes

$$\operatorname{curl} \mathbf{H} + \mathbf{j} = \mathbf{J}_e. \quad (3.16)$$

Eliminating \mathbf{H} from (3.1) and applying the definition (3.15), the boundary-value problem (3.1) becomes

$$(\omega)^{-1} \operatorname{curl} (\mu^{-1} \operatorname{curl} \mathbf{E}) + \mathbf{j} = \mathbf{F}, \quad (3.17a)$$

$$\mathbf{j} + \hat{\sigma} \mathbf{E} = \mathbf{0}, \quad (3.17b)$$

together with the magnetic boundary condition

$$\mathbf{n} \times \mu^{-1} \operatorname{curl} \mathbf{E} = \mathbf{n} \times \mathbf{h}. \quad (3.17c)$$

For convenience, the source and boundary terms in (3.1) are written as

$$\mathbf{h} := (\mu^{-1} \mathbf{J}_m), \quad (3.17d)$$

$$\mathbf{F} := \mathbf{J}_e + (\omega)^{-1} \operatorname{curl} \mathbf{h}. \quad (3.17e)$$

The transformation (3.15) is taken pointwise and involves no derivatives, so the boundary conditions remain unaffected in (3.17).

The substitution of the Helmholtz decomposition (3.4),(3.6) into (3.17) requires another boundary condition. It is well known that choosing

$$\mathbf{n} \cdot \mathbf{A} = 0 \quad \text{on } \partial\Omega \text{ and} \quad (3.18a)$$

$$\int_{\Omega} \phi dV = 0 \quad (3.18b)$$

is sufficient to guarantee that the Helmholtz decomposition is unique [46]. It is also possible to partition the boundary, prescribing (3.18a) on one portion of

$\partial\Omega$ and prescribing a Neumann-type condition on ϕ over the remainder of $\partial\Omega$ [90]. In either case, as with the Neumann problem for Poisson's equation, the scalar field ϕ is determined up to a scalar constant, so either a point condition or an integral condition like (3.18b) is required to fix the field ϕ [30, 89, 103]. The new boundary-value problem, then, is the PDE

$$(\omega)^{-1} \mathbf{curl} (\mu^{-1} \mathbf{curl} \mathbf{A}) + \mathbf{j} = \mathbf{F}, \quad (3.19a)$$

$$\operatorname{div} \mathbf{A} = 0, \quad (3.19b)$$

$$\mathbf{j} + \widehat{\sigma}(\mathbf{A} + \mathbf{grad} \phi) = \mathbf{0}, \quad (3.19c)$$

with boundary conditions and constraint

$$\mathbf{n} \times (\mu^{-1} \mathbf{curl} \mathbf{A}) = \mathbf{n} \times \mathbf{h}, \quad (3.19d)$$

$$\mathbf{n} \cdot \mathbf{A} = 0, \quad (3.19e)$$

$$\int_{\Omega} \phi dV = 0. \quad (3.19f)$$

Since the BVP (3.17) is known to be well-posed [15] and since the Helmholtz decomposition with (3.19e,f) is also known to be unique, it follows that the BVP (3.19) also has a unique solution.

The dominant operator in the equation (3.19) is stabilized through subtraction of a term that lies in the kernel of the **curl** operator, namely the term $\mathbf{grad}(\mu^{-1} \operatorname{div} \mathbf{A})$. Rather than expressing the stabilized PDE as in (3.10a), introduce a new variable

$$\psi := \mu^{-1} \operatorname{div} \mathbf{A}. \quad (3.20)$$

The stabilizing term in (3.10a), then, is $\mathbf{grad} \psi$, and the equation (3.19a)

becomes

$$(\omega)^{-1} (\mathbf{curl} (\mu^{-1} \mathbf{curl} \mathbf{A}) - \mathbf{grad} \psi) + \mathbf{j} = \mathbf{F}. \quad (3.21)$$

If the Coulomb gauge condition applies, $\psi \equiv 0$ and the stabilizing term $\mathbf{grad} \psi$ in (3.21) also vanishes identically. Next, the divergence is taken of the equation (3.19a), yielding

$$\operatorname{div} \mathbf{j} = \operatorname{div} \mathbf{J}_e. \quad (3.22)$$

Replacing the Coulomb gauge condition with (3.22) gives

$$(\omega)^{-1} (\mathbf{curl} (\mu^{-1} \mathbf{curl} \mathbf{A}) - \mathbf{grad} \psi) + \mathbf{j} = \mathbf{F}, \quad (3.23a)$$

$$\operatorname{div} \mathbf{j} = \operatorname{div} \mathbf{J}_e, \quad (3.23b)$$

$$\mathbf{j} + \widehat{\sigma}(\mathbf{A} + \mathbf{grad} \phi) = \mathbf{0}, \quad (3.23c)$$

$$\mu\psi - \operatorname{div} \mathbf{A} = 0, \quad (3.23d)$$

with the two boundary conditions and the constraint (3.19d-f). The extra differentiation to get (3.23b) requires an additional boundary condition to close the PDE problem (3.23).

To derive the appropriate additional BC, write Ampère's law (3.1b) as

$$\mathbf{curl} \mathbf{H} + \mathbf{j} = \mathbf{J}_e \quad (3.24)$$

Assuming (3.24) holds on a small surface $S \subset \partial\Omega$, then, integrating the normal projection of (3.24) onto S (with the usual outward orientation) gives

$$\int_{\partial S} \mathbf{H} \cdot \boldsymbol{\tau} d\ell + \int_S \mathbf{n} \cdot \mathbf{j} dS = \int_S \mathbf{n} \cdot \mathbf{J}_e dS.$$

By (3.1c), the first integral vanishes, leaving

$$\int_S \mathbf{n} \cdot \mathbf{j} dS = \int_S \mathbf{n} \cdot \mathbf{J}_e dS \quad (3.25)$$

for any surface $S \subset \partial\Omega$. It follows that

$$\mathbf{n} \cdot \mathbf{j} = \mathbf{n} \cdot \mathbf{J}_e \text{ on } \partial\Omega. \quad (3.26)$$

The procedure above of integrating the normal component of Ampère's law corresponds exactly to the derivation of the pressure boundary condition for the pressure-Poisson equation as outlined by Gresho and Sani [50].

The importance of the boundary condition (3.26) is that, as in the context of incompressible fluid flow, it is consistent with the requirement $\operatorname{div} \mathbf{A} = 0$ on $\partial\Omega$ [51]. Take the divergence of (3.23a); by (3.22),

$$\Delta\psi = 0; \quad (3.27)$$

that is, ψ satisfies Laplace's equation. Writing the stabilized equation (3.21) as

$$\operatorname{curl} \mathbf{H} - (\imath\omega)^{-1} \operatorname{grad} \psi + \mathbf{j} = \mathbf{F} \quad (3.28)$$

and applying the same arguments used in deriving (3.26), it follows that ψ satisfies a homogeneous Neumann boundary condition, i.e., $\partial\psi/\partial n = 0$ on $\partial\Omega$. Hence, ψ is spatially constant; an additional constraint such as

$$\int_{\Omega} \psi dV = 0 \quad (3.29)$$

pins down ψ uniquely. The Coulomb gauge condition (3.6) is thus recovered throughout Ω .

Hence, the final boundary-value problem is

$$(\omega)^{-1} (\mathbf{curl} (\mu^{-1} \mathbf{curl} \mathbf{A}) - \mathbf{grad} \psi) + \mathbf{j} = \mathbf{F}, \quad (3.30a)$$

$$\operatorname{div} \mathbf{j} = \operatorname{div} \mathbf{J}_e, \quad (3.30b)$$

$$\mathbf{j} + \hat{\sigma}(\mathbf{A} + \mathbf{grad} \phi) = \mathbf{0}, \quad (3.30c)$$

$$\mu\psi - \operatorname{div} \mathbf{A} = 0, \quad (3.30d)$$

with boundary conditions

$$\mathbf{n} \times (\mu^{-1} \mathbf{curl} \mathbf{A}) = \mathbf{n} \times \mathbf{h}, \quad (3.30e)$$

$$\mathbf{n} \cdot \mathbf{A} = 0, \quad (3.30f)$$

$$\mathbf{n} \cdot \mathbf{j} = \mathbf{n} \cdot \mathbf{J}_e. \quad (3.30g)$$

and global constraints

$$\int_{\Omega} \psi dV = 0, \quad (3.30h)$$

$$\int_{\Omega} \phi dV = 0. \quad (3.30i)$$

An equivalent boundary-value problem in terms of the variables \mathbf{A} and ϕ alone is the PDE

$$\begin{aligned} & (\omega)^{-1} (\mathbf{curl} (\mu^{-1} \mathbf{curl} \mathbf{A}) - \mathbf{grad} (\mu^{-1} \operatorname{div} \mathbf{A})) - \hat{\sigma}(\mathbf{A} + \mathbf{grad} \phi) \\ &= \mathbf{J}_e + (\omega)^{-1} \mathbf{curl} (\mu^{-1} \mathbf{J}_m), \end{aligned} \quad (3.31a)$$

$$\operatorname{div} [\hat{\sigma}(\mathbf{A} + \mathbf{grad} \phi)] = -\operatorname{div} \mathbf{J}_e, \quad (3.31b)$$

with boundary conditions

$$\mathbf{n} \times (\mu^{-1} \mathbf{curl} \mathbf{A}) = \mathbf{n} \times (\mu^{-1} \mathbf{J}_m), \quad (3.32a)$$

$$\mathbf{n} \cdot \mathbf{A} = 0, \quad (3.32b)$$

$$\mathbf{n} \cdot \hat{\sigma}(\mathbf{A} + \mathbf{grad} \phi) = -\mathbf{n} \cdot \mathbf{J}_e. \quad (3.32c)$$

and constraints

$$\int_{\Omega} \mu^{-1} \operatorname{div} \mathbf{A} dV = 0, \quad (3.32d)$$

$$\int_{\Omega} \phi dV = 0. \quad (3.32e)$$

The boundary conditions (3.32a,c) involve the material coefficients; in the event that the material coefficients are in fact tensor fields, the interactions of σ , ϵ , and μ with the normal field on $\partial\Omega$ are still accounted for by (3.32). For the simple case of isotropic tensor fields considered here, some further simplifications can be made. In particular,

$$\mathbf{n} \times \mathbf{curl} \mathbf{A} = \mathbf{n} \times \mathbf{J}_m, \quad (3.33a)$$

$$\hat{\sigma} \frac{\partial \phi}{\partial n} = -\mathbf{n} \cdot \mathbf{J}_e. \quad (3.33b)$$

For most geophysical applications, it is undesirable to have action of the source fields at the boundary. If the source fields have bounded support, then the boundary conditions (3.33) are homogeneous.

3.2.1 Interface Conditions

With the introduction of different electromagnetic field variables, the new fields satisfy different jump conditions at the interfaces of conducting

media. The same procedure used to derive (2.28) (cf. Section 2.3.2) yields the conditions

$$\mathbf{n}^I \cdot [\mathbf{A}^I - \mathbf{A}^{II}] = 0, \quad (3.34a)$$

$$\mathbf{n}^I \times [\mathbf{A}^I - \mathbf{A}^{II}] = \mathbf{j}_m, \quad (3.34b)$$

$$\mathbf{n}^I \cdot [\epsilon^I(\mathbf{A}^I + \mathbf{grad} \phi^I) - \epsilon^{II}(\mathbf{A}^{II} + \mathbf{grad} \phi^{II})] = \varrho_e, \quad (3.34c)$$

$$\mathbf{n}^I \cdot [\mathbf{j}^I - \mathbf{j}^{II}] = \mathbf{n}^I \cdot [\mathbf{J}_e^I - \mathbf{J}_e^{II}] \quad (3.34d)$$

across any surface $\Gamma \subset \Omega$ (cf. Section 2.3.2). The surface magnetic current density \mathbf{J}_m is often identically zero; where $\mathbf{J}_m \neq \mathbf{0}$, it generally does not have surface layers. As a result,

$$\mathbf{n}^I \times [\mathbf{A}^I - \mathbf{A}^{II}] = \mathbf{0}, \quad (3.34e)$$

i.e., the tangential component of \mathbf{A} is continuous across Γ . Similarly, with the assumption $\epsilon \equiv \epsilon_0$ in Ω , (3.34a,c) imply

$$\mathbf{n}^I \cdot [\mathbf{grad} \phi^I - \mathbf{grad} \phi^{II}] = \varrho_e / \epsilon_0. \quad (3.34f)$$

Finally, provided the surface Γ does not coincide with a surface of discontinuity of the applied electric source current \mathbf{J}_e , the right-hand side of (3.34d) vanishes also, i.e.,

$$\mathbf{n}^I \cdot [\mathbf{j}^I - \mathbf{j}^{II}] = 0. \quad (3.34g)$$

The preceding assumptions are not particularly restrictive in the context of this work or even in more general contexts. The resulting interface conditions (3.34a,e-g) are of great utility in deriving discretizations in Section 4.3.

3.3 Weak Formulations

There are naturally many weak problems equivalent to the PDE problem (3.31) that can be examined in a variational context. However, beyond pointing the way to different numerical schemes and providing a basis for finite-element analysis, weak formulations can provide insight into the interplay of boundary conditions with the differential operators. Although demonstrating the existence of solutions from weak formulations falls outside the scope of this work, a brief discussion of one particular weak formulation (similar to that applied in [13]) is included for completeness.

In terms of the notation (2.33) introduced in Chapter 2, the divergence theorem implies

$$(\mathbf{curl} \boldsymbol{\xi}, \boldsymbol{\eta})_{\Omega} - (\boldsymbol{\xi}, \mathbf{curl} \boldsymbol{\eta})_{\Omega} = \langle \mathbf{n} \times \boldsymbol{\xi}, \boldsymbol{\eta} \rangle_{\partial\Omega}, \quad (3.35a)$$

$$(u, \operatorname{div} \mathbf{V})_{\Omega} + (\mathbf{grad} u, \mathbf{V})_{\Omega} = \langle u, \mathbf{n} \cdot \mathbf{V} \rangle_{\partial\Omega} \quad (3.35b)$$

for any $\boldsymbol{\xi}, \boldsymbol{\eta} \in \mathcal{H}(\mathbf{curl}; \Omega)$, $\mathbf{V} \in \mathcal{H}(\operatorname{div}; \Omega)$, and $u \in \mathcal{H}(\mathbf{grad}; \Omega)$. Multiplying (3.31a) by some test vector field $\boldsymbol{\xi}$ and integrating by parts with (3.35) gives the weak equality

$$\begin{aligned} (\imath\omega)^{-1} a_{\mu}(\mathbf{A}, \boldsymbol{\xi}) - (\widehat{\sigma}(\mathbf{A} + \mathbf{grad} \phi), \boldsymbol{\xi})_{\Omega} - \langle \mu^{-1} \operatorname{div} \mathbf{A}, \mathbf{n} \cdot \boldsymbol{\xi} \rangle_{\partial\Omega} \\ = f(\boldsymbol{\xi}) + (\imath\omega)^{-1} \langle \mathbf{n} \times (\mu^{-1}(\mathbf{J}_m - \mathbf{curl} \mathbf{A})), \boldsymbol{\xi} \rangle_{\partial\Omega}, \end{aligned} \quad (3.36a)$$

where

$$a_{\mu}(\mathbf{A}, \boldsymbol{\xi}) := (\mu^{-1} \mathbf{curl} \mathbf{A}, \mathbf{curl} \boldsymbol{\xi})_{\Omega} + (\mu^{-1} \operatorname{div} \mathbf{A}, \operatorname{div} \boldsymbol{\xi})_{\Omega}, \quad (3.36b)$$

$$f(\boldsymbol{\xi}) := (\mathbf{J}_e, \boldsymbol{\xi})_{\Omega} + (\imath\omega)^{-1} (\mu^{-1} \mathbf{J}_m, \mathbf{curl} \boldsymbol{\xi})_{\Omega}. \quad (3.36c)$$

Similarly, multiplying (3.31b) by a scalar test function v and integrating gives

$$\begin{aligned} (\widehat{\sigma}(\mathbf{A} + \mathbf{grad} \phi), \mathbf{grad} v)_\Omega &= -(\mathbf{J}_e, \mathbf{grad} v)_\Omega \\ &+ \langle \mathbf{n} \cdot (\widehat{\sigma}(\mathbf{A} + \mathbf{grad} \phi) + \mathbf{J}_e), v \rangle_{\partial\Omega}. \end{aligned} \quad (3.36d)$$

For a solution of the PDE (3.31), the boundary integrals on the right-hand sides of (3.36a,d) vanish by virtue of (3.32a,c); that is, the boundary conditions (3.32a,c) are natural boundary conditions for this choice of variational form. The term $\langle \mu^{-1} \operatorname{div} \mathbf{A}, \mathbf{n} \cdot \boldsymbol{\xi} \rangle_{\partial\Omega}$ on the left-hand side of (3.36a) does not vanish unless some constraint is imposed on the space of functions from which the trial and testing functions are drawn. Assuming $\mathbf{n} \cdot \boldsymbol{\xi} = 0$ for all admissible vector fields $\boldsymbol{\xi}$, then the boundary integral term in question vanishes. Thus, imposing (3.32b) is an essential boundary condition.

Combining the above arguments, define the spaces

$$\mathbb{A}^0 := \{\boldsymbol{\xi} \in \mathcal{H}(\operatorname{div}; \Omega) \cap \mathcal{H}(\operatorname{curl}; \Omega) : \mathbf{n} \cdot \boldsymbol{\xi} = 0 \text{ on } \partial\Omega\}, \quad (3.37a)$$

$$\Phi := \mathcal{H}(\mathbf{grad}; \Omega). \quad (3.37b)$$

A variational problem that is equivalent to the BVP (3.31) subject to boundary conditions (3.32) is to find $(\mathbf{A}, \phi) \in \mathbb{A}^0 \times \Phi$ such that

$$(\imath\omega)^{-1} a_\mu(\mathbf{A}, \boldsymbol{\xi}) - (\widehat{\sigma}(\mathbf{A} + \mathbf{grad} \phi), \boldsymbol{\xi})_\Omega = f(\boldsymbol{\xi}) \quad \forall \boldsymbol{\xi} \in \mathbb{A}^0, \quad (3.38a)$$

$$(\widehat{\sigma}(\mathbf{A} + \mathbf{grad} \phi), \mathbf{grad} v)_\Omega = -(\mathbf{J}_e, \mathbf{grad} v)_\Omega \quad \forall v \in \Phi. \quad (3.38b)$$

A strong solution of the classical BVP (3.31),(3.32) will also satisfy the variational problem (3.38). Inserting a test function $\boldsymbol{\xi} = \mathbf{grad} v \in \mathbb{A}^0$ into (3.38a) and using (3.38b), it is clear that a solution of the weak variational problem is also weakly divergence-free.

Chapter 4

Finite-Volume Discretizations

Having chosen an analytic formulation ((3.31) with (3.32)) for Maxwell's equations, the next step is to select a suitable discretization. While certain applications call for finite element discretizations in order to capture the geometry accurately (see [16, 63, 88, 87] among many others), for the family of geophysical applications of relevance here, finite-volume discretizations suffice. After presentation of a description of the discrete domain in Cartesian coordinates, the well-known *Yee scheme* is derived using standard finite-volume arguments. A finite-volume discretization of the PDE (3.31) is subsequently presented in Section 4.3; this discretization extends the ideas of the Yee scheme to account for inhomogeneous media in a logical manner. Finally, Section 4.4 shows some analysis and experiments that justify the choice of coarse discrete representations of the inhomogeneous media.

4.1 Domain of Discretization

Assume the domain of the continuous problem (3.31) in Cartesian co-

ordinates is the rectangular box $(0, L_x) \times (0, L_y) \times (0, L_z) \subset \mathbb{R}^3$. The various finite-volume discretizations are derived using a tensor-product grid of Cartesian coordinates whose coordinates correspond to points in space at which the discrete grid functions approximate the appropriate continuous functions. The same grid and notation in this section underlies the Yee discretization in Section 4.2 and the discretization of the desired system (3.31) presented in Section 4.3.

Consider first the grid in the x -direction. There are N_x subintervals partitioning the interval $(0, L_x)$. The widths of the subintervals are denoted h_i^x ($i = 1, \dots, N_x$) and the centers of the subintervals are x_i ($i = 1, \dots, N_x$). The end-points of the subintervals have half-integer indices, namely $x_{i-1/2}$ ($i = 1, \dots, N_x + 1$). The dual grid comprises the subintervals with end-points x_i of widths $h_{i-1/2}^x$ given by

$$h_{i-1/2}^x := x_i - x_{i-1} \quad (i = 1, \dots, N_x + 1). \quad (4.1)$$

The ghost points

$$x_0 := x_1 - h_1^x \text{ and } x_{N_x+1} := x_{N_x} + h_{N_x}^x \quad (4.2)$$

may be included to facilitate derivation of boundary conditions; any discrete unknowns associated with grid points are eliminated using discrete approximations of the boundary conditions (e.g. [44, 99, 113]).

Assume that the intervals $(0, L_y)$ and $(0, L_z)$ are partitioned into N_y and N_z subintervals respectively with dual grids defined analogously. The vertices $(x_{i\pm1/2}, y_{j\pm1/2}, z_{k\pm1/2})$ are the corners of the cells of the primary grid; that is, the

boxes

$$V_{i,j,k} := (x_{i-\frac{1}{2}}, x_{i+\frac{1}{2}}) \times (y_{j-\frac{1}{2}}, y_{j+\frac{1}{2}}) \times (z_{k-\frac{1}{2}}, z_{k+\frac{1}{2}}) \quad (4.3a)$$

$$(i = 1, \dots, N_x; j = 1, \dots, N_y; k = 1, \dots, N_z)$$

with faces

$$S_{i\pm\frac{1}{2},j,k}^x := \{x_{i\pm\frac{1}{2}}\} \times (y_{j-\frac{1}{2}}, y_{j+\frac{1}{2}}) \times (z_{k-\frac{1}{2}}, z_{k+\frac{1}{2}}), \quad (4.3b)$$

$$S_{i,j\pm\frac{1}{2},k}^y := (x_{i-\frac{1}{2}}, x_{i+\frac{1}{2}}) \times \{y_{j\pm\frac{1}{2}}\} \times (z_{k-\frac{1}{2}}, z_{k+\frac{1}{2}}), \quad (4.3c)$$

$$S_{i,j,k\pm\frac{1}{2}}^z := (x_{i-\frac{1}{2}}, x_{i+\frac{1}{2}}) \times (y_{j-\frac{1}{2}}, y_{j+\frac{1}{2}}) \times \{z_{k\pm\frac{1}{2}}\} \quad (4.3d)$$

$$(i = 1, \dots, N_x; j = 1, \dots, N_y; k = 1, \dots, N_z)$$

constitute the cells of the primary grid. The dual grid comprises the cells between the centroids of the primary grid cells; that is, the boxes

$$V_{i+\frac{1}{2},j+\frac{1}{2},k+\frac{1}{2}} := (x_i, x_{i+1}) \times (y_j, y_{j+1}) \times (z_k, z_{k+1}) \quad (4.4a)$$

$$(i = 1, \dots, N_x - 1; j = 1, \dots, N_y - 1; k = 1, \dots, N_z - 1)$$

with faces

$$S_{i+\frac{1}{2}\pm\frac{1}{2},j+\frac{1}{2},k+\frac{1}{2}}^x := \{x_{i+\frac{1}{2}\pm\frac{1}{2}}\} \times (y_j, y_{j+1}) \times (z_k, z_{k+1}), \quad (4.4b)$$

$$S_{i+\frac{1}{2},j+\frac{1}{2}\pm\frac{1}{2},k+\frac{1}{2}}^y := (x_i, x_{i+1}) \times \{y_{j+\frac{1}{2}\pm\frac{1}{2}}\} \times (z_k, z_{k+1}), \quad (4.4c)$$

$$S_{i+\frac{1}{2},j+\frac{1}{2},k+\frac{1}{2}\pm\frac{1}{2}}^z := (x_i, x_{i+1}) \times (y_j, y_{j+1}) \times \{z_{k+\frac{1}{2}\pm\frac{1}{2}}\} \quad (4.4d)$$

$$(i = 1, \dots, N_x - 1; j = 1, \dots, N_y - 1; k = 1, \dots, N_z - 1).$$

Notice that, while the centroids of the cells and faces of the primary grid coincide with points in the dual grid, the centroids of the cells and faces of the

dual grid do not necessarily coincide with points in the primary grid unless the grid spacings are uniform [80]. The basic geometry of the grids is illustrated for the case of uniform grid spacing in Figure 4.1.

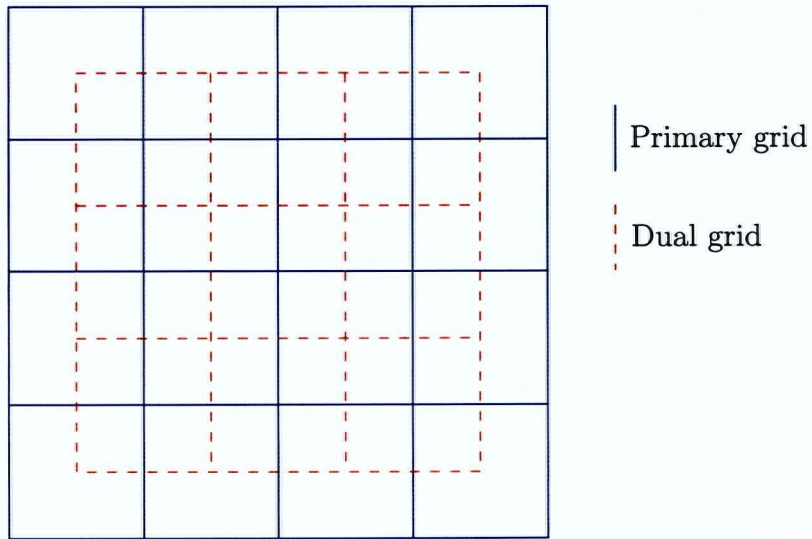


Figure 4.1: 2D cross-section of the primary and dual grids (uniform spacing). The corners of the dual grid are the cell centers of the primary grid and conversely.

4.2 The Yee Discretization

Yee [115] derived a set of finite-difference equations approximating Maxwell's equations in the time-domain. In this scheme, both the electric and magnetic fields \mathbf{E} and \mathbf{H} are discretized and are explicitly marched forward in time using the coupled curl equations (2.4a-b) as opposed to discretizing \mathbf{E} alone and using the second-order wave equation formulation (2.30). The finite-difference method derived is often called the *Yee algorithm* or the *Finite-*

Difference-Time-Domain algorithm (FD-TD) in the engineering literature (as in [104, 105]). The related spatial discretization in the frequency domain is the *Finite-Difference-Frequency-Domain algorithm*. In this thesis, the terminology “Yee algorithm” is avoided in favor of the more accurate terminology “Yee discretization” or “Yee scheme.” Yee’s important contribution lies in recognizing how to discretize Maxwell’s equations in space in conservative form; from the perspective of evolutionary ODEs or PDEs, the algorithmic aspects of the “Yee algorithm” come from well-established time-stepping techniques (e.g. [8, 91]).

The basic idea for the Yee discretization is to center the components of \mathbf{E} and \mathbf{H} in three-dimensional space so that each component of \mathbf{E} is surrounded by four circulating components of \mathbf{H} and conversely (except at the boundaries). With the unknown fields staggered on a grid, Faraday’s Law and Ampére’s Law are invoked and approximated along the contours. That is, the circulation of \mathbf{E} in a loop is linked with the flux of the magnetic field \mathbf{H} through that loop while the circulation of \mathbf{H} in a loop on a dual lattice is linked with the displacement current flux of the electric field \mathbf{E} through that loop.

For the engineering applications for which Yee’s discretization was originally derived, there are a number of practical advantages. Firstly, the locations of the components of \mathbf{E} and \mathbf{H} in the spatial lattice implicitly enforce discrete versions of the divergence conditions (2.4c-d). In fact, although originally derived as a finite-difference scheme, the Yee discretization can be derived as a

finite-volume method. Thus, the conservation properties arise as a common consequence of finite-volume techniques; for certain application families, it is important to preserve such global conservation laws [66, 104]. Secondly, the resulting finite-difference approximations for the space derivatives used in the curl operators are centered-difference approximations and hence are second-order accurate. Thirdly, when the staggered-grid spatial discretization is coupled with a leap-frog discretization in time, the resulting time-stepping method is explicit. The resulting discrete electromagnetic field can be evolved without solving large sparse linear systems at each time step. This can be useful for simulations of waveguides or other three-dimensional electronic structures over long time scales, since solving the linear systems involved would be prohibitive [104]. Finally, since the discrete fields are specified in terms of normal or tangential components, specification of certain boundary conditions can be simplified. For instance, given the tangential trace $\mathbf{n} \times \mathbf{e}$ of some known field \mathbf{e} , if the boundary condition $\mathbf{n} \times \mathbf{E} = \mathbf{n} \times \mathbf{e}$ on $\partial\Omega$ is given, the tangential components of the discrete electric field \mathbf{E}^h on the discrete boundary of a Cartesian tensor-product grid are given directly in the discretization.

4.2.1 The Discrete Fields

For the Yee discretization, the various components of the vector fields are staggered in space to approximate Maxwell's equations in a way that automatically ensures the integral conservation laws (2.4c-d) hold on a discrete level. In particular, the components of the discrete electric field \mathbf{E}^h are defined

at the centers of the edges of the cells of the primary grid and are tangential to those edges. Explicitly, if $\mathbf{E} = (E^x, E^y, E^z)^T$ in Cartesian coordinates, the discrete electric field unknowns are

$$E^x_{i,j\pm\frac{1}{2},k\pm\frac{1}{2}} \simeq E^x(x_i, y_{j\pm\frac{1}{2}}, z_{k\pm\frac{1}{2}}), \quad (4.5a)$$

$$E^y_{i\pm\frac{1}{2},j,k\pm\frac{1}{2}} \simeq E^y(x_{i\pm\frac{1}{2}}, y_j, z_{k\pm\frac{1}{2}}), \quad (4.5b)$$

$$E^z_{i\pm\frac{1}{2},j\pm\frac{1}{2},k} \simeq E^z(x_{i\pm\frac{1}{2}}, y_{j\pm\frac{1}{2}}, z_k), \quad (4.5c)$$

where $i = 1, \dots, N_x$, $j = 1, \dots, N_y$, and $k = 1, \dots, N_z$. From this, it follows that, for example,

$$\frac{\partial E^x}{\partial z}(x_i, y_{j+\frac{1}{2}}, z_k) = \frac{E^x_{i,j+\frac{1}{2},k+\frac{1}{2}} - E^x_{i,j+\frac{1}{2},k-\frac{1}{2}}}{h_k^z} + O((h_k^z)^2)$$

and similarly for other spatial derivatives of the components of \mathbf{E} ; that is, at the centers of cell faces, centered finite-difference approximations of derivatives of components of \mathbf{E} are second-order accurate.

The components of the discrete magnetic field \mathbf{H}^h are defined at the centers of the faces of the cells of the primary grid and are normal to those cell faces. Thus, given $\mathbf{H} = (H^x, H^y, H^z)^T$, the magnetic field discrete unknowns are

$$H^x_{i\pm\frac{1}{2},j,k} \simeq H^x(x_{i\pm\frac{1}{2}}, y_j, z_k), \quad (4.6a)$$

$$H^y_{i,j\pm\frac{1}{2},k} \simeq H^y(x_i, y_{j\pm\frac{1}{2}}, z_k), \quad (4.6b)$$

$$H^z_{i,j,k\pm\frac{1}{2}} \simeq H^z(x_i, y_j, z_{k\pm\frac{1}{2}}), \quad (4.6c)$$

with $i = 1, \dots, N_x$, $j = 1, \dots, N_y$, and $k = 1, \dots, N_z$. The placement of the various discrete solution components on the cell is depicted in Figure 4.2 and Figure 4.3.

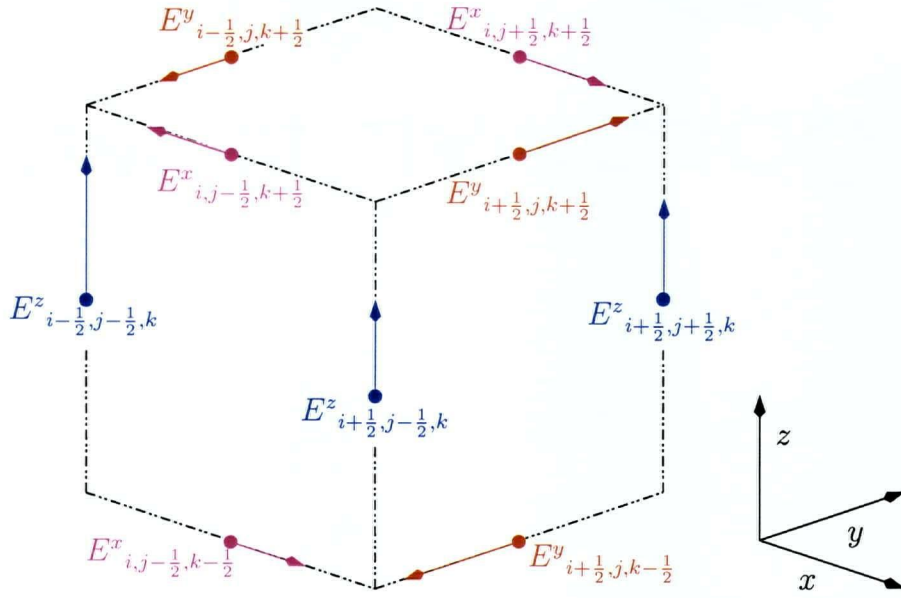


Figure 4.2: Staggering of components of the discrete electric field \mathbf{E}^h for the Yee scheme.

4.2.2 Derivation of Yee Scheme

The approach presented here uses finite-volume arguments along the lines of [27] or [80] as opposed to finite-difference arguments such as in [104] or Yee's original work [115]. Although the Yee scheme was originally derived on a uniform grid, the presentation here allows for nonuniform grids. Also, the frequency-domain Maxwell equations are discretized (as in [77, 84]) rather than the time-domain equations (2.4) used more often in engineering applications. Furthermore, for generality, a magnetic current source \mathbf{J}_m is included in the right-hand side of the discretization of Faraday's law, as in (2.16a); this generalization may be helpful for magnetotelluric models as in Section 2.2.7. Finally, for the moment, assume that the material parameters σ , ϵ , and μ

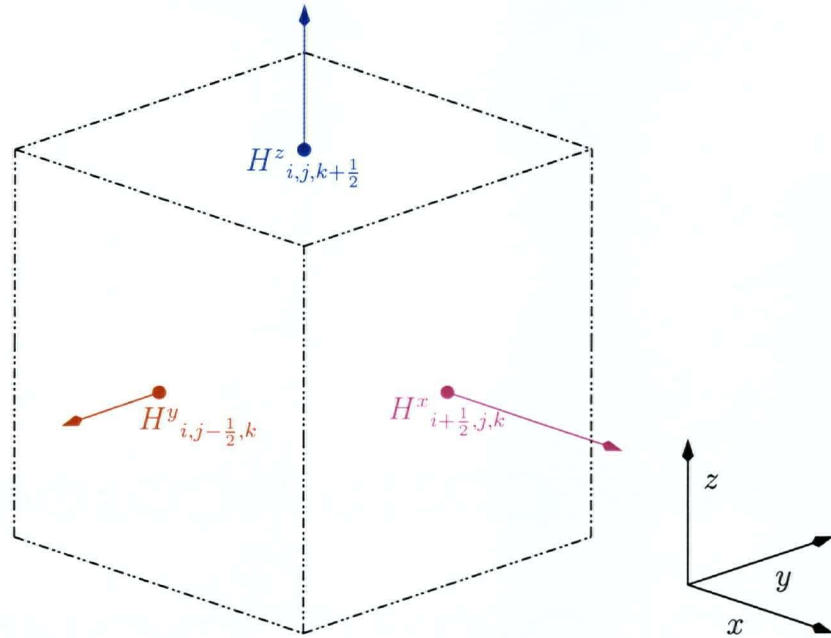


Figure 4.3: Staggering of components of the discrete magnetic field \mathbf{H}^h for the Yee scheme.

are all homogeneous and isotropic, i.e. scalar constants. This assumption is relaxed in Section 4.3 where the discretization of the system (3.31) is derived in terms of discrete vector and scalar potentials in inhomogeneous, isotropic media.

To approximate Maxwell's equations (2.16) on the nonuniform grid Ω^h , consider integrating the Maxwell curl equations (2.16a-b) as in [80, 104]. For any smooth surface $S \subset \Omega$ with boundary ∂S , Stokes' theorem and Faraday's Law (2.16a) give

$$\oint_{\partial S} \mathbf{E} \cdot \boldsymbol{\tau} d\ell - \omega \int_S \mu \mathbf{H} \cdot \mathbf{n} dS = \int_S \mathbf{J}_m \cdot \mathbf{n} dS. \quad (4.7)$$

The various discrete equations that correspond to the components of (2.16a)

are derived by choosing S as a face of the primary grid. First, take

$$S = S_{i-\frac{1}{2},j,k}^x := \{x_{i-\frac{1}{2}}\} \times (y_{j-\frac{1}{2}}, y_{j+\frac{1}{2}}) \times (z_{k-\frac{1}{2}}, z_{k+\frac{1}{2}})$$

in (4.7) as given in (4.3b). Approximating the line integral with four quadrature points at the midpoints at the center of each line segment and approximating the surface integrals with a single quadrature point at the centroid of S gives

$$\begin{aligned} h_k^z \left(E_{i-\frac{1}{2},j+\frac{1}{2},k}^z - E_{i+\frac{1}{2},j-\frac{1}{2},k}^z \right) - h_j^y \left(E_{i-\frac{1}{2},j,k+\frac{1}{2}}^y - E_{i-\frac{1}{2},j,k-\frac{1}{2}}^y \right) \\ - \omega \mu h_j^y h_k^z H_{i-\frac{1}{2},j,k}^x = h_j^y h_k^z J_{mi-\frac{1}{2},j,k}^x. \end{aligned} \quad (4.8a)$$

The remaining two discrete equations are obtained using

$$S = S_{i,j-\frac{1}{2},k}^y := (x_{i-\frac{1}{2}}, x_{i+\frac{1}{2}}) \times \{y_{j-\frac{1}{2}}\} \times (z_{k-\frac{1}{2}}, z_{k+\frac{1}{2}})$$

from (4.3c) and

$$S = S_{i,j,k-\frac{1}{2}}^z := (x_{i-\frac{1}{2}}, x_{i+\frac{1}{2}}) \times (y_{j-\frac{1}{2}}, y_{j+\frac{1}{2}}) \times \{z_{k-\frac{1}{2}}\}$$

from (4.3d) in (4.7); the corresponding finite-volume equations for the magnetic field \mathbf{H}^h are

$$\begin{aligned} h_i^x \left(E_{i,j-\frac{1}{2},k+\frac{1}{2}}^x - E_{i,j-\frac{1}{2},k-\frac{1}{2}}^x \right) - h_k^z \left(E_{i+\frac{1}{2},j-\frac{1}{2},k}^z - E_{i-\frac{1}{2},j-\frac{1}{2},k}^z \right) \\ - \omega \mu h_i^x h_k^z H_{i,j-\frac{1}{2},k}^y = h_i^x h_k^z J_{mi,j-\frac{1}{2},k}^y, \end{aligned} \quad (4.8b)$$

$$\begin{aligned} h_j^y \left(E_{i+\frac{1}{2},j,k-\frac{1}{2}}^y - E_{i-\frac{1}{2},j,k-\frac{1}{2}}^y \right) - h_i^x \left(E_{i,j+\frac{1}{2},k-\frac{1}{2}}^x - E_{i,j-\frac{1}{2},k-\frac{1}{2}}^x \right) \\ - \omega \mu h_i^x h_j^y H_{i,j,k-\frac{1}{2}}^z = h_i^x h_j^y J_{mi,j,k-\frac{1}{2}}^z. \end{aligned} \quad (4.8c)$$

To discretize the electric field equations, use the integral form of (2.16b), namely

$$\oint_{\partial S} \mathbf{H} \cdot \boldsymbol{\tau} d\ell - \int_S \hat{\sigma} \mathbf{E} \cdot \mathbf{n} dS = \int_S \mathbf{J}_e \cdot \mathbf{n} dS. \quad (4.8d)$$

The discrete equations for the electric field arise from choosing the surfaces S as the faces of the dual grid formed by joining the centroids of the cells of the primary grid. For instance, choosing

$$S = S_{i,j-\frac{1}{2},k-\frac{1}{2}}^x := \{x_i\} \times (y_{j-1}, y_j) \times (z_{k-1}, z_k)$$

from (4.4b) in (4.8d), and using one-point quadrature formulae to approximate the integrals gives

$$\begin{aligned} h_{k-\frac{1}{2}}^z \left(H_{i,j,k-\frac{1}{2}}^z - H_{i,j-1,k-\frac{1}{2}}^z \right) - h_{j-\frac{1}{2}}^y \left(H_{i,j-\frac{1}{2},k}^y - H_{i,j-\frac{1}{2},k-1}^y \right) \\ - h_{j-\frac{1}{2}}^y h_{k-\frac{1}{2}}^z \hat{\sigma} E_{i,j-\frac{1}{2},k-\frac{1}{2}}^x = h_{j-\frac{1}{2}}^y h_{k-\frac{1}{2}}^z J_{e,i,j-\frac{1}{2},k-\frac{1}{2}}^x. \end{aligned} \quad (4.8e)$$

For the corresponding equations in the y - and z -directions, substitute

$$S = S_{i-\frac{1}{2},j,k-\frac{1}{2}}^y := (x_{i-1}, x_i) \times \{y_j\} \times (z_{k-1}, z_k) \text{ as in (4.4c), and}$$

$$S = S_{i-\frac{1}{2},j-\frac{1}{2},k}^z := (x_{i-1}, x_i) \times (y_{j-1}, y_j) \times \{z_k\} \text{ as in (4.4d)}$$

into (4.8d), and repeat the procedure outlined above, respectively giving

$$\begin{aligned} h_{i-\frac{1}{2}}^x \left(H_{i-\frac{1}{2},j,k}^x - H_{i-\frac{1}{2},j,k-1}^x \right) - h_{k-\frac{1}{2}}^z \left(H_{i,j,k-\frac{1}{2}}^z - H_{i,j-1,k-\frac{1}{2}}^z \right) \\ - h_{i-\frac{1}{2}}^x h_{k-\frac{1}{2}}^z \hat{\sigma} E_{i-\frac{1}{2},j,k-\frac{1}{2}}^y = h_{i-\frac{1}{2}}^x h_{k-\frac{1}{2}}^z J_{e,i-\frac{1}{2},j,k-\frac{1}{2}}^y, \text{ and} \end{aligned} \quad (4.8f)$$

$$\begin{aligned} h_{j-\frac{1}{2}}^y \left(H_{i,j-\frac{1}{2},k}^y - H_{i,j-1,j-\frac{1}{2},k}^y \right) - h_{i-\frac{1}{2}}^x \left(H_{i-\frac{1}{2},j,k}^x - H_{i-\frac{1}{2},j-1,k}^x \right) \\ - h_{i-\frac{1}{2}}^x h_{j-\frac{1}{2}}^y \hat{\sigma} E_{i-\frac{1}{2},j-\frac{1}{2},k}^z = h_{i-\frac{1}{2}}^x h_{j-\frac{1}{2}}^y J_{e,i-\frac{1}{2},j-\frac{1}{2},k}^z. \end{aligned} \quad (4.8g)$$

For the cells adjacent to the boundary $\partial\Omega$, integrating (2.16a) with $S \subset \partial\Omega$ gives a discrete equation that can be simplified by appropriate boundary conditions (see [99] for examples).

With the discrete fields situated as they are on the staggered grids, the Yee scheme is second-order accurate on a uniform grid as can be determined by simple Taylor expansions [91, 104]; for greater accuracy on nonuniform grids, typically the sampling of the source terms has to be done more carefully (e.g. [7]). An alternative convergence analysis by Monk and Suli establishes the second-order accuracy of the discretization on nonuniform grids in suitable discrete energy norms [80]. The above finite-volume approach can also be extended to include systems involving inhomogeneous media and nonorthogonal or unstructured grids [66, 104]. Finally, highly accurate finite-volume discretizations of Maxwell's equations can also be derived from conservation-law form (e.g. [31]); such discretizations become more important in hyperbolic high-frequency transmission problems where accuracy is crucial.

4.3 Discretization Using Potentials

The goal now is to introduce a finite-volume discretization of the PDE system (3.31) derived in Chapter 3. For the case of $\mu = \mu_0 = \text{constant}$, a finite-volume discretization is derived in [54]; the presentation below considers the case where μ varies and is based on the original derivation in [53]. Piecewise continuity of the isotropic, inhomogeneous material tensor fields is assumed up to the resolution of the spatial grid.

The domain Ω is subdivided into cells as outlined already in Section 4.1. Within each cell $V_{i,j,k}$ of the primary grid, the conductivity σ , the permeability μ , and the permittivity ϵ are all assumed constant; that is,

$$\sigma \equiv \sigma_{i,j,k}, \quad \mu \equiv \mu_{i,j,k}, \quad \text{and} \quad \epsilon \equiv \epsilon_{i,j,k} \quad (4.9)$$

throughout the cell $V_{i,j,k}$. However, σ , μ , and ϵ may be discontinuous between adjacent cells. The material fields could be varying smoothly within cells, but it is simpler to assume that the material properties are constant in each cell. The domain, then, is composed of blocks of materials of distinct electric and magnetic properties. In practice, the variations in ϵ are much smaller in magnitude than those in σ and μ for geophysical problems (see Section 3.1).

For the purpose of deriving a discretization of (3.31) in terms of discrete grid functions (\mathbf{A}^h, ϕ^h) , it is advantageous to use the auxiliary or intermediate variables used in Section 3.2. Using the additional variables to derive a discretization is akin to mixed finite element methods that are commonly applied to problems with highly discontinuous coefficients [20, 21, 88]. This approach is employed in both [53] and [54] although the final discrete system is a discretization of (3.31) with discrete approximations (\mathbf{A}^h, ϕ^h) of (\mathbf{A}, ϕ) only. Thus, in terms of the variables introduced in Chapter 3, the system

under consideration is

$$\operatorname{curl} \mathbf{H} - (\imath\omega)^{-1} \operatorname{grad} \psi + \mathbf{j} = \mathbf{J}_e, \quad (4.10a)$$

$$\operatorname{div} \mathbf{j} = \operatorname{div} \mathbf{J}_e, \quad (4.10b)$$

$$\mu\psi - \operatorname{div} \mathbf{A} = 0, \quad (4.10c)$$

$$\mathbf{j} + \hat{\sigma}(\mathbf{A} + \operatorname{grad} \phi) = \mathbf{0}, \quad (4.10d)$$

$$\operatorname{curl} \mathbf{A} - \imath\omega\mu\mathbf{H} = \mathbf{J}_m. \quad (4.10e)$$

4.3.1 The Discrete Fields

Having decided to use the variables $(\mathbf{A}, \mathbf{j}, \mathbf{H}, \phi, \psi)$ to derive a finite-volume discretization, it is necessary to decide where on the staggered grid to place the components of the discrete approximations $(\mathbf{A}^h, \mathbf{j}^h, \mathbf{H}^h, \phi^h, \psi^h)$. This element is left out of the derivation of the Yee discretization in Section 4.2. There, the components of \mathbf{E}^h and \mathbf{H}^h are chosen as in (4.5) and (4.6) to ensure the discrete divergence conditions hold. It is equally reasonable, then, to reverse the roles of \mathbf{E}^h and \mathbf{H}^h on the staggered grid, yielding a discretization with \mathbf{H}^h tangential to cell edges and \mathbf{E}^h normal to cell faces; within homogeneous media, the choice is arbitrary.

With inhomogeneous media, certain field components are known to be continuous or discontinuous across material interfaces. It is the interface conditions (2.28) together with the discretization (4.9) of material coefficients that points towards more robust discretizations. Under the assumptions listed in Section 3.2.1, the interface conditions across cell surfaces for the variables \mathbf{A} ,

\mathbf{j} , \mathbf{H} , and ϕ are as in (2.28) and (3.34), i.e.,

$$\mathbf{n}^I \cdot [\mathbf{A}^I - \mathbf{A}^{II}] = 0, \quad (4.11a)$$

$$\mathbf{n}^I \times [\mathbf{A}^I - \mathbf{A}^{II}] = \mathbf{0}, \quad (4.11b)$$

$$\mathbf{n}^I \cdot [\mathbf{j}^I - \mathbf{j}^{II}] = 0, \quad (4.11c)$$

$$\mathbf{n}^I \times [\mathbf{H}^I - \mathbf{H}^{II}] = \mathbf{0}, \quad (4.11d)$$

$$\mathbf{n}^I \cdot [\mathbf{\nabla} \phi^I - \mathbf{\nabla} \phi^{II}] = \varrho_e / \epsilon_0, \quad (4.11e)$$

where ϱ_e is a surface charge density. The conditions (4.11) imply that $\mathbf{n} \cdot \mathbf{j}$ is continuous across material interfaces while $\mathbf{n} \cdot \mathbf{E}$ is not. Moreover, $\mathbf{n} \cdot \mathbf{\nabla} \phi$ inherits the discontinuity in $\mathbf{n} \cdot \mathbf{E}$, while \mathbf{A} is continuous.

Motivated by the conditions (4.11), the locations of the discrete unknowns become clear. Since discrete divergences are computed by integrating over cell volumes, the discrete unknowns \mathbf{A}^h and \mathbf{j}^h corresponding to the vector potential \mathbf{A} and the generalized current field \mathbf{j} respectively are prescribed on cell faces of the primary grid with components normal to cell faces.

By (4.10c), the unknowns comprising the discrete field ψ^h should be located at the centers of the cell volumes since that is where the discrete approximation to $\operatorname{div} \mathbf{A}$ is centered. Similarly, the discrete field ϕ^h sits at cell centers; with that choice, the approximation of $\mathbf{\nabla} \phi$ is normal to the centers of cell faces.

Since, from (2.28d), the tangential components of the magnetic field \mathbf{H} are continuous across interfaces in the absence of surface currents \mathbf{j}_e , the discrete unknowns \mathbf{H}^h are set at the centers of the edges of cells of the primary grid with components tangential to those edges. This contrasts with the

specification of \mathbf{H}^h in the Yee discretization as given in (4.6); \mathbf{H}^h is tangential to cell edges in this scheme while it is normal to cell faces in the Yee scheme.

Then, in Cartesian coordinates, the discrete approximations of $\mathbf{A} = (A^x, A^y, A^z)^T$, $\mathbf{j} = (j^x, j^y, j^z)^T$, $\mathbf{H} = (H^x, H^y, H^z)^T$, ϕ , and ψ are

$$A^x_{i \pm \frac{1}{2}, j, k} \simeq A^x(x_{i \pm \frac{1}{2}}, y_j, z_k), \quad (4.12a)$$

$$A^y_{i, j \pm \frac{1}{2}, k} \simeq A^y(x_i, y_{j \pm \frac{1}{2}}, z_k), \quad (4.12b)$$

$$A^z_{i, j, k \pm \frac{1}{2}} \simeq A^z(x_i, y_j, z_{k \pm \frac{1}{2}}), \quad (4.12c)$$

$$j^x_{i \pm \frac{1}{2}, j, k} \simeq j^x(x_{i \pm \frac{1}{2}}, y_j, z_k), \quad (4.12d)$$

$$j^y_{i, j \pm \frac{1}{2}, k} \simeq j^y(x_i, y_{j \pm \frac{1}{2}}, z_k), \quad (4.12e)$$

$$j^z_{i, j, k \pm \frac{1}{2}} \simeq j^z(x_i, y_j, z_{k \pm \frac{1}{2}}), \quad (4.12f)$$

$$H^x_{i, j \pm \frac{1}{2}, k \pm \frac{1}{2}} \simeq H^x(x_i, y_{j \pm \frac{1}{2}}, z_{k \pm \frac{1}{2}}), \quad (4.12g)$$

$$H^y_{i \pm \frac{1}{2}, j, k \pm \frac{1}{2}} \simeq H^y(x_{i \pm \frac{1}{2}}, y_j, z_{k \pm \frac{1}{2}}), \quad (4.12h)$$

$$H^z_{i \pm \frac{1}{2}, j, k} \simeq H^z(x_{i \pm \frac{1}{2}}, y_j, z_k), \quad (4.12i)$$

$$\phi_{i, j, k} \simeq \phi(x_i, y_j, z_k), \quad (4.12j)$$

$$\psi_{i, j, k} \simeq \psi(x_i, y_j, z_k), \quad (4.12k)$$

where $i = 1, \dots, N_x$, $j = 1, \dots, N_y$, and $k = 1, \dots, N_z$. The discrete source field \mathbf{J}_e^h is normal to cell faces as is \mathbf{A}^h while the discrete source field \mathbf{J}_m^h lies tangential to cell edges like \mathbf{H}^h .

4.3.2 Derivation of the Finite-Volume Scheme

The strategy to derive the discrete system is as follows:

1. Integrate (4.10a) over the faces of primary-grid cells.
2. Integrate (4.10b) over the primary-grid cells.
3. Integrate (4.10c) over the primary-grid cells to get discrete equations for ψ^h .
4. Integrate (4.10d) over lines between centers of adjacent primary-grid cells to get discrete equations for \mathbf{j}^h .
5. Integrate (4.10e) over the faces of dual-grid cells to get discrete equations for \mathbf{H}^h .

In the last three steps, the discrete equations derived are used to eliminate the discrete fields ψ^h , \mathbf{j}^h , and \mathbf{H}^h from the discrete equations derived in the first two steps. Where appropriate, the boundary conditions (3.32) can be applied to close the resulting discrete equations [44, 99, 113]. The end result is a large linear system that involves only the unknown discrete fields \mathbf{A}^h and ϕ^h .

To begin, integrate the stabilized equation (4.10a) over faces of the primary grid as in the derivation of the Yee scheme. For any surface $S \subset \Omega$, (4.10a) together with Stokes' Theorem gives

$$\oint_{\partial S} \mathbf{H} \cdot \boldsymbol{\tau} d\ell - (\imath\omega)^{-1} \int_S \mathbf{grad} \psi \cdot \mathbf{n} dS + \int_S \mathbf{j} \cdot \mathbf{n} dS = \int_S \mathbf{J}_e \cdot \mathbf{n} dS. \quad (4.13)$$

The surfaces to use in (4.13) are the faces of the cells of the primary grid (the rectangles $S_{i-\frac{1}{2},j,k}^x$, $S_{i,j-\frac{1}{2},k}^y$, and $S_{i,j,k-\frac{1}{2}}^z$ from (4.3)). Substitute $S = S_{i-\frac{1}{2},j,k}^x$ into (4.13) and use a centered finite-differences to approximate $\partial_x \psi$. Then,

with the same discrete approximations as in (4.8a) for the remaining integral terms, the discrete equation resulting is

$$\begin{aligned} h_k^z \left(H_{i-\frac{1}{2}, j+\frac{1}{2}, k}^z - H_{i-\frac{1}{2}, j-\frac{1}{2}, k}^z \right) - h_j^y \left(H_{i-\frac{1}{2}, j, k+\frac{1}{2}}^y - H_{i-\frac{1}{2}, j, k-\frac{1}{2}}^y \right) \\ + h_j^y h_k^z \left(\frac{\psi_{i-1, j, k} - \psi_{i, j, k}}{\omega h_{i-\frac{1}{2}}^x} + j_{i-\frac{1}{2}, j, k}^x \right) = h_j^y h_k^z J_e^x_{i-\frac{1}{2}, j, k}. \end{aligned} \quad (4.14a)$$

The corresponding equations in the y - and z -directions are obtained using $S = S_{i, j-\frac{1}{2}, k}^y$ and $S_{i, j, k-\frac{1}{2}}^z$ respectively in (4.13); the resulting discrete equations are

$$\begin{aligned} h_i^x \left(H_{i, j-\frac{1}{2}, k+\frac{1}{2}}^x - H_{i, j-\frac{1}{2}, k-\frac{1}{2}}^x \right) - h_k^z \left(H_{i+\frac{1}{2}, j-\frac{1}{2}, k}^z - H_{i-\frac{1}{2}, j-\frac{1}{2}, k}^z \right) \\ + h_i^x h_k^z \left(\frac{\psi_{i, j-1, k} - \psi_{i, j, k}}{\omega h_{j-\frac{1}{2}}^y} + j_{i, j-\frac{1}{2}, k}^y \right) = h_i^x h_k^z J_e^y_{i, j-\frac{1}{2}, k}, \end{aligned} \quad (4.14b)$$

$$\begin{aligned} h_j^y \left(H_{i+\frac{1}{2}, j, k-\frac{1}{2}}^y - H_{i-\frac{1}{2}, j, k-\frac{1}{2}}^y \right) - h_i^x \left(H_{i, j+\frac{1}{2}, k-\frac{1}{2}}^x - H_{i, j-\frac{1}{2}, k-\frac{1}{2}}^x \right) \\ + h_i^x h_j^y \left(\frac{\psi_{i, j, k-1} - \psi_{i, j, k}}{\omega h_{k-\frac{1}{2}}^z} + j_{i, j, k-\frac{1}{2}}^z \right) = h_i^x h_j^y J_e^z_{i, j, k-\frac{1}{2}}. \end{aligned} \quad (4.14c)$$

Next, for any volume $V \subset \Omega$, (4.10b) gives

$$\oint_{\partial V} \mathbf{j} \cdot \mathbf{n} dS = \oint_{\partial V} \mathbf{J}_e \cdot \mathbf{n} dS.$$

Choose $V = V_{i, j, k}$ from (4.3a) to derive

$$\begin{aligned} h_j^y h_k^z \left(j_{i+\frac{1}{2}, j, k}^x - j_{i-\frac{1}{2}, j, k}^x \right) + h_i^x h_k^z \left(j_{i, j+\frac{1}{2}, k}^y - j_{i, j-\frac{1}{2}, k}^y \right) \\ + h_i^x h_j^y \left(j_{i, j, k+\frac{1}{2}}^z - j_{i, j, k-\frac{1}{2}}^z \right) = \\ h_j^y h_k^z \left(J_e^x_{i+\frac{1}{2}, j, k} - J_e^x_{i-\frac{1}{2}, j, k} \right) + h_i^x h_k^z \left(J_e^y_{i, j+\frac{1}{2}, k} - J_e^y_{i, j-\frac{1}{2}, k} \right) \\ + h_i^x h_j^y \left(J_e^z_{i, j, k+\frac{1}{2}} - J_e^z_{i, j, k-\frac{1}{2}} \right). \end{aligned} \quad (4.15)$$

Having derived (4.14) and (4.15), the remaining equations are integrated to eliminate the discrete unknowns ψ^h , \mathbf{j}^h , and \mathbf{H}^h . The resulting system involves \mathbf{A}^h and ϕ^h only; it is this system that is studied in subsequent chapters.

Eliminating ψ^h is straightforward; by (4.10c), for any volume $V \subset \Omega$,

$$\int_V \mu \psi dV - \int_V \operatorname{div} \mathbf{A} dV = 0.$$

Since $\mu = \mu_{i,j,k}$ is constant in cells, as in the derivation of (4.15), choose $V = V_{i,j,k}$, yielding

$$\begin{aligned} \psi_{i,j,k} &= \mu_{i,j,k}^{-1} \left[h_j^y h_k^z \left(A^x_{i+\frac{1}{2},j,k} - A^x_{i-\frac{1}{2},j,k} \right) + h_i^x h_k^z \left(A^y_{i,j+\frac{1}{2},k} - A^y_{i,j-\frac{1}{2},k} \right) \right. \\ &\quad \left. + h_i^x h_j^y \left(A^z_{i,j,k+\frac{1}{2}} - A^z_{i,j,k-\frac{1}{2}} \right) \right]. \end{aligned} \quad (4.16)$$

Since the field $\operatorname{grad} \phi$ is potentially less smooth than $\widehat{\sigma} \operatorname{grad} \phi$ across an interface between primary grid cells, it is preferable to express (4.10d) by dividing through by $\widehat{\sigma}$ first as in [54]. Then, for any path $\Gamma \subset \Omega$,

$$\int_{\Gamma} [\widehat{\sigma}^{-1} \mathbf{j} + \mathbf{A} + \operatorname{grad} \phi] \cdot \boldsymbol{\tau} d\ell = 0. \quad (4.17)$$

Choosing Γ in (4.17) to be a line between cell centers such as

$$\Gamma = \ell_{i-\frac{1}{2},j,k}^x := (x_{i-1}, x_i) \times \{y_j\} \times \{z_k\},$$

the line integral can be approximated by

$$h_{i-\frac{1}{2}}^x \left(\frac{j^x_{i-\frac{1}{2},j,k}}{\widehat{\sigma}_{i-\frac{1}{2},j,k}} + A^x_{i-\frac{1}{2},j,k} \right) + \phi_{i,j,k} - \phi_{i-1,j,k} = 0. \quad (4.18)$$

In (4.18), the *harmonic average* of $\widehat{\sigma}$ across the adjacent cells $V_{i-1,j,k}$ and $V_{i,j,k}$ is defined by

$$\widehat{\sigma}_{i-\frac{1}{2},j,k} := h_{i-\frac{1}{2}}^x \left(\int_{x_{i-1}}^{x_i} \frac{dx}{\widehat{\sigma}(x, y_j, z_k)} \right)^{-1}.$$

By (4.9), the integral above evaluates to

$$\widehat{\sigma}_{i-\frac{1}{2},j,k} = h_{i-\frac{1}{2}}^x \left(\frac{h_{i-1}^x}{\widehat{\sigma}_{i-1,j,k}} + \frac{h_i^x}{\widehat{\sigma}_{i,j,k}} \right)^{-1}. \quad (4.19a)$$

Similar averages taken in the y - and z -directions give

$$\widehat{\sigma}_{i,j-\frac{1}{2},k} = h_{j-\frac{1}{2}}^y \left(\frac{h_{j-1}^y}{\widehat{\sigma}_{i,j-1,k}} + \frac{h_j^y}{\widehat{\sigma}_{i,j,k}} \right)^{-1}, \quad (4.19b)$$

$$\widehat{\sigma}_{i,j,k-\frac{1}{2}} = h_{k-\frac{1}{2}}^z \left(\frac{h_{k-1}^z}{\widehat{\sigma}_{i,j,k-1}} + \frac{h_k^z}{\widehat{\sigma}_{i,j,k}} \right)^{-1}. \quad (4.19c)$$

The derivation of harmonic—rather than arithmetic—averages is natural in this context upon application of numerical considerations (viz. integration of rough quantities). Using harmonic averages becomes important in practice when the coefficient σ may jump by several orders of magnitude [54, 96, 113].

The discrete approximation (4.18) can be solved to yield an equation for $j^x_{i-\frac{1}{2},j,k}$, namely

$$j^x_{i-\frac{1}{2},j,k} = -\widehat{\sigma}_{i-\frac{1}{2},j,k} \left(A^x_{i-\frac{1}{2},j,k} + \frac{\phi_{i,j,k} - \phi_{i-1,j,k}}{h_{i-\frac{1}{2}}^x} \right). \quad (4.20a)$$

The integration of (4.17) along lines in the y - and z -directions yields

$$j^y_{i,j-\frac{1}{2},k} = -\widehat{\sigma}_{i,j-\frac{1}{2},k} \left(A^y_{i,j-\frac{1}{2},k} + \frac{\phi_{i,j,k} - \phi_{i,j-1,k}}{h_{j-\frac{1}{2}}^y} \right), \quad (4.20b)$$

$$j^z_{i,j,k-\frac{1}{2}} = -\widehat{\sigma}_{i,j,k-\frac{1}{2}} \left(A^z_{i,j,k-\frac{1}{2}} + \frac{\phi_{i,j,k} - \phi_{i,j,k-1}}{h_{k-\frac{1}{2}}^z} \right) \quad (4.20c)$$

for $j^y_{i,j-\frac{1}{2},k}$ and $j^z_{i,j,k-\frac{1}{2}}$ respectively. Thus, using the definitions (4.19), the equations (4.20) can be used to eliminate \mathbf{j}^h in (4.14) and (4.15).

It remains to eliminate the magnetic field unknowns \mathbf{H}^h from (4.14) by integrating the equation (4.10e). Since the tangential components of the field

$\mathbf{B} = \mu \mathbf{H}$ are discontinuous while the tangential components of the field \mathbf{H} are continuous across interfaces (see (2.28)), it makes more sense to integrate $\mu \mathbf{H}$ in (4.10e). Thus, the equation (4.10e) implies

$$\imath\omega \int_S \mu \mathbf{H} \cdot \mathbf{n} dS = - \int_S \mathbf{J}_m \cdot \mathbf{n} dS + \oint_{\partial S} \mathbf{A} \cdot \boldsymbol{\tau} d\ell \quad (4.21)$$

for any surface S .

The surfaces of integration to use in (4.21) are the faces of the dual grid, namely $S_{i,j-\frac{1}{2},k-\frac{1}{2}}^x$, $S_{i-\frac{1}{2},j,k-\frac{1}{2}}^y$, and $S_{i-\frac{1}{2},j-\frac{1}{2},k}^z$ from (4.4b-d). Taking $S_{i,j-\frac{1}{2},k-\frac{1}{2}}^x$, use single quadrature points to approximate the integrals above, so

$$\begin{aligned} \imath\omega h_{j-\frac{1}{2}}^y h_{k-\frac{1}{2}}^z \mu_{i,j-\frac{1}{2},k-\frac{1}{2}} H_{i,j-\frac{1}{2},k-\frac{1}{2}}^x &= -h_{j-\frac{1}{2}}^y h_{k-\frac{1}{2}}^z J_{mi,j-\frac{1}{2},k-\frac{1}{2}}^x \\ h_{k-\frac{1}{2}}^z (A_{i,j,k-\frac{1}{2}}^z - A_{i,j-1,k-\frac{1}{2}}^z) - h_{j-\frac{1}{2}}^y (A_{i,j-\frac{1}{2},k}^y - A_{i,j-\frac{1}{2},k-1}^y). \end{aligned} \quad (4.22)$$

In (4.22), the value of μ on the surface $S_{i,j-\frac{1}{2},k-\frac{1}{2}}^x$ is approximated by the ordinary average

$$\mu_{i,j-\frac{1}{2},k-\frac{1}{2}} := \left(h_{j-\frac{1}{2}}^y h_{k-\frac{1}{2}}^z \right)^{-1} \int_{S_{i,j-\frac{1}{2},k-\frac{1}{2}}^x} \mu(x_i, y, z) dy dz. \quad (4.23)$$

Assuming the permeability μ is piecewise constant, this simplifies to

$$\begin{aligned} \mu_{i,j-\frac{1}{2},k-\frac{1}{2}} &= \left(4h_{j-\frac{1}{2}}^y h_{k-\frac{1}{2}}^z \right)^{-1} (h_{j-1}^y h_{k-1}^z \mu_{i,j-1,k-1} + h_{j-1}^y h_k^z \mu_{i,j-1,k} \\ &\quad + h_j^y h_{k-1}^z \mu_{i,j,k-1} + h_j^y h_k^z \mu_{i,j,k}) \\ &= \left(4h_{j-\frac{1}{2}}^y h_{k-\frac{1}{2}}^z \right)^{-1} \sum_{q,r=\pm\frac{1}{2}} h_{j-\frac{1}{2}+q}^y h_{k-\frac{1}{2}+r}^z \mu_{i,j-\frac{1}{2}+q,k-\frac{1}{2}+r}, \end{aligned} \quad (4.24a)$$

with corresponding averages

$$\mu_{i-\frac{1}{2},j,k-\frac{1}{2}} = \left(4h_{i-\frac{1}{2}}^x h_{k-\frac{1}{2}}^z\right)^{-1} \sum_{p,r=\pm\frac{1}{2}} h_{i-\frac{1}{2}+p}^x h_{k-\frac{1}{2}+r}^z \mu_{i-\frac{1}{2}+p,j,k-\frac{1}{2}+r}, \quad (4.24b)$$

$$\mu_{i-\frac{1}{2},j-\frac{1}{2},k} = \left(4h_{i-\frac{1}{2}}^x h_{j-\frac{1}{2}}^y\right)^{-1} \sum_{p,q=\pm\frac{1}{2}} h_{i-\frac{1}{2}+p}^x h_{j-\frac{1}{2}+q}^y \mu_{i-\frac{1}{2}+p,j-\frac{1}{2}+q,k} \quad (4.24c)$$

in the y - and z -directions respectively. The discrete equations for \mathbf{H}^h are

$$H_{i,j-\frac{1}{2},k-\frac{1}{2}}^x = (\omega \mu_{i,j-\frac{1}{2},k-\frac{1}{2}})^{-1} \left(\frac{A_{i,j,k-\frac{1}{2}}^z - A_{i,j-1,k-\frac{1}{2}}^z}{h_{j-\frac{1}{2}}^y} \right) \quad (4.25a)$$

$$- \frac{A_{i,j-\frac{1}{2},k}^y - A_{i,j-\frac{1}{2},k-1}^y}{h_{k-\frac{1}{2}}^z} - J_{mi,j-\frac{1}{2},k-\frac{1}{2}}^x, \quad (4.25b)$$

$$H_{i-\frac{1}{2},j,k-\frac{1}{2}}^y = (\omega \mu_{i-\frac{1}{2},j,k-\frac{1}{2}})^{-1} \left(\frac{A_{i-\frac{1}{2},j,k}^x - A_{i-\frac{1}{2},j,k-1}^x}{h_{k-\frac{1}{2}}^z} \right) \quad (4.25c)$$

$$- \frac{A_{i,j,k-\frac{1}{2}}^z - A_{i-1,j,k-\frac{1}{2}}^z}{h_{i-\frac{1}{2}}^x} - J_{mi-\frac{1}{2},j,k-\frac{1}{2}}^y,$$

$$H_{i-\frac{1}{2},j-\frac{1}{2},k}^z = (\omega \mu_{i-\frac{1}{2},j-\frac{1}{2},k})^{-1} \left(\frac{A_{i,j-\frac{1}{2},k}^y - A_{i-1,j,k-\frac{1}{2}}^y}{h_{i-\frac{1}{2}}^x} \right) \quad (4.25d)$$

$$- \frac{A_{i-\frac{1}{2},j,k}^x - A_{i-\frac{1}{2},j-1,k}^x}{h_{j-\frac{1}{2}}^y} - J_{mi-\frac{1}{2},j-\frac{1}{2},k}^z.$$

Substituting (4.25) into (4.14) eliminates \mathbf{H}^h from the discrete linear system.

4.3.3 The Discrete Linear System

This discretization can be viewed as an extension of Yee's method suitable for discontinuous coefficients. The difference operators are centered, conservative, and second-order accurate, as seen in [53, 54]. Throughout, a consistent, compact discretization of the operators **grad**, **div**, and **curl** is used;

the corresponding discrete operators can be denoted \mathbf{grad}^h , \mathbf{div}^h , \mathbf{curl}_f^h , and \mathbf{curl}_e^h . Notice that two discrete operators are needed for \mathbf{curl} ; \mathbf{curl}_f^h that operates on discrete vector fields defined normal to cell faces (like \mathbf{A}^h in (4.12a-c)) and \mathbf{curl}_e^h acts on discrete vector fields defined to be tangential to cell edges (like \mathbf{H}^h in (4.12g-i)). With these definitions, the identities

$$\mathbf{curl}_f^h \mathbf{grad}^h \phi^h = \mathbf{0}^h, \quad (4.26a)$$

$$\mathbf{div}^h \mathbf{curl}_e^h \mathbf{H}^h = \mathbf{0}^h, \text{ and} \quad (4.26b)$$

$$\mathbf{grad}^h \mathbf{div}^h \mathbf{A}^h - \mathbf{curl}_e^h \mathbf{curl}_f^h \mathbf{A}^h = \Delta^h \mathbf{A}^h \quad (4.26c)$$

follow immediately (cf. [53, 54, 64, 65, 100]). The discrete identities (4.26) are analogues of vector calculus identities. For a more thorough treatment of the finite-volume discretizations of standard vector calculus operators in (4.26), consult [64, 65].

The equations (4.10) in discrete form are

$$\mathbf{curl}_e^h \mathbf{H}^h - (\omega)^{-1} \mathbf{grad}^h \psi^h + \mathbf{j}^h = \mathbf{J}_e^h, \quad (4.27a)$$

$$\mathbf{div}^h \mathbf{j}^h = \mathbf{div}^h \mathbf{J}_e^h, \quad (4.27b)$$

$$\mu_c^h \psi^h - \mathbf{div}^h \mathbf{A}^h = \mathbf{0}^h, \quad (4.27c)$$

$$\mathbf{j}^h + \widehat{\sigma}^h (\mathbf{A}^h + \mathbf{grad}^h \phi^h) = \mathbf{0}^h, \quad (4.27d)$$

$$\mathbf{curl}_f^h \mathbf{A}^h - \omega \mu_e^h \mathbf{H}^h = \mathbf{J}_m^h. \quad (4.27e)$$

The boundary conditions (3.32) are included in the definitions of the discrete operators in (4.26) and (4.27). The operators $\widehat{\sigma}^h$, μ_c^h , and μ_e^h are discrete approximations of the operators $\widehat{\sigma}$ and μ respectively; notice two operators are needed for μ , one at cell centers, the other at cell edges.

After eliminating the discrete fields \mathbf{H}^h , \mathbf{j}^h , and ϕ^h in (4.27), the final linear system can be formally represented as

$$\mathbf{A}^h \mathbf{x}^h = \mathbf{b}^h \quad (4.28a)$$

where

$$\mathbf{A}^h := \begin{pmatrix} (\omega)^{-1} \mathcal{L}_\mu^h - \widehat{\sigma}^h & -\widehat{\sigma}^h \mathbf{grad}^h \\ \operatorname{div}^h \widehat{\sigma}^h & \operatorname{div}^h \widehat{\sigma}^h \mathbf{grad}^h \end{pmatrix}, \quad (4.28b)$$

$$\mathcal{L}_\mu^h := \mathbf{curl}_e^h(\mu_e^h)^{-1} \mathbf{curl}_f^h - \mathbf{grad}^h(\mu_c^h)^{-1} \operatorname{div}^h, \quad (4.28c)$$

$$\mathbf{x}^h := \begin{pmatrix} \mathbf{A}^h \\ \phi^h \end{pmatrix}, \quad (4.28d)$$

and \mathbf{b}^h represents the appropriate source and boundary data. The operator \mathcal{L}_μ^h in (4.28c) has a 19-point stencil; the distinction between this discretization (in which \mathbf{H}^h and ψ^h have to be eliminated) and a direct discretization of the operator $\mathbf{curl}(\mu^{-1} \mathbf{curl}(\cdot)) - \mathbf{grad}(\mu^{-1} \operatorname{div}(\cdot))$ is that μ_e^h (the value of μ on cell edges) is naturally given by an arithmetic average and not a harmonic average. With $\mu = \mu_0$, (4.26c) implies that \mathcal{L}_μ^h in (4.28d) simplifies to a scalar multiple of the discrete vector Laplacian operator Δ^h , so

$$\mathbf{A}^h = \begin{pmatrix} -(\omega \mu_0)^{-1} \Delta^h - \widehat{\sigma}^h & -\widehat{\sigma}^h (\mathbf{grad})^h \\ (\operatorname{div})^h \widehat{\sigma}^h & (\operatorname{div})^h \widehat{\sigma}^h (\mathbf{grad})^h \end{pmatrix}. \quad (4.29)$$

Now, applying div^h to (4.27a) and simplifying with (4.27b) and (4.26b) gives

$$\operatorname{div}^h \mathbf{grad}^h \psi^h = 0^h.$$

Moreover, the boundary conditions (3.32c) and the discrete equation (4.27a) imply that the discrete normal derivative of ψ^h vanishes on the boundary. Setting, say, $\psi_{1,1,1} = 0$ at a single point (or applying the global constraint (3.32d)) determines that $\psi^h \equiv 0^h$ throughout the grid. It follows, then, that this scheme yields a discrete divergence-free vector potential, namely

$$\operatorname{div}^h \mathbf{A}^h = 0^h. \quad (4.30)$$

Given the exact solution (\mathbf{A}, ϕ) of (3.31), the stabilization term $\mathbf{grad} \psi$ in (4.10a) vanishes. With this scheme, (4.30) holds also, so the discrete system is indeed stabilized by this term and not penalized (e.g. [21]). This is not the case with nodal finite element methods as in [33, 69]. When an approximate solution \mathbf{A}^h fails to satisfy (4.30), the stabilization term may grow when the permeability μ varies over a few orders of magnitude, or $\operatorname{div}^h \mathbf{A}^h$ grows in attempting to keep the discrete approximation of $\mu^{-1} \operatorname{div} \mathbf{A}$ approximately constant across interfaces [69].

4.4 Grid Effects

For general physical problems, the material parameters σ , μ , and ϵ are tensor fields that are functions of spatial coordinates (and possibly of frequency as well). An inherent limitation of the discretization (4.28) lies in the decision to approximate the material coefficients by functions that are piecewise constant on a tensor-product grid (cf. (4.9)). The geometry of the earth is not brick-like for realistic geophysical problems; that is, interfaces do

not naturally align with a simple grid.

This crude model is chosen to simplify the inverse problem within which the forward-modeling problem (3.1) is embedded. For inverse problems, recovering the material coefficient σ is typically the goal, so the locations of interfaces between distinct media are not known *a priori*. Given that many forward solves are needed and that any physical data is sparse and contaminated by noise, it is not reasonable to expect to be able to resolve the interfaces to arbitrary accuracy. This motivates the use of a simple model of the media like (4.9) in which the isotropic material coefficients are piecewise constant on a Cartesian tensor-product grid (4.3). More complicated finite-element discretizations could give accurate solutions for arbitrary geometries more effectively but would require more *a priori* information about the material coefficients. Even highly accurate finite-volume or finite-difference discretizations are obtainable on simple Cartesian grids, but the interfaces within grid cells are assumed *a priori* (e.g. [74, 113]).

For high-frequency electromagnetic simulations, staircase approximations of interfaces are avoided (e.g. [104, Chap. 10]. In such applications, careful resolution of the geometry is crucial because errors computed will propagate throughout the solution [104]. This is to be expected for a hyperbolic PDE model where noise in the approximate solutions can propagate along characteristics. At low frequencies, however, Maxwell's equations are primarily parabolic in character, so noise in solutions tends to get smoothed out or damped by the naturally diffusive flow. Thus, the coarse approximations cho-

sen for the material coefficients do not upset the accuracy of solutions obtained provided that the frequencies are moderate in magnitude.

4.4.1 Model Problem Analysis

To what degree do solutions of Maxwell's equations change when the material coefficients are coarsely resolved as in the numerical discretizations (4.28)? To answer this question, consider first the model diffusion problem in n dimensions,

$$-\operatorname{div}(\sigma \operatorname{grad} \phi) = f \quad (\boldsymbol{x} \in \Omega), \quad (4.31a)$$

with homogeneous boundary conditions

$$\phi = 0 \quad (\boldsymbol{x} \in \partial\Omega_D), \quad (4.31b)$$

$$\boldsymbol{n} \cdot (\sigma \operatorname{grad} \phi) = 0 \quad (\boldsymbol{x} \in \partial\Omega_N). \quad (4.31c)$$

In (4.31b-c), the boundary $\partial\Omega = \partial\Omega_D \cup \partial\Omega_N$ is partitioned into two disjoint portions $\partial\Omega_D$ and $\partial\Omega_N$ on which the Dirichlet and Neumann boundary conditions apply respectively. Inhomogeneous boundary conditions can be handled also (see [21, Section IV.1]) but the homogeneous boundary conditions (4.31b-c) are studied here for simplicity. Similarly, assume that the diffusion coefficient σ is a positive scalar field satisfying

$$0 < \sigma_{\min} \leq \sigma(\boldsymbol{x}) \leq \sigma_{\max} \quad (\boldsymbol{x} \in \Omega).$$

The extension to the case where σ is an $n \times n$ tensor field requires that σ is symmetric and positive-definite with smallest eigenvalue uniformly bounded away from 0 independent of \boldsymbol{x} .

A variational formulation of the boundary-value problem (4.31) is to find $\phi \in \mathcal{H}_E^1(\Omega)$ such that

$$(\sigma \mathbf{grad} \phi, \mathbf{grad} \psi)_\Omega = \int_\Omega f \psi \, dV \quad \forall \psi \in \mathcal{H}_E^1(\Omega), \quad (4.32a)$$

where the space of test functions is

$$\mathcal{H}_E^1(\Omega) := \{\psi \in \mathcal{H}(\mathbf{grad}; \Omega) : \psi = 0 \text{ on } \partial\Omega_D\}. \quad (4.32b)$$

Under standard assumptions on f and σ , the solution ϕ is known to be in $\mathcal{H}_E^1(\Omega)$; moreover, the gradient $\mathbf{grad} \phi$ is also bounded (see [21, 46, 89]).

Consider also a perturbed problem where the data are identical except for the coefficient σ ; that is, for some $h > 0$, given a slightly perturbed coefficient $\tilde{\sigma}$, the perturbed boundary-value problem is

$$-\operatorname{div}(\tilde{\sigma} \mathbf{grad} \tilde{\phi}) = f \quad (\mathbf{x} \in \Omega), \quad (4.33)$$

with the associated homogeneous boundary conditions (4.31b,c) for $\tilde{\phi}$. The corresponding weak problem is to find $\tilde{\phi} \in \mathcal{H}_E^1(\Omega)$ such that

$$(\tilde{\sigma} \mathbf{grad} \tilde{\phi}, \mathbf{grad} \psi)_\Omega = \int_\Omega f \psi \, dV \quad \forall \psi \in \mathcal{H}_E^1(\Omega). \quad (4.34a)$$

The coefficient $\tilde{\sigma}$ satisfies

$$0 < \sigma_{\min} \leq \tilde{\sigma}(\mathbf{x}) \leq \sigma_{\max} \quad (\mathbf{x} \in \Omega),$$

and $\tilde{\sigma}$ approximates σ in the sense that there is a set $S^h \subset \Omega$ of measure $O(h)$ ($0 < h \ll 1$) on which $\tilde{\sigma} - \sigma$ is supported. That is, $\tilde{\sigma} = \sigma$ almost everywhere, except on a small volume near material interfaces where $\tilde{\sigma}$ fails

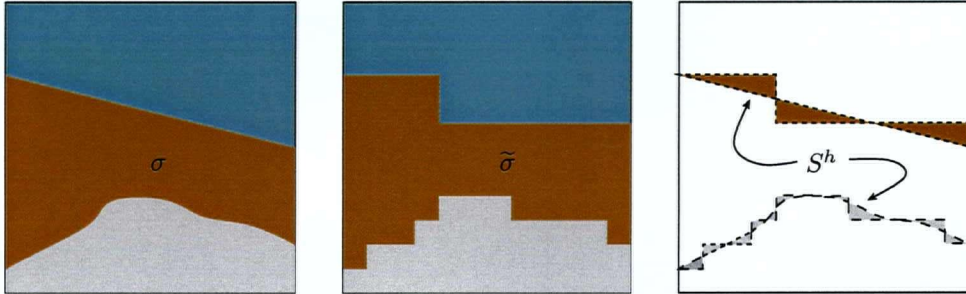


Figure 4.4: Cross-sections of the coefficient σ , the perturbed coefficient $\tilde{\sigma}$, and the support S^h of the perturbation $\tilde{\sigma} - \sigma$.

to resolve the interface (see Figure 4.4). With the preceding assumptions, assuming $\text{meas}(S^h) = O(h)$ is the n -dimensional volume of S^h , then

$$\|\tilde{\sigma} - \sigma\|_\infty \leq K := \sigma_{\max} - \sigma_{\min} \text{ and} \quad (4.35a)$$

$$\|\tilde{\sigma} - \sigma\|_p \leq (K \text{ meas}(S^h))^{\frac{1}{p}} = O(h^{\frac{1}{p}}) \quad (1 \leq p < \infty). \quad (4.35b)$$

In particular, although the discrepancy $\|\tilde{\sigma} - \sigma\|_p$ vanishes as $h \downarrow 0$ in standard L_p -norms, the difference is $O(1)$ in the L_∞ -norm.

Unfortunately, deriving a bound on $\|\tilde{\phi} - \phi\|_p$ is not straightforward in general. There is a general result bounding $\|\mathbf{grad}(\tilde{\phi} - \phi)\|_2$.

Proposition 4.1. *Let ϕ and $\tilde{\phi}$ be solutions of the problems (4.32) and (4.34) respectively. Then,*

$$\|\mathbf{grad}(\tilde{\phi} - \phi)\|_2 = O\left(h^{\frac{1}{2}}\right).$$

Proof. With a bit of algebraic manipulation, subtracting the equations (4.32) and (4.34) yields

$$\left(\tilde{\sigma} \mathbf{grad}(\tilde{\phi} - \phi), \mathbf{grad} \psi\right)_\Omega = \frac{1}{2} ((\tilde{\sigma} - \sigma) \mathbf{grad} \phi, \mathbf{grad} \psi)_\Omega. \quad (4.36)$$

Substituting $\psi = \tilde{\phi} - \phi$ into the left-hand side of (4.36) gives

$$\left| \int_{\Omega} \tilde{\sigma} |\mathbf{grad}(\tilde{\phi} - \phi)|_2^2 dV \right| \geq \sigma_{\min} \left\| \mathbf{grad}(\tilde{\phi} - \phi) \right\|_2^2.$$

The same substitution $\psi = \tilde{\phi} - \phi$ into the right-hand side of (4.36) yields

$$\begin{aligned} \left| \left((\tilde{\sigma} - \sigma) \mathbf{grad} \phi, \mathbf{grad}(\tilde{\phi} - \phi) \right)_\Omega \right| &\leq \int_{\Omega} |\mathbf{grad} \phi| \left| (\tilde{\sigma} - \sigma) \mathbf{grad}(\tilde{\phi} - \phi) \right| dV \\ &\leq \|\mathbf{grad} \phi\|_\infty \left\| (\tilde{\sigma} - \sigma) \mathbf{grad}(\tilde{\phi} - \phi) \right\|_1 \\ &\leq \|\mathbf{grad} \phi\|_\infty \|(\tilde{\sigma} - \sigma)\|_2 \left\| \mathbf{grad}(\tilde{\phi} - \phi) \right\|_2 \end{aligned}$$

by applying Hölder's inequality twice. Combining the preceding inequalities,

$$\begin{aligned} \|\mathbf{grad}(\tilde{\phi} - \phi)\|_2 &\leq \frac{1}{\sigma_{\min}} \|\mathbf{grad} \phi\|_\infty \|(\tilde{\sigma} - \sigma)\|_2 \\ &\leq \frac{1}{\sigma_{\min}} \|\mathbf{grad} \phi\|_\infty K^{\frac{1}{2}} (\text{meas}(S^h))^{\frac{1}{2}} \\ &= O(h^{\frac{1}{2}}). \end{aligned}$$

□

In some circumstances, the field $\mathbf{grad} \phi$ may be more relevant than ϕ itself. For instance, in electrostatics, ϕ would be a potential field whereas $\mathbf{grad} \phi$ would be an electric field that is measurable by physical means. The bound on $\|\mathbf{grad}(\tilde{\phi} - \phi)\|_2$ in Proposition 4.1 is valuable in such cases, giving a quantitative bound on the measure of difference that staircasing makes to the computed gradients.

In one dimension, it is straightforward to derive a stronger bound on $\|\tilde{\phi} - \phi\|_\infty$ directly.

Proposition 4.2. Consider the PDE problems (4.32) and (4.34) in one dimension on the domain $\Omega = (0, L)$ for some $L > 0$. Assume that ϕ and $\tilde{\phi}$ are solutions of (4.32) with the boundary conditions

$$\phi(0) = \phi'(L) = 0 \quad (4.37)$$

with similar boundary conditions for $\tilde{\phi}$ in (4.34). Then,

$$\|\tilde{\phi} - \phi\|_\infty = O(h).$$

Proof. With the boundary conditions (4.37), the exact solutions to (4.32) and (4.34) can be derived directly in one dimension, namely

$$\phi(x) = \int_0^x \frac{F(\xi)}{\sigma(\xi)} d\xi, \quad (4.38a)$$

$$\tilde{\phi}(x) = \int_0^x \frac{F(\xi)}{\tilde{\sigma}(\xi)} d\xi, \quad (4.38b)$$

where

$$F(\xi) := \int_\xi^L f(s) ds. \quad (4.38c)$$

Then,

$$\begin{aligned} |\tilde{\phi}(x) - \phi(x)| &= \left| \int_0^x \left(\frac{1}{\tilde{\sigma}(\xi)} - \frac{1}{\sigma(\xi)} \right) F(\xi) d\xi \right| \\ &\leq \frac{1}{\sigma_{\min}^2} \int_0^x |\tilde{\sigma}(\xi) - \sigma(\xi)| \cdot |F(\xi)| d\xi \\ &\leq \frac{\|F\|_\infty}{\sigma_{\min}^2} \|\tilde{\sigma} - \sigma\|_1 \\ &= O(h). \end{aligned}$$

□

As a direct consequence of Proposition 4.2, similar bounds in the \mathcal{L}_1 - and \mathcal{L}_2 -norms hold.

Corollary 4.3. *In one dimension, under the same assumptions as in Proposition 4.2, $\|\tilde{\phi} - \phi\|_1 = O(h)$ and $\|\tilde{\phi} - \phi\|_2 = O(h)$.*

Proof. The desired bounds follow directly from applying Hölder's inequality on a bounded domain. In particular,

$$\begin{aligned}\|\tilde{\phi} - \phi\|_1 &= \int_0^L |\tilde{\phi} - \phi| dx \leq L \|\tilde{\phi} - \phi\|_\infty \leq O(h), \text{ and} \\ \|\tilde{\phi} - \phi\|_2 &= \left(\int_0^L |\tilde{\phi} - \phi|^2 dx \right)^{\frac{1}{2}} \\ &\leq \left(\|\tilde{\phi} - \phi\|_1 \cdot \|\tilde{\phi} - \phi\|_\infty \right)^{\frac{1}{2}} = O(h).\end{aligned}$$

□

The main feature that makes Proposition 4.2 possible is that the Green's functions appropriate to both the unperturbed and perturbed problems have a particular form; specifically, the solution ϕ in (4.38a-b) is can be written in the form

$$\phi(x) = \int_{\Omega} \frac{1}{\sigma(\xi)} \mathcal{F}(f; x; \xi) d\xi, \quad (4.39)$$

where the expression $\mathcal{F}(f; x; \xi)$ does not depend on σ . It is reasonable to conjecture an extension of Proposition 4.2 beyond one dimension; that is, assuming the fundamental solutions of the perturbed and unperturbed PDE problems have similar structure to (4.39), the discrepancy pointwise is

$$|\tilde{\phi}(\mathbf{x}) - \phi(\mathbf{x})| \leq \int_{\Omega} \left| \frac{1}{\tilde{\sigma}} - \frac{1}{\sigma} \right| \cdot |\mathcal{F}(f; \mathbf{x}; \xi)| d\xi$$

and an $O(h)$ bound for $\|\tilde{\phi} - \phi\|_\infty$ results (as well as Corollary 4.3). However, even in one dimension, with boundary conditions other than (4.37), the term \mathcal{F} within the Green's function depends on σ (or $\tilde{\sigma}$), i.e., $\mathcal{F} = \mathcal{F}(\sigma; f; x; \xi)$, making the proof slightly more complicated.

4.4.2 Numerical Study

In the following tests, a reference coefficient σ and a family of perturbed coefficients $\{\tilde{\sigma}_k\}_{k=1}^m$ are prescribed in the fixed domain $\Omega = [-1, 1]^3$. For a fixed right-hand side f , associated with each of these structures are the boundary-value problems (4.31) and (4.33) (with the substitutions $\tilde{\sigma} = \tilde{\sigma}_k$ in each case).

Within this section, to avoid confusion of exact and numerical solutions of perturbed and unperturbed PDEs, a discrete approximation of a continuous function ϕ on a grid as described in Section 4.1 is denoted Φ rather than the customary ϕ^h . Thus,

Φ approximates ϕ , where $-\operatorname{div}(\sigma \operatorname{grad} \phi) = f$ and

$\tilde{\Phi}_k$ approximates $\tilde{\phi}_k$, where $-\operatorname{div}(\tilde{\sigma}_k \operatorname{grad} \tilde{\phi}_k) = f$ ($k = 1, \dots, m$).

Solving the preceding $m + 1$ numerical problems and computing the relative discrepancies

$$\frac{\|\tilde{\Phi}_k - \Phi\|_p}{\|\Phi\|_p} \text{ and } \frac{\|\operatorname{grad}(\tilde{\Phi}_k - \Phi)\|_p}{\|\operatorname{grad} \Phi\|_p} \quad (4.40)$$

in suitable discrete norms gives some estimation of the effect of the family of perturbations $\{\tilde{\sigma}_k\}_{k=1}^m$ on reference solution ϕ . It is assumed that the dis-

cretization is sufficiently accurate that the numerical discrepancies $\|\tilde{\Phi}_k - \Phi\|_p$ provide reasonable information about the analytic discrepancies $\|\tilde{\phi}_k - \phi\|_p$.

The cell-centered finite-volume discretization coinciding with the (2,2) block of A^h in (4.28b) is applied in the experiments with a homogeneous Neumann boundary condition (i.e. $\partial\Omega_D = \emptyset$ in (4.31b) and $\partial\Omega_N = \partial\Omega$ in (4.31c)). The right-hand sides vectors f^h are generated randomly. The resulting linear systems are solved with Dendy's BOXMG multigrid solver [35, 36]. For the purpose of comparison, discrete \mathcal{L}_∞ -, \mathcal{L}_1 - and \mathcal{L}_2 -norms for cell-centered grid functions are respectively given by

$$\|\Phi\|_\infty = \max_{1 \leq i \leq N_x, 1 \leq j \leq N_y, 1 \leq k \leq N_z} |\Phi_{i,j,k}|, \quad (4.41a)$$

$$\|\Phi\|_1 = \sum_{i=1}^{N_x} \sum_{j=1}^{N_y} \sum_{k=1}^{N_z} h_i^x h_j^y h_k^z |\Phi_{i,j,k}|, \quad (4.41b)$$

$$\|\Phi\|_2 = \left(\sum_{i=1}^{N_x} \sum_{j=1}^{N_y} \sum_{k=1}^{N_z} h_i^x h_j^y h_k^z |\Phi_{i,j,k}|^2 \right)^{\frac{1}{2}}. \quad (4.41c)$$

Two particular reference coefficients are used in the experiments. The first is a model of a diffusive half-space

$$\sigma_{HS}(x, y, z) := \begin{cases} \sigma_{air} & z > 0, \\ \sigma_{ground} & z < 0, \end{cases} \quad (4.42a)$$

for some positive scalars σ_{air} and σ_{ground} . For experiments with $\sigma = \sigma_{HS}$, the coefficient in the air is fixed as $\sigma_{air} = 10^{-7}\text{S/m}$. This test case is not difficult to solve numerically, although the jumps in σ may be quite large. The simple geometry suffices to see the effect of moving the interface.

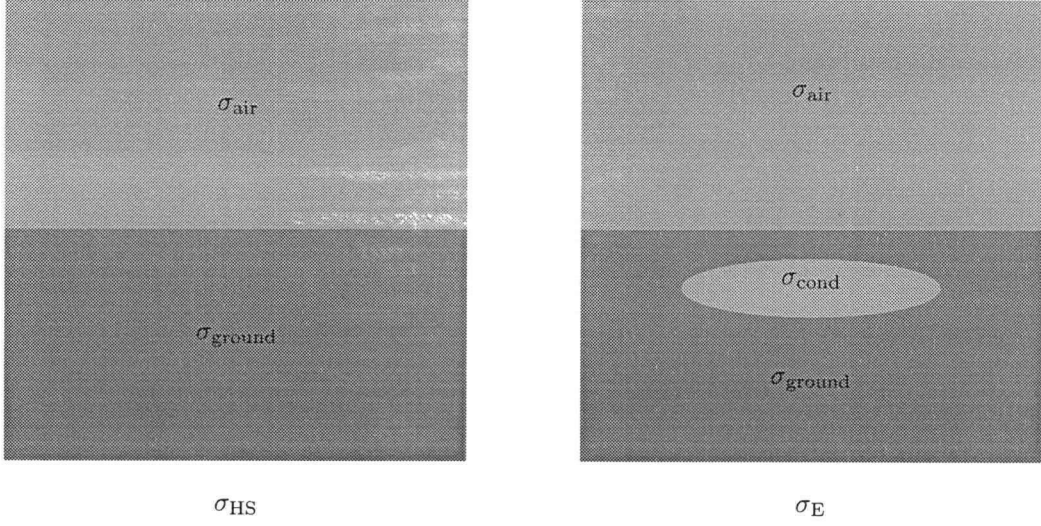


Figure 4.5: Cross-sections of σ_{HS} and σ_{E} for perturbation experiments.

For a more complicated geometry, consider also the coefficient σ_{E} describing a diffusive ellipsoid buried in a half-space. In this model,

$$\sigma_{\text{E}}(x, y, z) := \begin{cases} \sigma_{\text{air}} & z > 0, \\ \sigma_{\text{cond}} & \frac{x^2}{a^2} + \frac{y^2}{b^2} + \frac{(z+z_0)^2}{c^2} < 1, \\ \sigma_{\text{ground}} & z < 0, \end{cases} \quad (4.42\text{b})$$

for some positive constants σ_{cond} , a , b , c , and z_0 with $z_0 \geq c$. The values $\sigma_{\text{air}} = 10^{-8}\text{S/m}$, $\sigma_{\text{ground}} = 10^{-3}\text{S/m}$, $a = b = 0.5$, and $c = z_0 = 0.25$ are fixed in experiments. The diffusion coefficient σ_{E} is particularly useful for a more critical evaluation of grid effects because the Cartesian grid cannot resolve the curved ellipsoid accurately. Cross-sections of the models σ_{HS} and σ_{E} are illustrated in Figure 4.5.

Based on the reference coefficients (4.42), a first family of perturbations to consider is based on vertical shifts of the reference model by individual grid

σ_{ground}	Norm	$\Phi - \tilde{\Phi}_1$	$\Phi - \tilde{\Phi}_2$	$\Phi - \tilde{\Phi}_3$	$\Phi - \tilde{\Phi}_4$	Rate
10^{-4}	$\ \cdot\ _\infty$	1.451×10^{-1}	2.440×10^{-1}	2.440×10^{-1}	2.902×10^{-1}	0.574
	$\ \cdot\ _1$	4.337×10^{-2}	8.953×10^{-2}	1.346×10^{-1}	1.788×10^{-1}	1.033
	$\ \cdot\ _2$	3.803×10^{-2}	7.569×10^{-2}	1.126×10^{-1}	1.492×10^{-1}	0.989
10^{-3}	$\ \cdot\ _\infty$	1.112×10^{-1}	1.868×10^{-1}	1.942×10^{-1}	2.495×10^{-1}	0.613
	$\ \cdot\ _1$	4.283×10^{-2}	8.340×10^{-2}	1.250×10^{-1}	1.648×10^{-1}	0.969
	$\ \cdot\ _2$	4.072×10^{-2}	8.207×10^{-2}	1.256×10^{-1}	1.686×10^{-1}	1.020
10^{-2}	$\ \cdot\ _\infty$	2.553×10^{-1}	4.091×10^{-1}	4.491×10^{-1}	4.995×10^{-1}	0.560
	$\ \cdot\ _1$	5.810×10^{-2}	1.043×10^{-1}	1.491×10^{-1}	1.920×10^{-1}	0.855
	$\ \cdot\ _2$	6.204×10^{-2}	1.108×10^{-1}	1.555×10^{-1}	1.983×10^{-1}	0.837
10^{-1}	$\ \cdot\ _\infty$	1.562×10^{-1}	3.036×10^{-1}	3.535×10^{-1}	3.820×10^{-1}	0.782
	$\ \cdot\ _1$	3.319×10^{-2}	7.126×10^{-2}	1.104×10^{-1}	1.480×10^{-1}	1.092
	$\ \cdot\ _2$	3.474×10^{-2}	7.007×10^{-2}	1.051×10^{-1}	1.379×10^{-1}	1.005
10^0	$\ \cdot\ _\infty$	2.292×10^{-1}	3.573×10^{-1}	5.050×10^{-1}	5.210×10^{-1}	0.651
	$\ \cdot\ _1$	8.344×10^{-2}	1.598×10^{-1}	2.299×10^{-1}	3.051×10^{-1}	0.932
	$\ \cdot\ _2$	7.582×10^{-2}	1.435×10^{-1}	2.055×10^{-1}	2.709×10^{-1}	0.916

σ_{ground}	Norm	$\nabla\Phi - \nabla\tilde{\Phi}_1$	$\nabla\Phi - \nabla\tilde{\Phi}_2$	$\nabla\Phi - \nabla\tilde{\Phi}_3$	$\nabla\Phi - \nabla\tilde{\Phi}_4$	Rate
10^{-4}	$\ \cdot\ _\infty$	6.852×10^{-1}	8.764×10^{-1}	8.765×10^{-1}	8.765×10^{-1}	0.252
	$\ \cdot\ _1$	3.371×10^{-2}	6.312×10^{-2}	9.094×10^{-2}	1.182×10^{-1}	0.904
	$\ \cdot\ _2$	1.187×10^{-1}	1.887×10^{-1}	2.399×10^{-1}	2.815×10^{-1}	0.644
10^{-3}	$\ \cdot\ _\infty$	6.057×10^{-1}	7.630×10^{-1}	8.469×10^{-1}	8.469×10^{-1}	0.293
	$\ \cdot\ _1$	3.524×10^{-2}	6.888×10^{-2}	1.008×10^{-1}	1.321×10^{-1}	0.959
	$\ \cdot\ _2$	1.176×10^{-1}	1.911×10^{-1}	2.437×10^{-1}	2.881×10^{-1}	0.670
10^{-2}	$\ \cdot\ _\infty$	6.487×10^{-1}	8.427×10^{-1}	8.427×10^{-1}	8.427×10^{-1}	0.268
	$\ \cdot\ _1$	3.682×10^{-2}	6.905×10^{-2}	9.844×10^{-2}	1.269×10^{-1}	0.898
	$\ \cdot\ _2$	1.233×10^{-1}	1.954×10^{-1}	2.461×10^{-1}	2.901×10^{-1}	0.637
10^{-1}	$\ \cdot\ _\infty$	6.320×10^{-1}	9.176×10^{-1}	9.176×10^{-1}	9.176×10^{-1}	0.382
	$\ \cdot\ _1$	3.548×10^{-2}	6.699×10^{-2}	9.637×10^{-2}	1.238×10^{-1}	0.909
	$\ \cdot\ _2$	1.190×10^{-1}	1.903×10^{-1}	2.435×10^{-1}	2.854×10^{-1}	0.653
10^0	$\ \cdot\ _\infty$	6.164×10^{-1}	7.705×10^{-1}	7.705×10^{-1}	7.705×10^{-1}	0.229
	$\ \cdot\ _1$	3.545×10^{-2}	6.660×10^{-2}	9.627×10^{-2}	1.245×10^{-1}	0.908
	$\ \cdot\ _2$	1.234×10^{-1}	1.921×10^{-1}	2.452×10^{-1}	2.889×10^{-1}	0.626

Table 4.1: Half-space coefficient σ_{HS} : results with vertical shifts

cells of height h . That is,

$$\tilde{\sigma}_k(x, y, z) = \sigma(x, y, z - kh) \quad (k = 1, \dots, m). \quad (4.43)$$

Tables 4.1 and 4.2 present results of applying this family of perturbations (4.43) to both σ_{HS} and σ_{E} on a grid of $72 \times 72 \times 72$ cells. The rates of convergence are computed in each row are found by averaging

$$\frac{\ln \|\Phi - \tilde{\Phi}_k\| - \ln \|\Phi - \tilde{\Phi}_1\|}{\ln k} \quad (k > 1)$$

across each row (with a similar definition for the gradients).

The second set of perturbed coefficients is generated by resolving the reference model on successively coarser grids. That is, given σ resolved on a fine grid of spacing h , $\tilde{\sigma}_k$ is obtained by resolving σ on a grid $(k+1)$ times as coarse (i.e. of spacing $(k+1)h$) and injecting the values back into the original fine mesh (see Figure 4.6). The solutions Φ and $\tilde{\Phi}_k$ are then computed and compared on the same fine grid of $72 \times 72 \times 72$ cells. Table 4.3 gives results of using this family of perturbations with the ellipsoid model σ_{E} .

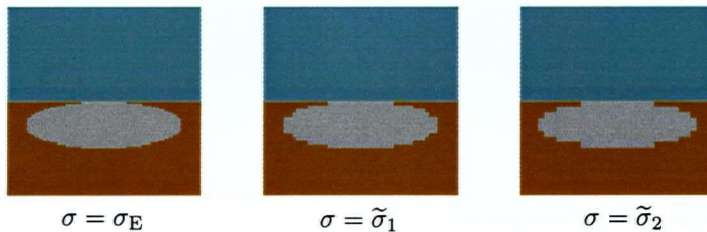


Figure 4.6: Cross-sections of ellipsoid coefficient σ_{E} resolved on fine and coarse grids.

The experiments of Tables 4.1 and 4.2 support the hypothesis that a perturbation $\tilde{\sigma} - \sigma$ of $O(h)$ support induces a perturbation $\tilde{\phi} - \phi$ of $O(h)$ in the

σ_{ground}	Norm	$\Phi - \tilde{\Phi}_1$	$\Phi - \tilde{\Phi}_2$	$\Phi - \tilde{\Phi}_3$	$\Phi - \tilde{\Phi}_4$	Rate
10^{-2}	$\ \cdot\ _\infty$	1.620×10^{-1}	2.986×10^{-1}	3.101×10^{-1}	4.645×10^{-1}	0.744
	$\ \cdot\ _1$	3.458×10^{-2}	6.932×10^{-2}	1.106×10^{-1}	1.561×10^{-1}	1.049
	$\ \cdot\ _2$	4.507×10^{-2}	8.541×10^{-2}	1.267×10^{-1}	1.692×10^{-1}	0.939
10^{-1}	$\ \cdot\ _\infty$	2.241×10^{-1}	3.171×10^{-1}	4.010×10^{-1}	4.536×10^{-1}	0.513
	$\ \cdot\ _1$	3.120×10^{-2}	6.644×10^{-2}	1.050×10^{-1}	1.420×10^{-1}	1.096
	$\ \cdot\ _2$	4.416×10^{-2}	8.414×10^{-2}	1.239×10^{-1}	1.630×10^{-1}	0.937
10^0	$\ \cdot\ _\infty$	1.630×10^{-1}	2.688×10^{-1}	3.323×10^{-1}	3.673×10^{-1}	0.652
	$\ \cdot\ _1$	3.673×10^{-2}	7.358×10^{-2}	1.097×10^{-1}	1.455×10^{-1}	0.997
	$\ \cdot\ _2$	4.546×10^{-2}	8.837×10^{-2}	1.286×10^{-1}	1.663×10^{-1}	0.947
10^1	$\ \cdot\ _\infty$	1.446×10^{-1}	2.498×10^{-1}	3.145×10^{-1}	3.617×10^{-1}	0.719
	$\ \cdot\ _1$	6.289×10^{-2}	1.312×10^{-1}	2.008×10^{-1}	2.706×10^{-1}	1.057
	$\ \cdot\ _2$	5.667×10^{-2}	1.168×10^{-1}	1.780×10^{-1}	2.392×10^{-1}	1.041
10^2	$\ \cdot\ _\infty$	1.548×10^{-1}	2.905×10^{-1}	3.420×10^{-1}	3.823×10^{-1}	0.760
	$\ \cdot\ _1$	3.868×10^{-2}	7.754×10^{-2}	1.159×10^{-1}	1.544×10^{-1}	1.000
	$\ \cdot\ _2$	4.444×10^{-2}	8.672×10^{-2}	1.276×10^{-1}	1.681×10^{-1}	0.962

σ_{ground}	Norm	$\nabla\Phi - \nabla\tilde{\Phi}_1$	$\nabla\Phi - \nabla\tilde{\Phi}_2$	$\nabla\Phi - \nabla\tilde{\Phi}_3$	$\nabla\Phi - \nabla\tilde{\Phi}_4$	Rate
10^{-2}	$\ \cdot\ _\infty$	6.481×10^{-1}	8.785×10^{-1}	8.785×10^{-1}	8.785×10^{-1}	0.312
	$\ \cdot\ _1$	3.799×10^{-2}	7.093×10^{-2}	1.011×10^{-1}	1.307×10^{-1}	0.894
	$\ \cdot\ _2$	1.278×10^{-1}	1.992×10^{-1}	2.498×10^{-1}	2.939×10^{-1}	0.617
10^{-1}	$\ \cdot\ _\infty$	6.982×10^{-1}	8.153×10^{-1}	8.153×10^{-1}	8.636×10^{-1}	0.173
	$\ \cdot\ _1$	3.678×10^{-2}	6.962×10^{-2}	1.001×10^{-1}	1.303×10^{-1}	0.915
	$\ \cdot\ _2$	1.243×10^{-1}	1.988×10^{-1}	2.508×10^{-1}	2.972×10^{-1}	0.648
10^0	$\ \cdot\ _\infty$	6.181×10^{-1}	7.459×10^{-1}	8.274×10^{-1}	8.274×10^{-1}	0.249
	$\ \cdot\ _1$	3.890×10^{-2}	7.391×10^{-2}	1.044×10^{-1}	1.322×10^{-1}	0.903
	$\ \cdot\ _2$	1.257×10^{-1}	2.023×10^{-1}	2.549×10^{-1}	2.964×10^{-1}	0.650
10^1	$\ \cdot\ _\infty$	6.288×10^{-1}	8.107×10^{-1}	8.357×10^{-1}	8.513×10^{-1}	0.281
	$\ \cdot\ _1$	3.624×10^{-2}	6.980×10^{-2}	1.003×10^{-1}	1.296×10^{-1}	0.931
	$\ \cdot\ _2$	1.200×10^{-1}	1.973×10^{-1}	2.489×10^{-1}	2.948×10^{-1}	0.676
10^2	$\ \cdot\ _\infty$	6.278×10^{-1}	9.572×10^{-1}	9.572×10^{-1}	9.572×10^{-1}	0.432
	$\ \cdot\ _1$	4.064×10^{-2}	7.712×10^{-2}	1.103×10^{-1}	1.424×10^{-1}	0.913
	$\ \cdot\ _2$	1.258×10^{-1}	2.044×10^{-1}	2.582×10^{-1}	3.040×10^{-1}	0.664

Table 4.2: Ellipsoid coefficient σ_E : results with vertical shifts

\mathcal{L}_1 - and \mathcal{L}_2 -norms. Further, the \mathcal{L}_2 -norm field $\mathbf{grad}(\tilde{\phi} - \phi)$ seems to decrease with h at a rate close to $O(h^{\frac{1}{2}})$ and clearly less than $O(h)$, consistent with the prediction of Proposition 4.1. There is a marked difference in the convergence of the \mathcal{L}_{∞} -norms of $\Phi - \tilde{\Phi}_k$ versus the other norms; this is indicative of the fact that the difference is very strongly concentrated near the set S^h and rapidly decays away from there.

Measurement of convergence rates in Table 4.3 is not as straightforward where the ellipsoidal model σ_E is resolved on a family of successively coarser grids. However, it is reassuring to notice that the relative differences in the numerical solutions are extremely small even with the coarse resolution of the ellipsoid's curvature. The results shown here demonstrate that staircasing is not as problematic in diffusive problems as it is in dispersive ones; such is the case for Maxwell's equations considered at sufficiently low frequencies also.

σ_{ground}	Norm	$\Phi - \tilde{\Phi}_1$	$\Phi - \tilde{\Phi}_2$	$\Phi - \tilde{\Phi}_3$	Rate
10^{-2}	$\ \cdot\ _\infty$	1.331×10^{-6}	2.148×10^{-6}	2.190×10^{-6}	0.572
	$\ \cdot\ _1$	3.321×10^{-6}	6.001×10^{-6}	4.060×10^{-6}	0.518
	$\ \cdot\ _2$	1.779×10^{-6}	3.221×10^{-6}	2.240×10^{-6}	0.533
10^{-1}	$\ \cdot\ _\infty$	1.400×10^{-6}	1.775×10^{-6}	1.860×10^{-6}	0.300
	$\ \cdot\ _1$	1.705×10^{-7}	3.447×10^{-7}	4.141×10^{-7}	0.911
	$\ \cdot\ _2$	2.107×10^{-7}	3.567×10^{-7}	4.603×10^{-7}	0.735
10^0	$\ \cdot\ _\infty$	2.232×10^{-6}	4.279×10^{-6}	4.287×10^{-6}	0.294
	$\ \cdot\ _1$	3.410×10^{-7}	7.221×10^{-7}	1.078×10^{-6}	1.074
	$\ \cdot\ _2$	4.398×10^{-7}	7.566×10^{-7}	1.073×10^{-6}	0.726
10^1	$\ \cdot\ _\infty$	1.999×10^{-6}	2.476×10^{-6}	2.715×10^{-6}	0.326
	$\ \cdot\ _1$	2.270×10^{-7}	4.901×10^{-7}	7.111×10^{-7}	1.260
	$\ \cdot\ _2$	3.252×10^{-7}	5.337×10^{-7}	7.311×10^{-7}	0.850
10^2	$\ \cdot\ _\infty$	2.147×10^{-6}	2.506×10^{-6}	3.443×10^{-6}	0.767
	$\ \cdot\ _1$	2.473×10^{-7}	5.977×10^{-7}	9.732×10^{-7}	1.065
	$\ \cdot\ _2$	3.632×10^{-7}	6.437×10^{-7}	9.497×10^{-7}	0.797

σ_{ground}	Norm	$\nabla\Phi - \nabla\tilde{\Phi}_2$	$\nabla\Phi - \nabla\tilde{\Phi}_3$	$\nabla\Phi - \nabla\tilde{\Phi}_4$	Rate
10^{-2}	$\ \cdot\ _\infty$	4.985×10^{-6}	6.917×10^{-6}	7.087×10^{-6}	0.396
	$\ \cdot\ _1$	3.906×10^{-7}	6.271×10^{-7}	8.363×10^{-7}	0.688
	$\ \cdot\ _2$	1.104×10^{-6}	1.495×10^{-6}	1.858×10^{-6}	0.456
10^{-1}	$\ \cdot\ _\infty$	5.803×10^{-6}	6.446×10^{-6}	6.721×10^{-6}	0.143
	$\ \cdot\ _1$	4.631×10^{-7}	7.136×10^{-7}	9.450×10^{-7}	0.637
	$\ \cdot\ _2$	1.300×10^{-6}	1.730×10^{-6}	2.101×10^{-6}	0.425
10^0	$\ \cdot\ _\infty$	6.574×10^{-6}	1.107×10^{-5}	1.107×10^{-5}	0.613
	$\ \cdot\ _1$	4.770×10^{-7}	7.398×10^{-7}	9.938×10^{-7}	0.651
	$\ \cdot\ _2$	1.306×10^{-6}	1.784×10^{-6}	2.178×10^{-6}	0.458
10^1	$\ \cdot\ _\infty$	5.781×10^{-6}	6.386×10^{-6}	6.655×10^{-6}	0.136
	$\ \cdot\ _1$	4.456×10^{-7}	7.039×10^{-7}	9.403×10^{-7}	0.670
	$\ \cdot\ _2$	1.300×10^{-6}	1.737×10^{-6}	2.122×10^{-6}	0.432
10^2	$\ \cdot\ _\infty$	6.546×10^{-6}	6.566×10^{-6}	7.256×10^{-6}	0.049
	$\ \cdot\ _1$	4.550×10^{-7}	7.127×10^{-7}	9.808×10^{-7}	0.673
	$\ \cdot\ _2$	1.309×10^{-6}	1.733×10^{-6}	2.153×10^{-6}	0.429

Table 4.3: Ellipsoid coefficient σ_E : results with fine & coarse resolutions

Chapter 5

Construction and Analysis of Iterative Solvers

Since the frequency-domain problem (3.1) needs to be solved many times for various frequencies and sources within a single geophysical inverse problem, the major objective of this work is to construct fast solvers for the forward-modeling problem. A major obstacle in achieving this goal is the ill-conditioning of the corresponding discretizations due to the near-vanishing conductivity σ in a large portion of the domain. Another obstacle is the strong coupling between solution components as a result of the double-**curl** PDE operator in (3.1a). Finally, the presence of strong discontinuities in the coefficients σ (and possibly μ) contributes also to ill-conditioning in the linear systems that can inhibit solver performance. The PDE formulation and discretization in preceding chapters deal with these concerns in part. It remains to find robust algorithms for the solution of the linear algebraic equations.

Among iterative methods for solving linear systems of algebraic equations, two particular families stand out for this application: preconditioned

Krylov-subspace methods [10, 49, 93] and multigrid methods [19, 18, 22, 56]. In considering these strategies, a particular multigrid preconditioner approximating the dominant diagonal blocks of the coefficient matrix is a natural choice for an iterative solver. After development of a Fourier analysis in the spirit of [17, 24, 38] to determine bounds of the spectrum of the preconditioned system under certain assumptions, some numerical experiments demonstrate the efficacy of this solver.

5.1 Iterative Methods

With the analytic reformulation of (3.1) as the boundary-value problem (3.31), the discretization (4.28) derived in Chapter 4 yields a set of equations

$$Ax = b \tag{5.1}$$

describing the discrete fields (\mathbf{A}^h, ϕ^h) over a three-dimensional domain. For a typical problem using a grid of $40 \times 40 \times 40$ cells, there are over 250,000 complex unknowns to determine. In the absence of unusual structure in the sparse coefficient matrix, problems of this size rule out direct solvers, so iterative solvers are required for (5.1).

5.1.1 Preconditioned Krylov-Subspace Methods

With a lexicographic ordering to the unknowns (\mathbf{A}^h, ϕ^h) , the basic block

structure of the coefficient matrix A in (5.1) is

$$A = \begin{pmatrix} A_{11} - \omega B_{11} & -\omega B_{12} \\ B_{21} & A_{22} \end{pmatrix} \quad (5.2)$$

In the general case, A_{11} is a matrix representation of the real discrete difference operator

$$\mathcal{L}_\mu^h = \mathbf{curl}_e^h(\mu_e^h)^{-1} \mathbf{curl}_f^h - \mathbf{grad}^h(\mu_c^h)^{-1} \mathbf{div}^h$$

as in (4.28c). The operator has a 19-point stencil that simplifies to a 7-point stencil for the vector Laplacian operator in the case that $\mu \equiv \mu_0$, as in (4.29). The block A_{22} represents the difference operator $\mathbf{div}^h \hat{\sigma}^h \mathbf{grad}^h$ as in (4.28), while the matrix blocks B_{11} , B_{12} , and B_{21} are discrete representations of lower-order operators. Given that the diagonal blocks A_{11} and A_{22} correspond to discretizations of second-order differential operators, for a sufficiently fine grid, these blocks are dominant. This dominance is strongly dependent on the frequency ω ; for high frequencies, the grid spacing h has to be quite small to ensure dominance of A_{11} in the top block row of (5.2).

With suitable boundary conditions and scaling, the coefficient matrix A in (5.2) is complex symmetric, but non-Hermitian and indefinite. As such, the well-known method of conjugate gradients and the associated theory cannot be applied to solve the system of linear equations [49, 61, 93]. Even so, non-Hermitian Krylov-subspace iterations such as BiCGStab or GMRES are known to perform well for a wide range of applications with suitable preconditioners (i.e. matrices M such that M approximates A^{-1}) to improve convergence behavior (e.g. [38, 87, 62]).

As a simple example of a preconditioner for (5.1), consider a single step of SSOR (Symmetric Successive Over-Relaxation [34, 10]). Like other preconditioners based on a single step of a classical, stationary iterative method, an SSOR preconditioner is simple to implement, requiring only knowledge of the splitting

$$A = D - L - U, \quad (5.3a)$$

where L and U are strictly lower- and upper-triangular matrices and D is a diagonal matrix. With the splitting (5.3a), the SSOR preconditioner is

$$M_S(\alpha) := (D - \alpha U)^{-1}(\alpha L + (1 - \alpha)D)(D - \alpha L)^{-1}(\alpha U + (1 - \alpha)D), \quad (5.3b)$$

where $\alpha \in (0, 2)$ is the relaxation parameter¹[10]. For certain second-order elliptic PDE problems, a choice of the relaxation parameter α_{opt} exists that reduces the spectral condition number of $\text{cond}(M_S(\alpha_{\text{opt}})A)$ optimally; however, practical computation of α_{opt} requires information about the spectrum of A that is prohibitively expensive [48]. If the forward-modeling problem (5.1) must be solved repeatedly for many different frequencies ω , the preconditioner $M_S(\alpha)$ must be computed for each ω since both D and U in (5.3a) depend on ω .

The block structure of A suggests a different preconditioner. Given the diagonal dominance of the blocks A_{11} and A_{22} in (5.2), the matrix

$$M_E := \begin{pmatrix} A_{11}^{-1} \\ & A_{22}^{-1} \end{pmatrix} \quad (5.4)$$

¹The relaxation parameter is denoted with α here rather than the customary symbol ω to avoid confusion with the frequency.

is an approximation of A^{-1} to leading order. The frequency dependent blocks ωB_{11} , ωB_{22} , and ωB_{12} are ignored in defining M_E in (5.4). If numerous systems of the form (5.1) need to be solved for different frequencies, since M_E is independent of ω , then only a single *LU*-factorization of M_E need be computed and stored.

Of course, for large three-dimensional problems, computing M_E exactly by *LU*-factorization of A_{ii} is almost as much work as doing computing an *LU*-factorization of A itself. As such, some approximation of M_E is sought. A well-known method for doing this is through applying *ILU* (Incomplete *LU*) factorizations to the diagonal blocks of A (e.g. [93, Chap. 10]). That is, rather than finding the exact *LU*-factorizations of A_{11} and A_{22} , approximate factors

$$\tilde{L}_{11}\tilde{U}_{11} \simeq A_{11} \text{ and } \tilde{L}_{22}\tilde{U}_{22} \simeq A_{22}$$

are computed. The triangular factors \tilde{L}_{ii} and \tilde{U}_{ii} ($i = 1, 2$) are computed as in the usual *LU*-factorization, and either fill elements below a prescribed drop tolerance are rejected (*ILU* with a threshold) or all fill elements are disregarded (*ILU(0)*). The block-*ILU* preconditioner

$$M_I := \begin{pmatrix} \tilde{L}_{11}\tilde{U}_{11} & \\ & \tilde{L}_{22}\tilde{U}_{22} \end{pmatrix}^{-1} \quad (5.5)$$

turns out to be an effective approximation of M_E that in turn approximates A^{-1} for sufficiently low frequencies. By ignoring the off-diagonal blocks of A , computing M_I requires much less work and storage than a similar *ILU*-factorization of A .

The efficacy of the ILU factorization approximating M_E comes in part from some additional structure; in particular, both of the blocks of M_E come from the discretization of second-order elliptic differential equations. For such problems, *multigrid methods* have been extensively studied and developed that exploit the smoothing properties of the underlying elliptic operators [19, 18, 56, 113]. As an alternative to applying a preconditioned Krylov-subspace iteration to solve the linear system (5.1), a full multigrid method could be developed to solve the system (4.28). That is, a multigrid method could approximate the inverse of A directly in (5.1) rather than choosing a preconditioner M and applying a Krylov-subspace iteration. Such a full multigrid method could be derived through traditional geometric arguments from the discrete operator in (4.28), or algebraically directly from the matrix representation A in (5.1). The geometric-multigrid approach is somewhat difficult for systems of PDEs discretized on a staggered grid; development of the inter-grid transfer operators is fairly straightforward, but distributive smoothers in three dimensions require more effort [18, 17]. The algebraic-multigrid approach is more amenable to a black-box implementation and is adaptable to unstructured grids as well; however, in algebraic-multigrid solvers, the construction of a hierarchy of coarse grids is not obvious and the theoretical details are often more complicated than for geometric multigrid [92]. The results of an experiment applying an AMG solver are documented in Section 5.4.

A sensible middle ground adopted here is to apply a multigrid method as a preconditioner for a Krylov-subspace iteration [114, 9, 32, 62, 108]. In

this particular case, a practical multigrid preconditioner M_M approximates the action of M_E in (5.4) by a multigrid method. That is,

$$M_M := \begin{pmatrix} \widetilde{M}_{11} & \\ & \widetilde{M}_{22} \end{pmatrix}, \quad (5.6)$$

where \widetilde{M}_{ii} represents the action of a single multigrid V(2,1)-cycle approximating the action of A_{ii}^{-1} ($i=1,2$). For a homogeneous permeability $\mu \equiv \mu_0$, the block A_{11} in (5.2) reduces to a 3×3 block-diagonal matrix. In that case, the block preconditioner M_E is a 4×4 block-diagonal matrix, as are M_I in (5.5) and M_M in (5.6). The multigrid preconditioner, then, is

$$M_M := \begin{pmatrix} M_{11} & & & \\ & M_{22} & & \\ & & M_{33} & \\ & & & M_{44} \end{pmatrix}. \quad (5.7)$$

The diagonal blocks of M_M in (5.7) represent the action of multigrid methods for solving four uncoupled PDE problems in the scalar fields A^x , A^y , A^z , and ϕ (specifically, three Poisson problems and one inhomogeneous diffusion problem). Constructing M_M in (5.7) is simpler than in (5.6) because \widetilde{M}_{11} requires building a multigrid solver for a 3×3 coupled PDE system discretized on a staggered grid. The preconditioner M_M in (5.7) is analyzed in the next section. For the practical implementation in the experiments of Section 5.4, a black-box multigrid solver—in particular, the code BOXMG of Dendy [35, 36]—is applied.

5.2 Analytical Framework

To better understand the preconditioner M_E , consider the system (3.31) and its discretization (5.1) under simplifying assumptions that ensure that the eigenvectors of all the blocks of A are Fourier modes. That is, for discrete wavenumbers $0 \leq \alpha, \beta, \gamma \leq n - 1$, the grid function $\psi^{\alpha\beta\gamma}$ given by

$$\psi_{ijk}^{\alpha\beta\gamma} := e^{(2\pi\alpha ih)\imath} e^{(2\pi\beta jh)\imath} e^{(2\pi\gamma kh)\imath} \quad i, j, k = 0, 1, \dots, n - 1 \quad (5.8)$$

should be an eigenvector of all the blocks of A in (5.1). This is true under the assumptions:

1. The boundary conditions are periodic.
2. The grid is uniform.
3. The material properties σ , μ , and ϵ are all constant.

Under the first assumption, upon discretization, the indexing is done in arithmetic modulo n . For instance, grid points on, say, the top boundary are identified with opposite points on the bottom boundary, and centers of cells touching the top boundary are considered as neighbors of centers of cells touching the bottom boundary. The scalar grid functions A^{xh} , A^{yh} , A^{zh} , and ϕ^h each consist of $N := n^3$ unknowns, the matrix blocks are square of dimension $N \times N$, and the resulting system to be solved has dimension $4N \times 4N$.

The first assumption seems unreasonable in light of the boundary conditions (3.32) actually implemented. However, for a class of realistic geophysical

problems, the fields are expected to vanish or decay in the absence of source currents, and the sources are frequently of compact support. Thus, for a sufficiently large domain Ω , the effect of boundary data on the fields inside the domain is often negligible. In such cases, the assumption of periodicity in the following analysis is particularly reasonable and does not compromise the model.

Further, as in Section 2.2.4, make the quasistatic assumption $\hat{\sigma} = \sigma$ and make a slight regularizing assumption

$$\sigma \leftarrow \max(\sigma, \sigma_{\text{air}}), \quad (5.9)$$

with $\sigma_{\text{air}} > 0$ small (on the order of 10^{-9} to 10^{-6} S/m). The regularizing assumption (5.9) ensures $\sigma \neq 0$ everywhere (which would not be the case ordinarily in the air). These assumptions simplify the presentation without loss of essence in the obtained theoretical results. In the experiments reported in Section 5.4, these simplifying assumptions on σ are relaxed as are most other assumptions of the present section.

5.2.1 Discrete Operators on a Periodic Grid

With the preceding assumptions, the matrix (4.28) reduces to (4.29) since the permeability μ is constant. Furthermore, since the conductivity σ is also constant, the block matrix $\hat{\sigma}^h$ reduces to σI . The entire coefficient matrix

A can be written as

$$\begin{pmatrix} (\omega\mu_0)^{-1}\Delta^h + \sigma I_N & & & \sigma D_x^h \\ & (\omega\mu_0)^{-1}\Delta^h + \sigma I_N & & \sigma D_y^h \\ & & (\omega\mu_0)^{-1}\Delta^h + \sigma I_N & \sigma D_z^h \\ -\sigma(D_x^h)^* & -\sigma(D_y^h)^* & -\sigma(D_z^h)^* & \sigma\Delta^h \end{pmatrix} \quad (5.10)$$

where the matrices D_x^h , D_y^h , and D_z^h correspond to discretizations of first-order derivative operators with periodic boundary conditions in (5.10). That is, assuming standard lexicographic ordering of the unknowns describing the grid functions, let

$$D^- := \frac{1}{h} \begin{pmatrix} 1 & & & -1 \\ -1 & 1 & & \\ & \ddots & \ddots & \\ & & -1 & 1 \end{pmatrix} \in \mathbb{C}^{n \times n} \quad (5.11)$$

be the matrix for the periodic primitive backwards difference operator in one dimension. Then,

$$\begin{aligned} D_x^h &:= I_n \otimes I_n \otimes D^- \in \mathbb{C}^{N \times N}, \\ D_y^h &:= I_n \otimes D^- \otimes I_n \in \mathbb{C}^{N \times N}, \text{ and} \\ D_z^h &:= D^- \otimes I_n \otimes I_n \in \mathbb{C}^{N \times N}, \end{aligned}$$

where \otimes denotes the conventional Kronecker product (e.g. [34, p. 274]). Likewise, the matrices $-(D_x^h)^*$, $-(D_y^h)^*$, and $-(D_z^h)^*$ in the fourth block row of (5.10) correspond to forward difference operators. Finally, the discretization Δ^h of the Laplacian operator Δ with periodic boundary conditions satisfies

$$\Delta^h = -D_x^h(D_x^h)^* - D_y^h(D_y^h)^* - D_z^h(D_z^h)^*.$$

The primary advantage of considering the discretization (4.28) on a periodic lattice is that the discrete difference operators in (5.10) share common eigenvectors. Explicitly, for $\alpha, \beta, \gamma = 0, \dots, n - 1$, the discrete grid functions $\psi^{\alpha\beta\gamma}$ defined by

$$\psi_{ijk}^{\alpha\beta\gamma} := e^{(2\pi\alpha ih)i} e^{(2\pi\beta j h)j} e^{(2\pi\gamma k h)k} \quad (i, j, k = 0, 1, \dots, n - 1)$$

are common eigenvectors of the difference operators D_x^h , D_y^h , D_z^h , Δ^h , and of the identity matrix I_N . The corresponding eigenvalues are

$$d_x^{\alpha\beta\gamma} := h^{-1} (1 - e^{-(2\alpha\pi h)i}) \text{ for } D_x^h, \quad (5.12a)$$

$$d_y^{\alpha\beta\gamma} := h^{-1} (1 - e^{-(2\beta\pi h)j}) \text{ for } D_y^h, \quad (5.12b)$$

$$d_z^{\alpha\beta\gamma} := h^{-1} (1 - e^{-(2\gamma\pi h)k}) \text{ for } D_z^h, \quad (5.12c)$$

$$\delta^{\alpha\beta\gamma} := -\frac{4}{h^2} (\sin^2(\alpha\pi h) + \sin^2(\beta\pi h) + \sin^2(\gamma\pi h)) \text{ for } \Delta^h. \quad (5.12d)$$

In particular, the nonzero eigenvalues $\delta^{\alpha\beta\gamma}$ of Δ^h satisfy

$$0 < \frac{h^2}{12} \leq -\frac{1}{\delta^{\alpha\beta\gamma}} \leq \frac{1}{16} \quad (\alpha, \beta, \gamma = 0, \dots, n - 1; \alpha^2 + \beta^2 + \gamma^2 > 0) \quad (5.13)$$

for $n \geq 2$. The upper bound of $1/16$ on $-1/\delta^{\alpha\beta\gamma}$ is obtained for a very coarse mesh when $n = 2$; as n increases, this upper bound decreases.

With the eigenvalues (5.12) of the blocks of A in (5.10), determine now the eigenvalues and singular values of the preconditioned iteration matrix $M^{-1}A$, where

$$M := \begin{pmatrix} \Delta^h & & & \\ & \Delta^h & & \\ & & \Delta^h & \\ & & & \sigma\Delta^h \end{pmatrix}. \quad (5.14)$$

The matrix M is *real* and, up to a scalar multiple, consists of the dominant diagonal blocks of the matrix A , excluding the Helmholtz shift σI_N in the first three block rows.

Note that the solution u of $\Delta u = b$ with periodic boundary conditions is determined only up to a constant. Thus, M in (5.14) has a zero eigenvalue of multiplicity four (corresponding to four distinct constant grid functions for A^{x^h} , A^{y^h} , A^{z^h} , and ϕ^h). However, as in [38], if S_0 denotes the space spanned by the constant grid function $\psi^{000} \in \mathbb{C}^N$ and S_0^\perp denotes the orthogonal complement of S_0 in \mathbb{C}^N , then $\Delta^h|_{S_0^\perp}$ is invertible. Further, the operator $(\Delta^h|_{S_0^\perp})^{-1}$ extends to an operator $(\Delta^h)_*^{-1}$ defined over all of \mathbb{C}^N by defining it to be 0 on S_0 . Thus, it makes sense to consider the matrix $M^{-1}A$ restricted to a subspace S that excludes the 4-dimensional constant null-space of M , as in (5.13). Denote this matrix by $M^{-1}A|_S$.

5.3 Spectral Bounds

The goal now is to derive bounds on the eigenvalue range and the l_2 -condition number of $M^{-1}A|_S$; this is possible due to the fact that the blocks of A in (5.10) all share common eigenvectors. The eigenvalues and singular values of this matrix are determined by considering the eigenvalues of a 4×4 matrix with the same structure, as the following lemma indicates.

Lemma 5.1. *Let $A \in \mathbb{C}^{(mn) \times (mn)}$ be a block matrix with blocks $A_{ij} \in \mathbb{C}^{n \times n}$ ($i, j = 1, \dots, m$). Let the blocks A_{ij} all share a common eigenvector $\mathbf{v} \in \mathbb{C}^n$ with corresponding eigenvalues $\alpha_{ij} \in \mathbb{C}$ ($i, j = 1, \dots, m$). Furthermore let*

$B = (\alpha_{ij}) \in \mathbb{C}^{m \times m}$ have the eigenvalues α_{ij} as its elements, and let λ be an eigenvalue of B with an eigenvector $\mathbf{u} \in \mathbb{C}^m$.

Then λ is also an eigenvalue of A with an eigenvector $\mathbf{u} \otimes \mathbf{v}$.

Proof. Although this lemma is standard, the proof is included for completeness. By definition,

$$A_{ij}\mathbf{v} = \alpha_{ij}\mathbf{v} \quad (i, j = 1, 2, \dots, m)$$

$$B\mathbf{u} = \lambda\mathbf{u}.$$

Thus, the i th block of $A(\mathbf{u} \otimes \mathbf{v})$ is

$$\begin{aligned} [A(\mathbf{u} \otimes \mathbf{v})]_i &= \sum_{j=1}^m A_{ij}u_j\mathbf{v} = \sum_{j=1}^m u_j\alpha_{ij}\mathbf{v} \\ &= \lambda u_i\mathbf{v} = \lambda [\mathbf{u} \otimes \mathbf{v}]_i. \end{aligned}$$

□

Next, find the eigenvalues and singular values of the 4×4 matrix corresponding to $M^{-1}A|_S$ in Fourier space. Introduce the parameter

$$\chi := \omega\mu\sigma > 0 \tag{5.15}$$

that has dimensions of L^{-2} , where L is a unit of length.

Lemma 5.2. *Let $dx, dy, dz \in \mathbb{C}$ be prescribed scalars such that $\delta := -dxdx^* - dydy^* - dzdz^* < 0$. Given $\sigma, \chi > 0$, define the complex 4×4 matrix $\widetilde{M}^{-1}\widetilde{A}$,*

where

$$\widetilde{M} := \begin{pmatrix} \delta & & \\ & \delta & \\ & & \delta \\ & & \sigma\delta \end{pmatrix}, \text{ and } \widetilde{A} := \begin{pmatrix} \delta + i\chi & & i\chi dx \\ & \delta + i\chi & i\chi dy \\ & & \delta + i\chi \\ -\sigma dx^* & -\sigma dy^* & -\sigma dz^* & \sigma\delta \end{pmatrix}.$$

Then, the eigenvalues $\tilde{\lambda}$ of $\widetilde{M}^{-1}\widetilde{A}$ are

$$\tilde{\lambda}_1 := 1 + \frac{i}{2\delta} (\chi + \sqrt{\chi(\chi - 4\delta i)}), \quad (5.16a)$$

$$\tilde{\lambda}_2 = \tilde{\lambda}_3 := 1 + \frac{\chi}{\delta} i, \quad (5.16b)$$

$$\tilde{\lambda}_4 := 1 + \frac{i}{2\delta} (\chi - \sqrt{\chi(\chi - 4\delta i)}). \quad (5.16c)$$

Further, the singular values $\tilde{\eta}$ of $\widetilde{M}^{-1}\widetilde{A}$ are

$$\tilde{\eta}_1 := \left[1 + \frac{c}{2} + \frac{1}{2} \sqrt{c(c+4)} \right]^{\frac{1}{2}}, \quad (5.17a)$$

$$\tilde{\eta}_2 = \tilde{\eta}_3 := \left[1 + \frac{\chi^2}{\delta^2} \right]^{\frac{1}{2}}, \quad (5.17b)$$

$$\tilde{\eta}_4 := \left[1 + \frac{c}{2} - \frac{1}{2} \sqrt{c(c+4)} \right]^{\frac{1}{2}}, \quad (5.17c)$$

where $c = c(-\frac{1}{\delta}, \chi) := (-\frac{1}{\delta}) (1 + \chi^2 (1 - \frac{1}{\delta})) > 0$.

Proof. Although the derivation of (5.16) and (5.17) requires tedious algebraic manipulations, the formulae are verifiable directly by inspection. \square

Notice that the eigenvalues and singular values of $\widetilde{M}^{-1}\widetilde{A}$ in Lemma 5.2 depend only on the parameters $\delta > 0$ and χ . Next, derive bounds for $|\tilde{\lambda}|$ and $\tilde{\eta}$ in terms of δ and χ .

Lemma 5.3. Assume $0 < -1/\delta \leq \frac{1}{16}$. Then, the eigenvalues $\tilde{\lambda}$ of $\widetilde{M}^{-1}\widetilde{A}$ given in (5.16) all satisfy

$$0 < \tilde{\lambda}_{\min} \leq |\tilde{\lambda}| \leq \tilde{\lambda}_{\max}$$

for some positive constants that depend on χ but not on δ . Similarly, the singular values $\tilde{\eta}$ given in (5.17) all satisfy

$$0 < \tilde{\eta}_{\min} \leq \tilde{\eta} \leq \tilde{\eta}_{\max}$$

for some positive constants that depend on χ but not on δ . Further, as $\chi \rightarrow \infty$,

$$\frac{\tilde{\lambda}_{\max}}{\tilde{\lambda}_{\min}} = O(\chi^2) \text{ and } \frac{\tilde{\eta}_{\max}}{\tilde{\eta}_{\min}} = O(\chi^2).$$

Proof. Denote $\zeta = \sqrt{\chi^2 + 16\delta^2} > \chi$. From (5.16), it is apparent that

$$|\tilde{\lambda}_1| = \left[\frac{\chi}{4\delta^2} (\chi + \zeta + \sqrt{2\chi}\sqrt{\zeta + \chi}) - \frac{\sqrt{2\chi}}{2\delta} \sqrt{\zeta - \chi} + 1 \right]^{\frac{1}{2}}, \quad (5.18a)$$

$$|\tilde{\lambda}_2| = |\tilde{\lambda}_3| = \left[1 + \frac{\chi^2}{\delta^2} \right]^{\frac{1}{2}}, \quad (5.18b)$$

$$|\tilde{\lambda}_4| = \left[\frac{\chi}{4\delta^2} (\chi + \zeta - \sqrt{2\chi}\sqrt{\zeta + \chi}) + \frac{\sqrt{2\chi}}{2\delta} \sqrt{\zeta - \chi} + 1 \right]^{\frac{1}{2}}. \quad (5.18c)$$

It follows from the analytic expressions in (5.18) that

$$|\tilde{\lambda}_1| \geq |\tilde{\lambda}_2| = |\tilde{\lambda}_3| \geq |\tilde{\lambda}_4|$$

for any valid choices of χ and δ . Examining $|\tilde{\lambda}_1|$ and $|\tilde{\lambda}_4|$ in (5.18a,c) as δ varies over the interval $(-\infty, -16]$, it follows that

$$\tilde{\lambda}_{\max} := \max \left\{ |\tilde{\lambda}_1| : \delta \in (-\infty, -16] \right\} = \left| \tilde{\lambda}_1 \right|_{\delta=-16}, \text{ and} \quad (5.19a)$$

$$\tilde{\lambda}_{\min} := \min \left\{ |\tilde{\lambda}_4| : \delta \in (-\infty, -16] \right\} = \left| \tilde{\lambda}_4 \right|_{\delta=-16}. \quad (5.19b)$$

Thus, using the analytic expressions in (5.19), as $\chi \rightarrow \infty$,

$$\frac{\tilde{\lambda}_{\max}}{\tilde{\lambda}_{\min}} = \left| \frac{\tilde{\lambda}_1}{\tilde{\lambda}_4} \right|_{\delta=-16} = \frac{\chi^2}{256} + 6 + O\left(\frac{1}{\chi^2}\right) = O(\chi^2).$$

Examining the singular values (5.17) in the same manner yields

$$\tilde{\eta}_1 \geq \tilde{\eta}_2 = \tilde{\eta}_3 \geq \tilde{\eta}_4.$$

Thus,

$$\tilde{\eta}_{\max} := \max \{ \tilde{\eta}_1 : \delta \in (-\infty, -16] \} = \tilde{\eta}_1|_{\delta=-16}, \text{ and} \quad (5.20a)$$

$$\tilde{\eta}_{\min} := \min \{ \tilde{\eta}_4 : \delta \in (-\infty, -16] \} = \tilde{\eta}_4|_{\delta=-16}. \quad (5.20b)$$

Hence, the bounds in (5.20) yield

$$\frac{\tilde{\eta}_{\max}}{\tilde{\eta}_{\min}} = \frac{17}{256} \chi^2 + \frac{33}{16} + O\left(\frac{1}{\chi^2}\right) = O(\chi^2).$$

□

Lemma 5.3 indicates that the ratio of the largest to smallest eigenvalues significantly underestimates the ratio of the largest to smallest singular values (which is the ℓ_2 -condition number) in the case that χ is large. In Figure 5.1, the curves plotted are based on the above estimates for the eigenvalue range and the ℓ_2 -condition number of $\tilde{M}^{-1}\tilde{A}$ as a function of χ . Also, Figure 5.1 shows the actual values (in Fourier space) for a given instance $n = 10^4$.

With the bounds established for the 4×4 case, Lemma 5.1 gives the eigenvalues and singular values of the full coefficient matrix $M^{-1}A|_S$.

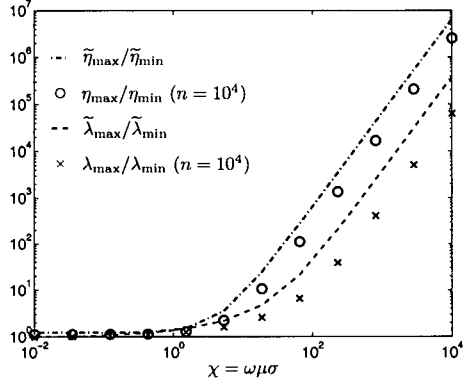


Figure 5.1: Eigenvalue range $\tilde{\lambda}_{\max}/\tilde{\lambda}_{\min}$ and the condition number $\tilde{\eta}_{\max}/\tilde{\eta}_{\min}$ as a function of χ , based on the formulae in Lemma 5.4; also plotted are actual values ($\lambda_{\max}/\lambda_{\min}$ and η_{\max}/η_{\min} , respectively) for $n = 10^4$.

Lemma 5.4. *The eigenvalues of $M^{-1}A|_S$ are given by*

$$\lambda_1^{\alpha\beta\gamma} = 1 + \frac{\imath}{2\delta^{\alpha\beta\gamma}} \left(\chi + \sqrt{\chi(\chi - 4\delta^{\alpha\beta\gamma}\imath)} \right), \quad (5.21a)$$

$$\lambda_2^{\alpha\beta\gamma} = \lambda_3^{\alpha\beta\gamma} := 1 + \frac{\chi}{\delta^{\alpha\beta\gamma}} \imath, \quad (5.21b)$$

$$\lambda_4^{\alpha\beta\gamma} = 1 + \frac{\imath}{2\delta^{\alpha\beta\gamma}} \left(\chi - \sqrt{\chi(\chi - 4\delta^{\alpha\beta\gamma}\imath)} \right) \quad (5.21c)$$

$(\alpha, \beta, \gamma = 0, \dots, n-1; \alpha^2 + \beta^2 + \gamma^2 > 0)$. The singular values of $M^{-1}A|_S$ are given by

$$\eta_1^{\alpha\beta\gamma} := \left[1 + \frac{c^{\alpha\beta\gamma}}{2} + \frac{1}{2} \sqrt{c^{\alpha\beta\gamma}(c^{\alpha\beta\gamma} + 4)} \right]^{\frac{1}{2}}, \quad (5.22a)$$

$$\eta_2^{\alpha\beta\gamma} = \eta_3^{\alpha\beta\gamma} := \left[1 + \frac{\chi^2}{\delta^{\alpha\beta\gamma} 2} \right]^{\frac{1}{2}}, \quad (5.22b)$$

$$\eta_4^{\alpha\beta\gamma} := \left[1 + \frac{c^{\alpha\beta\gamma}}{2} - \frac{1}{2} \sqrt{c^{\alpha\beta\gamma}(c^{\alpha\beta\gamma} + 4)} \right]^{\frac{1}{2}}, \quad (5.22c)$$

where $c^{\alpha\beta\gamma} = c(-\frac{1}{\delta^{\alpha\beta\gamma}}, \chi) := \left(-\frac{1}{\delta^{\alpha\beta\gamma}}\right) \left(1 + \chi^2 \left(1 - \frac{1}{\delta^{\alpha\beta\gamma}}\right)\right) > 0$.

Proof. Apply Lemma 5.1 using the scalar eigenvalues and singular values of

the 4×4 matrix from Lemma 5.2 along with the eigenvalues (5.12) of the difference operators constituting (5.10). \square

Combining the results of the preceding lemmata gives the final result.

Theorem 5.5. *The eigenvalues and singular values of $M^{-1}A|_S$ are bounded above and below independent of the grid size h . Further, the eigenvalue range $\lambda_{\max}/\lambda_{\min}$ and the ℓ_2 -condition number η_{\max}/η_{\min} are bounded independent of the grid, but grow quadratically with the parameter $\chi := \omega\mu\sigma$; i.e.*

$$\frac{\lambda_{\max}}{\lambda_{\min}} = O(\chi^2) \text{ and } \frac{\eta_{\max}}{\eta_{\min}} = O(\chi^2).$$

The practical implication of Theorem 5.5 is that the number of iterations required for convergence (up to a set positive tolerance) of a Krylov method for (5.10) preconditioned by the real parts of the leading blocks is expected to be small and independent of the grid size. As the frequency ω increases in a range where $\omega\mu\sigma \gg 1$, the number of iterations is expected to grow like ω^2 .

The full inversions of the Laplacians on the main block diagonal of M may be prohibitively expensive as a preconditioner. Instead, consider applying just one multigrid cycle. Denote by B the approximate inverse for $M|_S$ obtained in this way. It is well known (e.g. [56, 113]) that for a W -cycle using standard grid transfer and coarse grid operators and a sufficiently good smoothing rate (e.g. two red-black Gauss-Seidel sweeps before and after the coarse grid correction), there is a constant c independent of the grid size such

that

$$\|I - BM|_S\| \leq c < 1.$$

This implies that the condition number of $BM|_S$ is bounded. Writing

$$\text{cond}(BA) \leq \text{cond}(BM|_S) \text{ cond}(M|_S^{-1}A)$$

and applying Theorem 5.5 now yields similar results for the one multigrid cycle preconditioner.

Corollary 5.6. *The condition number of $BA|_S$, the problem matrix preconditioned by one multigrid cycle, is bounded independent of the grid size h . This condition number increases quadratically with the parameter $\chi := \omega\mu\sigma$.*

As a result of the preceding corollary, it is hoped that at low- to mid-range frequencies ω , using a few multigrid W - or V -cycles to approximate the inversion of the diagonal blocks yields a robust preconditioner for the linear system (5.1).

5.4 Numerical Experiments

In the experiments that follow, the parameters $\epsilon = \epsilon_0 = 8.8542 \times 10^{-12}$ F/m and the permittivity $\mu = \mu_0 = 4\pi \times 10^{-7}$ H/m are fixed constants. The grids used are either uniform or exponentially-widening (as described in [6]). The domain Ω is the cube $[-1, 1]^3$ and the homogeneous boundary conditions (3.32) are imposed on $\partial\Omega$ as described in Chapter 3. Although use of the boundary conditions (3.32) requires a domain Ω that is sufficiently

large, the experiments here focus on the performance of iterative solvers based on multigrid algorithms; this is unrelated to the specific boundary conditions implemented [18].

In comparing the performances of BiCGStab, QMR, and GMRES [10] in solving the linear systems of [6], BiCGStab performs significantly better; hence, consistent with the experiments of [6, 53, 54], preconditioned BiCGStab is chosen as the Krylov-subspace solver for the linear systems in the experiments that follow. As a convergence criterion for all BiCGStab iterations, a reduction of the relative residual to within a tolerance of 10^{-7} is required. Results from all experiments are given in terms of iteration counts.

Several preconditioning strategies are compared for performance.

1. Exact solves of diagonal blocks (M_E): The real parts of the diagonal blocks, namely

$$\text{diag}(\Delta^h + \omega^2\epsilon I, \Delta^h + \omega^2\epsilon I, \Delta^h + \omega^2\epsilon I, (\text{div})^h \sigma^h (\text{grad})^h),$$

are inverted exactly in each iteration by iterating a multigrid solver to convergence. This differs slightly from (5.4) due to the nonvanishing Helmholtz shift $\omega^2\epsilon$. For the range of frequencies considered, the difference between this preconditioning strategy and the one analyzed in Section 5.3 is negligible.

2. Multigrid preconditioning (M_M): Single V(2,1)-cycles are applied for each of the diagonal blocks to approximate the effect of M_E as in (5.7). For the (1,1), (2,2), and (3,3) blocks of M_M , point red-black Gauss-Seidel

smoothing is used if the grid is uniform. Otherwise, alternating-plane smoothing is used. For the (4,4) block, alternating-plane smoothing is used in all cases.

3. ILU preconditioning (M_I): An incomplete-LU factorization is computed using the real part of the matrix M_E as in (5.5). A drop tolerance 10^{-2} is applied.
4. SSOR preconditioning (M_S): The value $\alpha = 1.0$ used for the over-relaxation parameter in (5.3b).

The multigrid solver used is Dendy's code BOXMG (a black-box multigrid solver, see [35, 36]). For Poisson or simple Helmholtz problems on uniform grids, point red-black Gauss-Seidel smoothing cheaply inverts the (1,1), (2,2), and (3,3) blocks. For the inhomogeneous diffusion operator in the (4,4) block and for problems on non-uniform grids, alternating-plane smoothing is required to achieve reasonable multigrid performance, as observed in [1, 35, 36]. This gives a slight cause for concern due to the greater cost of plane relaxations. However, for large, highly inhomogeneous problems, the multigrid preconditioner applied with alternating-plane smoothing yields a robust solver.

In terms of computing costs (floating point operations or wall-clock time), the SSOR preconditioner M_S is cheapest. The ILU preconditioner M_I is slightly more expensive per iteration (depending on the level of fill) and requires some cost to set up, but is still fairly cheap. When on uniform grids and point red-black Gauss-Seidel smoothing is used on the Laplacian blocks, the multigrid preconditioner M_M takes roughly four times as long per iteration

as the preconditioner M_I ; for nonuniform grids, alternating-plane relaxation is needed, so each iteration of M_M is roughly 8.5 times as long as one of M_I .

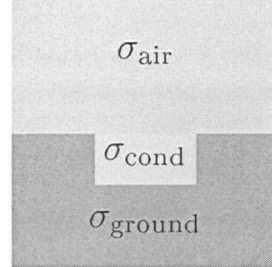


Figure 5.2: Cross-section of σ_B (a conducting block in a half-space).

As a first model, define the conductivity σ_B in Ω by

$$\sigma_B(x, y, z) = \begin{cases} \sigma_{\text{air}}, & z > 0; \\ \sigma_{\text{cond}}, & |x| \leq \frac{1}{5}, |y| \leq \frac{1}{5}, -\frac{1}{5} \leq z \leq 0; \\ \sigma_{\text{ground}}, & \text{otherwise.} \end{cases} \quad (5.23)$$

This models a conducting block of conductivity σ_{cond} embedded in a half-space. For the second test, consider the conductivity σ_E describing an ellipsoid buried underground (cf. (4.42b)). This constitutes a more difficult problem because the material interfaces do not align with the grid. The conductivity σ_{ground} of the earth is $\sigma_{\text{ground}} = 10^{-3}$ S/m and the conductivity σ_{air} of the air is $\sigma_{\text{air}} = 10^{-7}$ S/m (which regularizes σ as in (5.9)). Thus, the parameters σ_{cond} and ω are varied to compare performances of various preconditioners. The applied electromagnetic source term \mathbf{J}_e in (3.31) is either an electric or a magnetic dipole source as in [53, 110], while $\mathbf{J}_m \equiv 0$.

Consider first varying ω over the moderate range $[10^0, 10^4]$ Hz, and

σ_{cond} (S/m)	# of cells	BiCGStab iterations											
		$\omega = 10^0 \text{Hz}$				$\omega = 10^2 \text{Hz}$				$\omega = 10^4 \text{Hz}$			
		M_E	M_M	M_I	M_S	M_E	M_M	M_I	M_S	M_E	M_M	M_I	M_S
10^{-2}	10^3	1	3	7	19	3	3	7	19	6	6	11	20
	20^3	2	2	13	34	2	2	13	34	5	5	22	35
	30^3	2	2	20	44	3	3	20	44	5	5	34	50
	40^3	3	3	27	58	3	3	27	61	5	5	46	70
	50^3	3	3	33	72	3	3	33	79	5	5	61	86
10^0	10^3	3	3	9	25	3	3	9	25	6	6	12	25
	20^3	3	3	18	44	3	3	19	44	5	5	35	48
	30^3	3	3	30	66	3	3	30	50	5	5	56	63
	40^3	3	3	41	73	3	3	41	73	5	5	66	82
	50^3	3	3	44	100	3	3	44	100	5	5	100	111
10^2	10^3	3	3	9	20	3	3	9	25	6	6	12	25
	20^3	3	3	20	44	3	3	20	44	6	6	37	48
	30^3	3	3	30	67	3	3	27	59	6	6	55	67
	40^3	3	3	40	73	3	3	40	73	6	6	76	86
	50^3	3	3	49	95	3	3	48	96	6	6	97	109

Table 5.1: $\sigma = \sigma_B$ and electric dipole source on uniform grids. Each iteration of M_M is roughly 4 times as long as a single iteration of M_I .

varying σ_{cond} over the range $[10^{-2}, 10^2]$ S/m. These ranges translate to the parameter χ in (5.15) lying in the interval $[4\pi \times 10^{-9}, 4\pi \times 10^{-1}] \text{ m}^{-2}$. The jump discontinuities in σ for this range of σ_{cond} are between 5 and 9 orders of magnitude. For an electric dipole source, the results when discretized on uniform and nonuniform grids are tabulated in Tables 5.1 and 5.2 respectively. Tables 5.3 and 5.4 present results from similar trials on uniform and nonuniform grids respectively with a divergence-free magnetic dipole source term instead. Table 5.5 presents results of a similar set of trials with the model σ_E discretized on a set of uniform grids with an electric dipole source term.

All of the trials summarized in Tables 5.1–5.5 clearly show evidence of grid-independent rates of convergence of the Krylov method when preconditioned by M_E or M_M , as opposed to M_I or M_S . In spite of the seemingly strong

		BiCGStab iterations											
σ_{cond} (S/m)	# of cells	$\omega = 10^0 \text{Hz}$				$\omega = 10^2 \text{Hz}$				$\omega = 10^4 \text{Hz}$			
		M_E	M_M	M_I	M_S	M_E	M_M	M_I	M_S	M_E	M_M	M_I	M_S
10^{-2}	30^3	1	3	18	47	3	3	18	49	5	5	34	52
	40^3	4	4	27	59	4	4	26	64	7	7	40	68
	50^3	2	2	28	76	2	2	28	71	4	4	48	84
10^0	30^3	3	3	26	65	3	3	26	62	5	5	55	76
	40^3	4	4	31	76	4	4	34	78	7	7	76	91
	50^3	2	2	43	101	2	2	43	102	4	4	98	139
10^2	30^3	3	3	25	65	3	3	25	64	6	6	53	76
	40^3	4	4	31	79	4	4	34	80	7	7	76	102
	50^3	2	2	43	105	2	2	43	102	5	5	100	132

Table 5.2: $\sigma = \sigma_B$ and electric dipole source on nonuniform grids. Each iteration of M_M is roughly 8.5 times as long as a single iteration of M_I .

restrictions of the Fourier analysis of Section 5.2, the convergence behavior of the exact block inversion M_E measures up to theoretical predictions. That is, the analysis succeeds in capturing the essential local behavior of discrete operators for physically reasonable problems unhindered by the additional complications of nonuniform grids, of different boundary conditions, and, most significantly, of highly discontinuous conductivity models.

The results also show virtually identical performance in terms of iteration counts for the exact preconditioner M_E versus the single multigrid V(2,1)-cycle M_M . This observation suggests that solving the diagonal blocks exactly is unnecessary, at least within this frequency range. In particular, single V(2,1)-cycles work as effectively as the preconditioner M_E , with considerable savings in computational work.

Another interesting aspect of these results is that the iteration counts for all the preconditioners do not appear to depend strongly on ω or σ_{cond} . Looking at Figure 5.1, the spread of eigenvalues and the l_2 -condition number

BiCGStab iterations													
σ_{cond} (S/m)	# of cells	$\omega = 10^0 \text{Hz}$				$\omega = 10^2 \text{Hz}$				$\omega = 10^4 \text{Hz}$			
		M_E	M_M	M_I	M_S	M_E	M_M	M_I	M_S	M_E	M_M	M_I	M_S
10^{-2}	10^3	1	4	6	13	4	4	6	13	4	4	6	13
	20^3	4	4	13	25	4	4	13	25	4	4	15	25
	30^3	4	4	19	32	4	4	19	32	4	4	21	32
	40^3	4	4	27	42	4	4	27	42	4	4	32	41
	50^3	4	4	32	51	4	4	32	53	4	4	36	53
10^0	10^3	4	4	6	13	4	4	6	13	4	4	6	13
	20^3	4	4	13	25	4	4	13	25	4	4	15	25
	30^3	4	4	19	32	4	4	19	32	4	4	21	32
	40^3	4	4	27	43	4	4	27	41	4	4	32	43
	50^3	4	4	32	51	4	4	32	51	4	4	37	48
10^2	10^3	5	5	7	13	5	5	7	13	5	5	7	13
	20^3	5	5	13	26	5	5	13	26	5	5	15	26
	30^3	4	4	19	32	4	4	19	32	4	4	22	32
	40^3	5	5	27	42	5	5	27	42	5	5	32	43
	50^3	5	5	31	52	5	5	31	50	5	5	37	56

Table 5.3: $\sigma = \sigma_B$ and magnetic dipole source on uniform grids. Each iteration of M_M is roughly 4 times as long as a single iteration of M_I .

BiCGStab iterations													
σ_{cond} (S/m)	# of cells	$\omega = 10^0 \text{Hz}$				$\omega = 10^2 \text{Hz}$				$\omega = 10^4 \text{Hz}$			
		M_E	M_M	M_I	M_S	M_E	M_M	M_I	M_S	M_E	M_M	M_I	M_S
10^{-2}	30^3	1	3	23	41	3	3	23	42	3	3	25	42
	40^3	3	3	30	45	3	3	30	50	3	3	36	51
	50^3	2	2	37	61	2	2	37	60	2	2	47	62
10^0	30^3	3	3	23	42	3	3	23	41	3	3	26	41
	40^3	3	3	30	47	3	3	30	44	3	3	37	48
	50^3	3	3	37	60	3	3	37	65	3	3	47	65
10^2	30^3	3	3	21	41	3	3	21	41	4	4	27	48
	40^3	4	4	30	54	4	4	30	49	4	4	37	49
	50^3	3	3	37	57	3	3	37	57	4	4	47	59

Table 5.4: $\sigma = \sigma_B$ and magnetic dipole source on nonuniform grids. Each iteration of M_M is roughly 8.5 times as long as a single iteration of M_I .

BiCGStab iterations										
σ_{cond} (S/m)	# of cells	$\omega = 10^0 \text{Hz}$			$\omega = 10^2 \text{Hz}$			$\omega = 10^4 \text{Hz}$		
		M_E	M_M	M_I	M_E	M_M	M_I	M_E	M_M	M_I
10^{-2}	30^3	2	4	20	2	4	20	4	8	72
	40^3	2	4	30	2	4	30	4	6	107
	50^3	2	4	34	2	4	34	4	6	146
10^0	30^3	2	4	18	4	4	18	9	6	64
	40^3	2	4	25	2	4	24	5	6	98
	50^3	2	4	29	3	4	33	5	5	133
10^2	30^3	3	4	19	4	5	23	9	10	59
	40^3	2	4	24	2	4	29	8	9	92
	50^3	2	4	33	2	4	33	9	8	133

Table 5.5: $\sigma = \sigma_E$ and electric dipole source on uniform grids. Each iteration of M_M is roughly 4 times as long as a single iteration of M_I .

is quite flat until $\chi \simeq 10^1 \text{ m}^{-2}$. Once χ gets larger, however, the quadratic dependence of both quantities on χ becomes apparent and we can see the condition number getting far worse. Since χ is at most $4\pi \times 10^{-1} \text{ m}^{-2}$ in the trials so far, the iterations do not change much as σ_{cond} and ω are varied within this range.

BiCGStab iterations								
# of cells	ω (Hz)							
		10^1	10^2	10^3	10^4	10^5	10^6	
M_M	30^3	3	3	3	6	12	98	
	40^3	3	3	3	6	13	116	
	50^3	3	3	3	6	12	128	
M_I	30^3	30	27	31	55	166	642	
	40^3	40	40	42	76	210	1180	
	50^3	46	48	51	97	273	1551	

Table 5.6: $\sigma = \sigma_B$ over a range of frequencies.

To better observe the effect of increasing the parameter χ , fix the underlying conductivity model with $\sigma_{\text{cond}} = 10^2 \text{ S/m}$ and vary the frequency ω over a larger range using an electric dipole source. The multigrid pre-

conditioner M_M and the ILU preconditioner M_I are compared for problems discretized on uniform grids and the results are summarized in Table 5.6. Table 5.6 demonstrates the degradation of both preconditioning strategies M_M and M_I with increasing frequency. As in the other trials, iteration counts for the ILU-preconditioned system grow as the grid is refined, as opposed to the grid-independent iteration counts observed for the multigrid-preconditioned system. At the highest frequency $\omega = 10^6$ Hz, $\chi \approx 4\pi$ m $^{-2}$. Moreover, the performance of both preconditioners worsens significantly in increasing ω from 10^5 Hz to 10^6 Hz. This is consistent with the sharp rise observed in $\tilde{\eta}_{\max}/\tilde{\eta}_{\min}$ in Figure 5.1 near $\chi \simeq 10$ m $^{-2}$. Thus, the observations for higher frequencies agree well with the predictions of the Fourier analysis. This example is set over a short length scale, but the same quantitative results apply in terms of iteration counts on larger domains.

The CPU-time required for each iteration² of the multigrid preconditioner is roughly 4 times more than that for the ILU preconditioner in case of a uniform grid, and roughly 8.5 times more in the case of the exponentially widening grid (due to the additional cost of alternating-plane relaxations). Thus, using the ILU preconditioner M_I actually results in a faster algorithm than using the multigrid preconditioner M_M for coarse discretizations. But for fine discretizations (i.e., all cases recorded in Table 5.6) the multigrid preconditioner is significantly more efficient. Obviously, there is a crossover point beyond which the multigrid preconditioner is more efficient, since it achieves

²The iteration times are compared by running trials with the preconditioners M_M and M_I on various machines. Precise computational work estimates for BOXMG are in [35, 36].

convergence to a fixed tolerance within a constant number of iterations independent of the grid spacing h . In this example, the crossover point occurs for grid sizes that are well within practical range. A more specific implementation of the multigrid cycle could improve the efficiency of the preconditioner further, and lead to an earlier crossover point.

As a final test, Figure 5.3 presents convergence curves comparing the performance of M_M -preconditioned BiCGStab with an algebraic multigrid code³. The test problem uses the ellipsoidal model coefficient σ_E from (4.42b) discretized on a grid of $30 \times 30 \times 30$ cells. The code BOXMG is applied as a black-box solver to the dominant diagonal blocks of A in (5.1) while the other code applies an algebraic multigrid method to the full system. The results for M_M are plotted for several frequencies, while those for the algebraic solver (denoted by AMG in the Figure 5.3) are only plotted for one frequency; with the algebraic multigrid method used, the convergence curves are virtually identical for the distinct frequencies considered. Although restricted to a small test case due to implementation details, the results summarized in Figure 5.3 are important in demonstrating the favorable convergence behavior for M_M in spite of the cruder approximation inherent in this preconditioning strategy. The multigrid-preconditioning strategy turns out to be competitive with the more intensive full AMG solver in spite of the added simplicity (indeed, for this comparison, the wall-clock time for AMG is nearly ten times greater). This emphasizes the utility in the approach adopted throughout this research of deriving preconditioners from the structure of the PDE model as opposed

³The AMG code was generously provided by Yair Shapira.

to more brute force solvers.

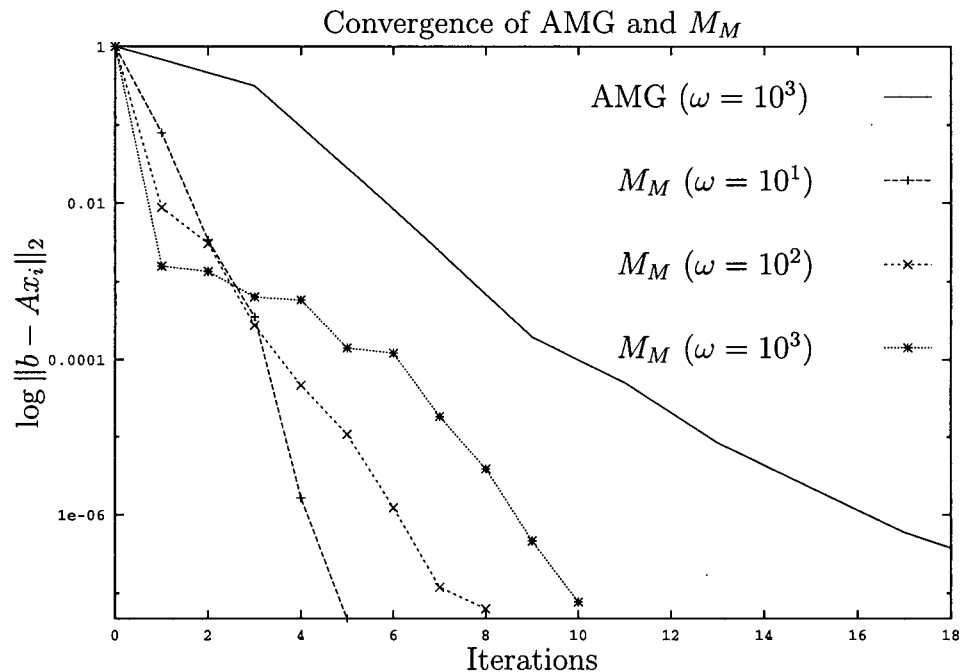


Figure 5.3: Comparison of AMG solver and M_M .

Chapter 6

Conclusions

6.1 Research Summary

Starting from the mathematical foundations of electromagnetic theory, this research addresses various concerns relevant to low-frequency electromagnetic simulation in geophysical or medical inverse problems. Drawing on the experience of practitioners of computational fluid dynamics, a PDE description suitable for moderate-frequency regimes is derived. With an appropriate continuous formulation, a finite-volume discretization is presented that possesses the conservation properties of the established Yee scheme and provides a sensible framework for respecting subtle interface conditions. A study of the consequences of staircase approximations to complex geometries in diffusive problems highlights the feasibility of Cartesian grids widely applied in practice. Finally, a family of preconditioners for the iterative solution of the resulting systems of equations is constructed, analyzed, implemented, and tested, yielding reliable solvers for large-scale three-dimensional problems.

An underlying contention of this work is that the construction of reliable numerical schemes and algorithms for the solution of PDEs is inextricably linked to the selection of physically meaningful and mathematically consistent forms of the associated continuous problems. The assumptions underlying the PDE model are critically examined from this perspective in Chapter 3. For the ranges of parameters considered, second-order boundary-value PDEs in the magnetic field \mathbf{H} are ruled out due to the strong discontinuities in the conductivity σ . To circumvent difficulties caused by the nontrivial kernel of the dominant **curl** operator, the electric field is split with a Helmholtz decomposition into divergence-free and curl-free components expressed in terms of vector and scalar potential variables \mathbf{A} and ϕ . The resulting indefinite PDE system is subsequently stabilized by subtracting a vanishing correction $\mathbf{grad}(\mu^{-1} \operatorname{div} \mathbf{A})$. Applying techniques established in the study of incompressible fluid flow, an extra differentiation yields a diffusion PDE for the scalar potential ϕ resembling a pressure-Poisson equation. The resulting diffusion equation replaces the gauge condition, yielding a PDE operator in Cartesian coordinates with much weaker coupling between solution components than the original PDE in the standard variables \mathbf{E} or \mathbf{H} . The new PDE problem is completed with two extra boundary conditions: one is needed to specify the Helmholtz decomposition and the other is required due to the additional differentiation. The logical progression outlined in Chapter 3 provides the analytical foundation on which the subsequent discretization and iterative methods stand.

With the PDE (3.31) expressed in terms of scalar and vector poten-

tials, the finite-volume discretization (4.28) is derived as in [53, 54]. As with the Yee scheme, the important conservation properties of the discretization (4.28) result from careful interlacing of field components on a grid staggered in space. In addition, the finite-volume arguments used to derive the discrete equations (4.28) provide a logical framework for the discrete representations of discontinuous material coefficients. As a result, discrete solutions approximate necessary interface conditions (3.34) at the junctions of distinct physical media. Furthermore, the coefficient matrix of the linear system stemming from the discretization (4.28) inherits block-diagonal dominance from the ellipticity and structure of the PDE operator in (3.31) expressed in Cartesian coordinates. The structure of this linear system is amenable to the preconditioners described in Chapter 5.

Discretization schemes widely used in practice for inverse problems are based on the assumption that the isotropic, inhomogeneous material coefficients are piecewise constant on grid cells. With standard Cartesian tensor-product grids, this supposition limits the resolution of interfaces between physical media to staircase approximations aligned with the faces of the cells of the grid. For straightforward scalar inhomogeneous diffusion problems, Proposition 4.1 states that if an interface between media is perturbed by $O(h)$, then the gradient of the solution of a perturbed diffusion problem differs from the gradient of a solution of an unperturbed diffusion problem by $O(h^{\frac{1}{2}})$ in the \mathcal{L}_2 -norm. Furthermore, in one dimension, the solution of the diffusion problem itself is perturbed by $O(h)$ in the \mathcal{L}_1 -, \mathcal{L}_2 -, and \mathcal{L}_{∞} -norms; this is particularly

surprising given that a perturbation of $O(h)$ of the interface generally results in a perturbation of $O(1)$ in the \mathcal{L}_∞ -norm of diffusion coefficient. While extension of the one-dimensional result to higher dimensions is not obvious, the numerical study of Section 4.4.2 suggests the same result holds in three dimensions. Thus, the implicit assumption of insensitivity of PDE solutions to staircase approximations of material interfaces is shown to be justifiable within the range of diffusive problems considered.

With the numerical scheme (4.28) and the corresponding sparse system of linear algebraic equations established, various preconditioned Krylov-subspace methods are considered for the iterative solution of the equations. A preconditioning strategy that stands out is one based on isolating the dominant diagonal blocks of the coefficient matrix. These blocks correspond to discretizations of uncoupled, scalar, elliptic PDEs with well-established solution techniques. Two robust preconditioners emerge that approximate inversions of the diagonal blocks, one based on ILU-factorization and another using a multigrid method. The reliability of these block-diagonal preconditioners follows directly from the properties of the PDE operator at moderate frequencies.

The Fourier analysis of Section 5.2 supports the preceding assertion. Under the assumptions outlined in Section 5.2, the coefficient matrix of the discrete linear system has a block structure wherein all blocks share Fourier modes as eigenvectors. As a result, Theorem 5.5 provides explicit bounds for the eigenvalue range and the ℓ_2 -condition number independent of the grid spacing. Moreover, these bounds are shown to grow quadratically with $\chi = \omega\mu\sigma$,

so degradation in the performance of block diagonal preconditioning strategies is expected as the frequency grows. In spite of the extreme limitations of the Fourier analysis, experiments in Section 5.4 strongly support the theoretical predictions for a variety of cases. Thus, for sources having compact support, the action near the boundary is negligible, so the local analysis captures the essential properties of the discrete operator well even in the presence of strong spatial inhomogeneities. Further, the block diagonal solver is observed to be competitive with an algebraic multigrid solver for the full discrete system, emphasizing the strength of the simpler block-diagonal preconditioning strategy.

6.2 Future Research

The formulation of the boundary-value problem (3.31) in terms of the vector and scalar potentials (\mathbf{A}, ϕ) is presented in Chapter 3 with the explicit assumption of existence of solutions. For Maxwell's equations expressed in the usual field variables \mathbf{E} and \mathbf{H} , establishing the existence and regularity of solutions in distinct physical contexts remains an area of active research in the mathematical community (e.g. [4, 97]). Complications within the geophysical context include the rough nature of the inhomogeneous coefficients and solutions and the selection of appropriate boundary conditions. For the purpose of applied computations within this work, proceeding with experimentation based on the assumption of well-posedness is justifiable. However, for the sake of mathematical consistency, the existence of solutions in appropriate spaces should be established.

Another mathematical question to address is the convergence of the finite-volume scheme (4.28). The derivation provided in Chapter 4 and the results of [54, 53] show that the method is consistent and second-order accurate; however, as is well-known in the numerical analysis community, given consistency of a numerical scheme, stability (in whatever appropriate sense) is generally required to conclude convergence. It is possible that searching for a relationship with established techniques using finite elements will point the way to a convergence proof (e.g., as in [81]).

The analysis and experiments of Section 4.4 raise a few interesting questions. It remains to extend Proposition 4.2 beyond the simple ODE case for one dimension; that is, is it true that a perturbation of $O(h)$ in the resolution of the interface between distinct media results in a perturbation of $O(h)$ in the solution of the inhomogeneous diffusion problem in the \mathcal{L}_∞ -norm? A similar theoretical result for more general elliptic PDE problems (including time-harmonic Maxwell's equations) would also be of practical utility. For more general boundary conditions and geometries in higher dimensions, more sophisticated analytical tools are needed to push the result up.

Approximate boundary conditions in computational electromagnetics constitute a broad area of research. An assumption implicit in many of the experiments and the analysis of this thesis is that the accuracy of the chosen boundary conditions for Maxwell's equations is not crucial for the family of applications studied herein. Although outside the scope of this work, it might be worthwhile to examine the suitability of this assumption with a numeri-

cal study comparing the solutions of Maxwell's equations with PML, PMC, absorbing, or other boundary conditions. There are some examples of such comparisons at high frequencies [31, 104, 105] but not at lower frequencies of interest here.

Another possible extension of the current work would be in the development of a time-domain code for Maxwell's equations. Some geophysical surveys rely on time-domain models of macroscopic electromagnetic behavior rather than time-harmonic frequency-domain models. For instance, in transient electromagnetic surveys, a DC source current in a steady state is abruptly shut off. The practical reason for shutting off the source in this manner is to allow receivers to measure the secondary electromagnetic fields due to currents induced in conductors without measuring the primary field caused by the source (that may be several orders of magnitude larger [82]). For transient electromagnetic phenomena and problems with discontinuous coefficients, the frequency-domain PDE models, spatial discretizations (see also [6, 53]) and solvers studied herein could be adapted for the time domain. For parabolic problems of interest, it is likely that implicit time-stepping is needed, unlike the explicit time-stepping used with the FD-TD method [104, 100, 112]. That being the case, the solvers described in Chapter 5 are of great utility; see [11, 70, 63] among other efforts.

Bibliography

- [1] R.E. Alcouffe, A. Brandt, J.E. Dendy, and J.W. Painter. The multi-grid methods for the diffusion equation with strongly discontinuous coefficients. *SIAM J. Sci. Stat. Comput.*, 2:430–454, 1981.
- [2] D. Alumbaugh and F. Morrison. Electromagnetic conductivity imaging with an iterative born inversion. *IEEE Trans. on geoscience and remote sensing*, 31:758–762, 1993.
- [3] D. Alumbaugh, G. Newman, L. Prevost, and J.N. Shadid. Three dimensional wideband electromagnetic modeling on a massively parallel computers. *Radio Science*, 31:1–23, 1996.
- [4] H. Ammari, A. Buffa, and J.-C. Nédélec. A justification of eddy currents model for the Maxwell’s equations. *SIAM J. Appl. Math.*, 60:1805–1823, 2000.
- [5] D. Aruliah and U. Ascher. Multigrid preconditioning for time-harmonic Maxwell’s equations. *submitted*, 2000.
- [6] D. Aruliah, U. Ascher, E. Haber, and D. Oldenburg. A method for the forward modelling of 3D electromagnetic quasi-static problems. *M3AS*, 11:1–21, 2001.
- [7] U. Ascher, R. Mattheij, and R. Russell. *Numerical Solution of Boundary Value Problems for Ordinary Differential Equations*. SIAM, 1995.
- [8] U. Ascher and L. Petzold. *Computer Methods for Ordinary Differential Equations and Differential-Algebraic Equations*. SIAM, Philadelphia, PA, 1998.
- [9] O. Axelsson and P. S. Vassilevski. A survey of multilevel preconditioned iterative methods. *BIT*, 29:769–793, 1989.

- [10] R. Barrett, M. Berry, T.F. Chan, J. Demmel, , J. Donato, J. Dongarra, V. Eijkhout, R. Pozo, C. Romine, and H. Van der Vorst. *Templates for the Solution of Linear Systems: Building Blocks for Iterative Methods*. SIAM, 1994.
- [11] R. Beck, P. Deuflhard, R. Hiptmair, R. Hoppe, and B. Wohlmuth. Adaptive multilevel methods for edge element discretizations of Maxwell's equations. *Surveys Math. Indust.*, 8:271–312, 1999.
- [12] J.-P. Berenger. A perfectly matched layer for the absorption of electromagnetic waves. *J. Comput. Phys.*, 114:185–200, 1994.
- [13] O. Bíró and K. Preis. On the use of the magnetic vector potential in the finite element analysis of three-dimensional eddy currents. *IEEE Trans., MAG*, 25:3145–3159, 1989.
- [14] M. Born. *Principles of Optics*. Pergamon Press, 1975.
- [15] A. Bossavit. Solving Maxwell's equations in a closed cavity, and the question of “spurious modes”. *IEEE Trans., MAG*, 26:702–705, 1990.
- [16] A. Bossavit. *Computational electromagnetism. Variational formulation, complementarity, edge elements*. Academic Press, 1998.
- [17] A. Brandt. Guide to multigrid development. In W. Hackbusch and U. Trottenberg, editors, *Multigrid Methods*, pages 220–312. Springer-Verlag, 1982.
- [18] A. Brandt. Multigrid techniques: 1984 Guide with applications to fluid Dynamics, 1984.
- [19] A. Brandt and N. Dinar. Multigrid solution to elliptic flow problems. In *Numerical Methods for PDE's*, pages 53–147. Academic Press, 1979.
- [20] F. Brezzi, J. Douglas Jr., and L.D. Marini. Two families of mixed finite elements for second order elliptic problems. *Numer. Math.*, 47:217–235, 1985.
- [21] F. Brezzi and M. Fortin. *Mixed and Hybrid Finite Element Methods*. Springer-Verlag, 1991.

- [22] William L. Briggs. *A Multigrid Tutorial*. SIAM, 1987.
- [23] G. Carey and T. Oden. *Finite Elements, a second course*. Prentice-Hall, 1983.
- [24] T.F. Chan and H.C. Elman. Fourier analysis of iterative methods for elliptic boundary value problems. *SIAM Review*, 31:20–49, 1989.
- [25] M. Clemens, R. Schuhmann, U. van Rienen, and T. Weiland. Modern Krylov subspace methods in electromagnetic field computation using the finite integration theory. *ACES J.*, 11:70–84, 1996.
- [26] M. Clemens and T. Weiland. Comparison of Krylov-type methods for complex linear systems applied to high-voltage problems. *IEEE Trans., MAG*, 34:3335–3338, 1998.
- [27] M. Clemens and T. Weiland. Numerical algorithms for the FDTD and FDFD simulation of slowly varying electromagnetic fields. *Int. J. Num. Modelling*, 12:3–22, 1999.
- [28] M. Clemens and T. Weiland. Transient Eddy-Current Calculation with the FI-Method. *IEEE Trans., MAG*, 35:1163–1166, 1999.
- [29] M. Costabel. A Coercive Bilinear Form for Maxwell’s Equations. *J. Math. Anal. Appl.*, 2:528–541, 1991.
- [30] R. Courant and D. Hilbert. *Partial Differential Equations*. Interscience Publishers, 1962.
- [31] F. El Dabaghi, K. Morgan, A.K. Parrott, and J. Periaux, editors. *Approximations and Numerical Methods for the Solution of Maxwell’s Equations*. Oxford University Press, 1998.
- [32] W. Dahmen and A. Kunoth. Multilevel preconditioning. *Numer. Math.*, 63:315–344, 1992.
- [33] N. A. Demerdash and R. Wang. Theoretical and numerical difficulties in 3D vector potential methods in finite element magnetostatic computations. *IEEE Trans., MAG*, MAG-26:1656–1658, 1990.
- [34] J. Demmel. *Applied Numerical Linear Algebra*. SIAM, 1997.

- [35] J.E. Dendy, Jr. Black Box Multigrid. *J. Comput. Phys.*, 48:366–386, 1982.
- [36] J.E. Dendy, Jr. Two multigrid methods for three-dimensional problems with discontinuous and anisotropic coefficients. *SIAM J. Sci. Stat. Comp.*, 8(2):673–685, Sept. 1987.
- [37] A. Dey and H.F. Morrison. Resistivity modeling for arbitrarily shaped three dimensional structures. *Geophysics*, 44:753–780, 1979.
- [38] H. Elman. Preconditioning for the steady-state Navier-Stokes equations with low viscosity. *SIAM J. Scient. Comput.*, 20:1299–1316, 1999.
- [39] H. Elman and D. Silvester. Fast Nonsymmetric Iterations and Preconditioning for Navier-Stokes Equations. *SIAM J. Scient. Comput.*, 17:33–46, 1996.
- [40] H.W. Engl, M. Hanke, and A. Neubauer. *Regularization of Inverse Problems*. Kluwer, 1996.
- [41] B. Engquist and A. Madja. Absorbing boundary conditions for the numerical simulation of waves. *Math. Comp.*, 31:1–24, 1977.
- [42] C. Farquharson and D. Oldenburg. Non-linear inversion using general measures of data misfit and model structure. *Geophysics J.*, 134:213–227, 1998.
- [43] R.P. Feynman, R.B. Leighton, and M. Sands. *The Feynman Lectures on Physics*. Addison-Wesley, 1977.
- [44] C.A.J. Fletcher. *Computational Techniques for Fluid Dynamics*, volume II. Springer-Verlag, 1988.
- [45] R. Freund and N. Nachtigal. QMR: A quasi-minimum residual method for non-Hermitian linear systems. *Numer. Math.*, 60:315–339, 1991.
- [46] V. Girault and P.A. Raviart. *Finite Element Methods for Navier-Stokes Equations*. Springer, 1986.
- [47] D. Givoli. *Numerical Methods for Problems in Infinite Domains*. Elsevier, 1992.

- [48] Gene H. Golub and Charles F. Van Loan. *Matrix Computations*. Johns Hopkins Univ. Press, 1996.
- [49] Anne Greenbaum. *Iterative methods for solving linear systems*. SIAM, 1997.
- [50] P.M. Gresho and R.L. Sani. On pressure boundary conditions for the incompressible Navier-Stokes equations. *Internat. J. Numer. Methods Fluids*, 7:1111–1145, 1987.
- [51] P.M. Gresho and R.L. Sani. *Incompressible Flow and the Finite Element Method: Advection-Diffusion and Isothermal Laminar Flow*. John Wiley & Sons Inc., 1998.
- [52] E. Haber. *Numerical Strategies for the Solution of Inverse Problems*. PhD thesis, University of British Columbia, 1997.
- [53] E. Haber and U. Ascher. Fast finite volume simulation of 3D electromagnetic problems with highly discontinuous coefficients. *SIAM J. Scient. Comput.*, 2001. To appear.
- [54] E. Haber, U. Ascher, D. Aruliah, and D. Oldenburg. Fast simulation of 3D electromagnetic using potentials. *J. Comput. Phys.*, 163:150–171, 2000.
- [55] E. Haber, U. Ascher, and D. Oldenburg. On optimization techniques for solving nonlinear inverse problems. *Inverse problems*, 2000. In press.
- [56] W. Hackbusch. *Multi-Grid methods and Applications*. Springer-Verlag, 1985.
- [57] T. Hagstrom, B. Alpert, L. Greengard, and S. Hariharan. Accurate Boundary Treatments for Maxwell's Equations and their Computational Complexity. *14th Annual Review of Progress in Applied Computational Electromagnetics*, to appear.
- [58] T. Hagstrom and S. Hariharan. A formulation of asymptotic and exact boundary conditions using local operators. *Appl. Num. Math.*, 27:403–416, 1998.

- [59] R.F. Harrington. *Field Computation by Moment Methods*. MacMillan, 1968.
- [60] M. Hestenes. *Conjugate Direction Methods in Optimization*. Springer-Verlag, 1980.
- [61] M. Hestenes and E. Stiefel. Methods of conjugate gradients for solving linear systems. *Cons. Reas. Nat. Bur. Stand.*, 49:409–436, 1952.
- [62] R. Hiptmair. *Multilevel preconditioning for mixed problems in three dimensions*. PhD thesis, University of Augsburg, 1996.
- [63] R. Hiptmair. Multigrid method for Maxwell’s equations. *SIAM J. Numer. Anal.*, 36:204–225, 1998.
- [64] J. M. Hyman and M. Shashkov. Natural discretizations for the divergence, gradient and curl on logically rectangular grids. *Int. J. Computers & Math. with Appl.*, 33:81–104, 1997.
- [65] J.M. Hyman and M. Shashkov. The adjoint operators for natural discretizations for the divergence, gradient and curl on logically rectangular grids. *IMACS J. Applied Numerical Math.*, 25:413–442, 1997.
- [66] J.M. Hyman and M. Shashkov. Mimetic discretizations for Maxwell’s equations. *J. Comp. Phys.*, 151:881–909, 1999.
- [67] R.S. Ingarden and A. Jamiolkowski. *Classical Electrodynamics*. Elsevier, 1985.
- [68] J.D. Jackson. *Classical Electrodynamics*. John Wiley & Sons Inc., 1975.
- [69] J. Jin. *The Finite Element in Electromagnetics*. John Wiley & Sons Inc., 1993.
- [70] P. Ciarlet Jr and J. Zou. Fully discrete finite element approaches for time-dependent Maxwell’s equations. *Numer. Math.*, 82:193–219, 1999.
- [71] A.A. Kaufman and G.V. Keller. *The magnetotelluric sounding method*. Elsevier, 1981.

- [72] D.J. LaBrecque. A scalar-vector potential solution for 3D EM finite-difference modeling. In M. Oristaglio and B. Spies, editors, *International Symposium on Three-Dimensional Electromagnetics*, pages 143–149. Schlumberger-Doll Research, 1995.
- [73] Rolf Leis. *Initial boundary value problems in mathematical physics*. John Wiley & Sons Inc., 1986.
- [74] R.J. LeVeque. *Numerical Methods for Conservation Laws*. Birkhauser, 1990.
- [75] Y. Li and D.W. Oldenburg. Inversion of 3-D DC resistivity data using an approximate inverse mapping. *Geophysical journal international*, 116:557–569, 1994.
- [76] P. Lorrain, D.P. Corson, and F. Lorrain. *Electromagnetic Fields and Waves*. W.H. Freeman and Company, 1988.
- [77] R.L. Mackie, T.R. Madden, and P.E. Wannamaker. Three dimensional magnetotelluric modeling using difference equations - theory and comparison to integral equation solutions. *Geophysics*, 58:215–226, 1993.
- [78] J.T. Marti. *Introduction to Sobolev Spaces and the Finite Element Solution of Elliptic Boundary Value Problems*. Academic Press, 1986.
- [79] C. Mattiussi. An analysis of finite volume, finite element, and finite difference methods using some concepts from algebraic topology. *Journal of Computational Physics*, 133:289–309, 1997.
- [80] P. Monk and E. Suli. A convergence analysis of Yee’s scheme on nonuniform grids. *SIAM J. Numer. Anal*, 31:393–412, 1994.
- [81] J.D. Moulton. *Numerical implementation of nodal methods*. PhD thesis, Institute of Applied Mathematics, University of British Columbia, 1996.
- [82] M.N. Nabighian and J.C. Macnae. Time domain electromagnetic prospecting methods. In *Electromagnetic methods in applied geophysics: applications*, pages 427–520. Soc. Expl. Geophys., 1991.

- [83] G. Newman and D. Alumbaugh. Three-dimensional massively parallel electromagnetic inversion—I. Theory. *Geophysical journal international*, 128:345–354, 1997.
- [84] G.A. Newman and D.L. Alumbaugh. Frequency-domain modelling of airborne electromagnetic responses using staggered finite differences. *Geophys. Prospecting*, 43:1021–1042, 1995.
- [85] D. W. Oldenburg. One-dimensional inversion of natural source magnetotelluric measurements. *Geophysics*, 44:1218–1244, 1979.
- [86] R. L. Parker. *Geophysical Inverse Theory*. Princeton University Press, Princeton NJ, 1994.
- [87] I. Perugia and V. Simoncini. An optimal indefinite preconditioner for a mixed finite element method. Technical Report 1098, Publ. I.A.N. C.N.R., 1998.
- [88] I. Perugia, V. Simoncini, and M. Arioli. Linear algebra methods in a mixed approximation of magnetostatic problems. *SIAM J. Scient. Comput.*, 21(3):1085–1101, 1999.
- [89] M. Renardy and R. Rogers. *An Introduction to Partial Differential Equations*. Springer-Verlag, 1993.
- [90] S.M. Richardson and A.R.H. Cornish. Solution of three-dimensional incompressible flow problems. *J. Fluid Mech.*, 82:309–319, 1977.
- [91] R.D. Richtmyer and K.W. Morton. *Difference Methods for Initial-Value Problems*. John Wiley and Sons, Inc., 1967.
- [92] J. W. Ruge and K. Stüben. Algebraic multigrid (AMG). In S. F. McCormick, editor, *Multigrid Methods*, pages 73–130. SIAM, 1987.
- [93] Y. Saad. *Iterative Methods for Sparse Linear Systems*. PWS Publishing Company, 1996.
- [94] Y. Saad and M.H. Schultz. GMRES: A generalized minimum residual algorithm for solving nonsymmetric linear systems. *SIAM J. Sci. Statist. Comp.*, 7:856–869, 1986.

- [95] J.E. Santos and D. Sheen. On the existence and uniqueness of solutions to Maxwell's equations in bounded domains with applications to magnetotellurics. *M3MAS*, 10:615–628, 2000.
- [96] S. Selberherr. *Analysis and Simulation of Semiconductor Devices*. Springer-Verlag, 1984.
- [97] D. Sheen. Approximation of electromagnetic fields: Part I. Continuous problems. *SIAM J. Appl. Math.*, 57:1716–1736, 1997.
- [98] J. Shen. *Computational Electromagnetics using Boundary Elements*. Computational Mechanics Publications, 1994.
- [99] D. Sidilkover and U. Ascher. A multigrid solver for the steady state Navier-Stokes equations using the pressure-Poisson formulation. *Comp. Appl. Math. (SBMAC)*, 14:21–35, 1995.
- [100] T. J. Smith. Conservative modeling of 3D electromagnetic fields; part I: properties and error analysis. *Geophysics*, 61:1308–1318, 1996.
- [101] D.C. Stinson. *Intermediate Mathematics of Electrmagnetics*. Prentice-Hall, 1976.
- [102] G. Strang and G.J. Fix. *An Analysis of the Finite Element Method*. Prentice-Hall, 1973.
- [103] J.C. Strikwerda. *Finite Difference Schemes and Partial Differential Equations*. Wadsworth & Brooks/Cole, 1989.
- [104] A. Taflove. *Computational Electrodynamics: the Finite-Difference Time-Domain Method*. Artech House Publishers, 1995.
- [105] Allen Taflove, editor. *Advances in computational electromagnetics: the finite-difference time-domain method*. John Wiley & Sons Inc., 1998.
- [106] S.V. Tsynkov. Numerical Solution of Problems on Unbounded Domains. A review. *Appl. Numer. Math.*, 27:465–532, 1998.
- [107] C.R. Vogel. Numerical solution of a non-linear ill-posed problem arising in inverse scattering. *Inverse Problems*, 1, 1985.

- [108] C. Vuik, J.J.I.M. van Kan, and P. Wesseling. A black box multi-grid preconditioner for second order elliptic partial differential equations. In G. Bugeda E. Onate and B. Suarez, editors, *Proceedings European Congress on Computational Methods in Applied Sciences and Engineering, ECCOMAS 2000, Barcelona, Spain, September 11-14, 2000*. CIMNE, 2000.
- [109] T. Wang and G.W. Hohmann. A finite-difference time-domain for three-dimensional electromagnetic modelling. *Geophysics*, 58:797–809, 1993.
- [110] S.H. Ward and G.W. Hohmann. Electromagnetic theory for geophysical applications. In *Electromagnetic Methods in Applied Geophysics*, pages 131–311. Soc. Expl. Geophys., 1988.
- [111] C. Weaver. *Mathematical Methods for Geo-Electromagnetic Induction*. John Wiley & Sons Inc, Philadelphia, 1994.
- [112] J.T. Weaver and A.K. Agarwal. Recent developments in three dimensional finite difference modelling of the magnetic field in geo-electric induction. *International Symposium on Three Dimensional Electromagnetics*, pages 131–142, 1995.
- [113] P. Wesseling. *An Introduction to Multigrid Methods*. John Wiley & Sons Inc., 1992.
- [114] J. Xu and J. Qin. Some remarks on a multigrid preconditioner. *SIAM J. Sci. Comput.*, 15:172–184, 1994.
- [115] K.S. Yee. Numerical solution of initial boundary value problems involving Maxwell's equations in isotropic media. *IEEE Trans. on antennas and propagation*, 14:302–307, 1966.